A techno-economic evaluation of a PV system providing simultaneous water heating and emergency power

SK Krieg

orcid.org/ 0000-0001-8930-1632

Dissertation accepted in fulfilment of the requirements for the degree *Master of Engineering in Mechanical Engineering* at the North-West University

Supervisor:	Dr WMK van Niekerk
Co-supervisor:	Prof M van Eldik

Graduation:	April 2024

Acknowledgements

I would like to acknowledge my supervisors, Dr. Willem van Niekerk and Prof. Martin van Eldik. Thank you for your guidance and patience. Thank you for always walking the extra mile while leading me through my dissertation.

I would also like to acknowledge my father Benno and mother Noreen, without you this would not have been possible. Thank you for believing in me and supporting me, throughout 6 years of study.

Lastly, thank you to my close friends for always having my back and making these last six years of studying worth it.

Abstract

With an increase in both loadshedding and the price of electricity, homeowners are looking to reduce their dependence on the national electricity grid, both for reliability and financial benefit. While water heating with an electric resistance heater accounts for approximately 40% of the total power consumption in a normal household, appliances like lightbulbs and a refrigerator consume relatively little power. Therefore, a PV system that can save money with water heating while providing reliable emergency power during grid loadshedding will benefit any homeowner. In this study, a combined PV system which can provide simultaneous water heating and emergency power is under techno-economic review.

A simulation model was developed to evaluate the proposed PV system. A single-diode model (SDM), which uses five parameters from a solar PV cell circuit, was used to model the power generation of a solar PV array. The model uses hourly solar radiation data from a climatic design year as input. The generated PV power is then used as input for the water heating and emergency power simulation. The water heating model uses thermodynamic conservation laws to determine the change in temperature within the geyser, taking into account a standard household water consumption profile, standing loss, and energy input from the PV system. The national grid is only used as an auxiliary power source to heat the water, should the water not be up to temperature after PV heating. Simultaneously, as the water is heated, the battery is also charged to be used as emergency power during loadshedding. Again, the grid is only used to charge the battery when the PV system is not sufficient. The model was verified with external literature and validated through experimental testing and hand calculations. The study focused on a side-by-side comparison of the different PV systems, defined in the study. Therefore, the model was not the main focus of the study, but rather means to compare the different systems.

Three different PV systems were simulated, each having the same water heating capacity and PV array, but with different battery capacities. The smallest system included a 12V, 20Ah battery, only used for lightbulbs and a Wi-Fi router during a 4-hour loadshedding period. The second system used a 12V, 80Ah battery to also power a refrigerator. Lastly, the third system used a 12V, 120Ah battery, which is capable of powering all the previously mentioned appliances as well as a microwave and hairdryer, albeit not at the same time. The system inverters were sized according to the load requirements of the systems. The simulation was performed for all three systems in four different locations over South-Africa, including two coastal cities and two in-land cities.

The study found that the PV systems generated around 2000 kWh for water heating in in-land cities, while only producing 1400 kWh for water-heating power in coastal cities. The savings,

with regard to emergency power, for each system increased as the system size increased. The PV system saved, on average, 195 kWh/year for emergency power with system C (largest system), while system A (smallest system) only saved 37 kWh/year. The cost savings for the system were calculated by comparing the grid electricity bill without the PV system to the grid electricity bill after the system was implemented.

The smallest system performed the best financially with a payback period of 6 years for in-land cities and levelised cost of energy of 1.73 ZAR, while the largest system, with its large battery capacity, saved the most kWh and provided more backup hours and capacity during loadshedding. The study concluded that: Firstly, the proposed combined system worked, providing reliable emergency power and financial benefit through savings in water heating. Secondly, the factors which the homeowner values more, convenience through emergency power or financial benefit through water heating, determine which system is better suited to the household.

Keywords: domestic water heating; solar photovoltaic; emergency power; simulation; modelling; performance; payback period; levelised cost of energy; combined PV system

Contents

LIST OF FIGURES

LIST OF TABLES

LIST OF ABBREVIATIONS

AC	Alternating current
ANC	African National Congress
BOS	Balance-of-System
C	Charge/Discharge rate
CAPEX	Capital expenditure
CFL	Compact fluorescent lamp
CIGS	Copper-indium/gallium-diselenide/sulfide
CSIR	Council for Scientific and Industrial Research
CSV	Comma-separated values
DC	Direct current
DPBP	Discounted payback period
DSTV	Digital Satellite Television
DVD	Digital versatile disc
IEEE	Institute of Electrical and Electronics Engineers
IRR	Internal rate of return
JPEG	Joint Photographic Experts Group
LCOE	Levelised cost of energy
LED	Light emitting diode
MPP	Maximum power point
MPPT	Maximum power point tracking
NAEP	Net annual energy production
NPV	Net present value
NREL	National Renewable Energy Laboratory
OPEX	Operating expenditure
PBP	Payback period
PV	Photovoltaic
PVGIS	Photovoltaic Geographical Information System
PVR	Personal(ised) video recorder
PWM	Pulse width modulation

SDM	Single-diode model
SQ	Shockly-Queisser
STC	Standard test conditions
TV	Television
VDC	Volts direct current

LIST OF SYMBOLS

a	Ideality factor
$C_{maintenance}$	Cost of the maintenance
c_p	Specific heat of water
C_{system}	Cost of the system
C_t	Net cash flow
d	Discount rate
dI/dV_{oc}	Slope at open circuit
dI/dV_{sc}	Slope at short circuit
E_{AUX}	Heating capacity of the geyser
E_{PV}	Energy supplied by PV system
G	Measured irradiance
$Grid_{evening1}$	Grid supply to geyser on
$Grid_{evening2}$	Grid supply to geyser on
$Grid_{morning1}$	Grid supply to geyser on
$Grid_{morning2}$	Grid supply to geyser on
G_{STC}	Irradiance at standard test conditions
G_{VAR}	Variable radiation
I	Terminal current of a single diode PV cell
i	Current hour
I_0	Reverse saturation current
$i-1$	Previous hour
I_d	Diode current
I_{MP}	Current at maximum power point
I_{mp}	Maximum power current
I_{ph}	Current source
I_{PV}	Photovoltaic current
I_R	Load current
I_{SC}	Current at short-circuit conditions
I_{sc_STC}	Short-circuit current at standard test conditions

I_{sh}	Shunt resistance current
k	Boltzmann’s constant
K_I	Thermal coefficient of ISC
K_I	Thermal coefficient of ISC
K_V	Thermal coefficient of VOC
K_V	Thermal coefficient of VOC
mS_{water}	Hot water consumption in the summer
mW_{water}	Hot water consumption in the winter
n	Lifetime of the system in years
N_s	Number of cells connected in series
P	Electrical power
P_{INT}	Intercept power
P_M	Maximum power
P_m	Rated power
q	Electron charge
Q_{LOSS}	Standing energy loss of water in the geyser
Q_{LOSS}	Standing energy loss of water in the geyser
Q_W	Change in thermal energy
R_b	Geometric ratio
R_{geyser}	Resistance of water heating element
R_S	Series resistance
R_{SH}	Shunt resistance
T	Cell temperature
T_{inlet}	Water temperature in
$Tmax_{GRID}$	Temperature setpoint when using grid energy
$Tmax_{PV}$	Temperature setpoint when using PV-generated energy
T_{STC}	Temperature at standard test conditions
Tt	Geyser temperature
Tt_0	Initial geyser temperature
U	Internal energy

V_d	Diode voltage
V_{MP}	Voltage at maximum power point
V_{mp}	Maximum power voltage
V_{OC}	Voltage at open-circuit conditions
V_{oc_STC}	STC open circuit voltage
Vt	Volume of water in the geyser
V_t	Thermal voltage
$\alpha_{V,STC}$	Temperature coefficient
β	Tilt angle
γ	Azimuth angle
δ	Declination angle
ΔT_{AUX}	Change in temperature due to the geyser using auxiliary energy
ΔT_{LOSS}	Change in temperature due to the standing loss
ΔT_m	Change in temperature due to hot water consumption
ΔT_{PV}	Change in temperature due to the generated PV power
φ	Latitude of Potchefstroom
ω	Hour angle of the sun

LIST OF UNITS

A	Ampere
°	Angular degrees
°C	Degrees Celsius
K	Kelvin
kg	Kilogram
kJ	Kilojoule
kW	Kilowatt
kWh	Kilowatt hour
L	Litre
m^2	Meter squared
min	Minute
Ω	Ohm
%	Percentage
V	Voltage
W	Watt
Wh	Watt hour
ZAR	South African Rand

1 - Introduction

1.1 Background

South Africa experienced its first loadshedding between November 2007 and January 2008. The power outages were a result of shortages in generating capacity at Eskom, South Africa's primary electricity supplier [2]. In 1998, an assumed demand growth of 4.2%, was predicted to fully use Eskom's generation capability by 2007 [3]. This prediction took into account a large rise in demand due the household electrification programme launched by the Department of Energy and Eskom. With the large increase in the population now using electricity, there was a steep increase in demand, while electricity prices stayed mostly unchanged between 2001 and 2008 [2]. The impact of this increase in demand was exacerbated by the lack of construction of new generating units, a negligence in maintenance activities on existing units, and the political struggles within the government [4]. The supply crisis prompted the launch of a new expansion programme in 2008. However, due to the subsidised cost of electricity, which neither reflected the marginal cost of supply nor included capital maintenance costs, there was a substantial lack of funds to finance the new programme [2]. In an attempt to raise the funds, the government increased the price of electricity by a cumulative 114% between 2008 and 2013. Eskom managed to avoid loadshedding in the following 6 years, but loadshedding was again implemented in March 2014 due to a shortage in generation capacity caused by the increased load and the summer maintenance programme [5]. Since 2019, Stage 4[1] loadshedding has become more and more prevalent, and the total amount of energy generated today (2023) is less than in 2010. The electricity is also produced at a much higher cost now than it was in 2010 [6].

With an increase in both loadshedding and the price of electricity, more homeowners are considering other, especially renewable, energy sources to heat water, save on electricity costs and be less dependent on Eskom. From an electricity cost perspective, water heating is the biggest single cost item, as water heating with an electric resistance heater, consumes approximately 40% of the total power in a normal household [7]. An electric resistance water heater is easily installed, with low capital investment, and is therefore the most common means of water heating in South Africa [7]. Electric geysers connected to the grid are, however, totally dependent on grid electricity and therefore vulnerable to loadshedding and the increasing price of electricity. Solar thermal geysers, heat pumps and photovoltaic (PV)

[1] Stage 4 loadshedding refers to the power being cut for four hours, twelve times over a period of eight days or twelve times over a period of four days for two hours at a time, resulting in 4000MW being shed from the grid.

modules are all viable alternative solutions to electric resistance geysers. Solar thermal geysers and heat pumps can only supply thermal energy for water heating. PV modules, however, generate electricity that can also be used for water heating and emergency power.

Providing emergency power during loadshedding is an increasing priority for households in South Africa. An easy solution to emergency power is the procurement of a generator to run during loadshedding. A generator can have a relatively low capital investment, but the operating costs are high. Batteries, charged from the grid, are another solution to emergency power, and although battery technology has improved and prices decreased, it is still a high capital investment. Both batteries charged from Eskom's grid and generators use non-renewable energy sources. Therefore, the energy generated by a generator or stored in batteries need to be replaced. This is accomplished by buying fuel for the generator or buying electricity from the grid, which increases the operating costs and therefore the lifetime cost of the system.

PV modules can generate electricity from the sun's irradiation, which is a renewable energy source. Excluding maintenance, PV modules have no operating costs, making them an attractive solution for emergency power. Smaller systems for emergency power are affordable for most middle to high income households, but as loadshedding increases from Stage 4 to Stage 6[2], appliances such as refrigerators also need to be powered, which increases the size of the backup power system requirements and therefore its costs.

When people want to reduce their consumption of electricity and reliance on the grid by installing alternative and renewable water heating technologies as well as emergency power systems, the economic viability is an important factor. The price of PV modules has decreased to such an extent that using them for water heating has become more economically viable. A single combined solar system that integrates water heating as well as emergency power generation from a single array of solar modules should therefore be more cost effective.

A typical PV system consists of four main components: the PV modules, an inverter, a charge controller and a backup battery. A 5kW inverter typically costs between 20 000 ZAR and 40 0000 ZAR, while a 1kW inverter plus geyser controller costs approximately 11 000 ZAR. A system that integrates the geyser, to be provided with DC power directly from the modules and power appliances during the day while storing power in a small battery for the provision of emergency power at night and during loadshedding, eliminates duplication and can therefore result in significant cost benefits. The absolute and relative sizes of the components mentioned above can be changed to form larger or smaller systems for different scenarios. As

[2] Stage 6 loadshedding refers to the power being cut for a total of 6 hours over a 24-hour period, resulting in 6000MW being shed from the grid.: and

the systems increase in size they can be described as more of a backup power system than an emergency power system.

To encourage the installation of solar systems, it is of great importance that homeowners have realistic expectations about the economic feasibility of such a system. Long exposure to the sun and other weather conditions such as humidity wears down components and therefore makes occasional device substitution necessary. Lithium-ion batteries, maximum power point tracking (MPPT) controllers and inverters typically have a 10 to 15-year life expectancy, while geyser elements have a lifespan of 5 to10 years [8, 9]. Replacing these components affects the economic feasibility of a solar system over its lifespan.

Although the prices of solar system components such as PV modules and batteries have decreased, it is still a large capital investment. Therefore, accurately evaluating the power a PV system can generate is very important, in order to correctly estimate the benefit of the economic investment [10]. This study aims to help enable homeowners to make an informed decision, depending on their budget and chosen comfort level, on the size of the system to install.

1.2 Problem statement

The economic viability of a combined residential PV solar system, without an inverter, that generates electricity for water heating and emergency power simultaneously, has not been systematically investigated for South African conditions.

1.2 Purpose of the study

The purpose of the study is to investigate the economic viability and feasibility of a solar PV system that combines water heating and emergency power generation with a single array of solar modules. With the current state of technology, the feasibility of having a combined system with two controllers, providing power from a single array to the battery and the electric geyser is yet unknown and was investigated throughout the study.

1.4 Scope

For the purpose of this study three scenarios were investigated, where the emergency load increased for each scenario. The most basic (smallest) system scenario is only able to provide emergency power to lights and Wi-Fi. A slightly larger system will be able to also sustain a refrigerator during loadshedding. Even larger systems are aimed towards more comfort as they can provide backup power for other household appliances like hairdryers and microwaves. System A had the smallest load capacity, and System C had the largest. The loadshedding schedule used throughout study had two blocks of Stage 4 loadshedding from 6:00 to 10:00 in the morning and between 18:00 and 22:00 in the evening. This profile was

chosen as it is the time of day when the household used the most electric load. No other loadshedding schedule was simulated in this study. The PV system for each scenario was simulated to evaluate whether it could provide power and to a 200L electric resistance water heater and household appliances from a single solar array. Each system consisted of a PV array, geyser controller, an electric resistance geyser, charge controller, a battery and inverter, as the main components. Throughout the study, the load capacity (number of appliances) of the systems could be altered to simulate how these changes affect the techno-economic viability of each system. The PV array was not optimized for different load profiles. As the goal of the study was to compare different scenarios where the backup capacity is changed, th number of solar panels was not varied. The number of panels were sufficient to heat the 200L water tank. High level modelling, which uses a simple model to analyse each component's input and output, was performed on the system, simulating the operations of the system. An experiment was conducted to verify parts of the simulation model with experimental data. The verified simulation model was then used to do a parametric techno-economic study of the different systems as well as their ability to provide emergency power during power cuts. Finally, the different systems were compared to assess each system's economic viability as well as its performance regarding water heating, power generating capacity and storage.

1.5 Methodology

As the technology used (PV modules, and batteries) is in a rapidly developing field, the study only focused on current technology and the most relevant literature reflected in Chapter 2, the literature study. The literature study gives a brief introduction to each technology used in the system, to properly understand its function. It also looks at the current state of technology in solar water heating and solar power generation. Different means of modelling, simulations and program developing were studied. The trend in component costs as well as the environmental factors that affect PV system operation and performance was investigated. The working principles of a PV system used for water heating and emergency power are introduced in the literature study.

The study focused on simulation for a household of four people (two adults and two children), with a middle to high household income. The distinguishing factor between the different scenarios and their systems was in the inverter providing AC power and the backup battery capacity of the system. The load capacity was changed according to the needs of the homeowner. The best-suited size, in terms of load capacity and backup battery capacity, for each system was therefore determined.

For the scope of this study, we assumed that the Balance-of-System components[3] stay constant for each system. The AC appliances that were included in each system are detailed in the table below. Note that water heating is included in each system.

Table 1: Appliances included in each scenario for emergency power

Provide power to:	Scenario A	Scenario B	Scenario C
Lights and WIFI	X	X	X
Refrigerator		X	X
Other appliances			X

The battery capacity was scaled according to the AC loads that needed to be powered for each system. The battery for System A had to be able to provide emergency power for up to 4 hours when used only for lights and Wi-Fi. The battery for System B had to be capable of also powering a refrigerator, and the battery for System C extra household appliances. The system had to be able to charge the battery and power the specified appliances during the day, while also heating water. During loadshedding the lights, Wi-Fi, refrigerator and household appliances were powered from the charged battery. Water heating was not powered from the battery, only PV power was used for water heating.

A normalised hot water consumption profile and data from a typical climatic design year were used as input data for the simulation model. System specifications, as well as capital and installation costs, were obtained from reputable suppliers across South Africa.

The entire simulation model was developed in Excel. To verify parts of the simulation model, the results of the model were compared to the data extracted from an experimental solar system set up in Potchefstroom.

[3] BOS or Balance-of-System components are the mechanical or electrical equipment and hardware used to assemble and integrate major components as well as conduct, distribute and control the flow of power in the system.

2 Literature study

The chapter begins with an introduction to the working principles of residential PV systems. The different technologies available and price of PV modules, controllers and batteries are discussed in the following sections. This is followed by a review of the different environmental and operating conditions, modelling techniques, and input parameters that influence the simulation model developed in this study. Different economic indicators that can be used for a techno-economic study of PV systems are also reviewed. The chapter is concluded with the findings of the reviewed literature relevant to this study.

2.1 Residential PV systems

As mentioned in Chapter 1, the aim of this study is to combine two photovoltaic systems into a single system. The combined system consists of a single PV array with a parallel connection to two controllers, namely a MPPT controller that charges the battery and the geyser controller that feeds the element with PV power. The parallel connection should allow the PV panels to charge the battery and heat the water simultaneously. First, the two separate residential PV systems are discussed to gain a better understanding of each system and how it functions.

2.1.1 PV system for power generation

Figure 1 illustrates the components found within a typical stand-alone solar PV system used for power generation and supply to household loads. The PV array, which is made up of multiple PV modules, generates direct current (DC) from solar irradiation [11]. The current flows from the modules through the charge controller. A charge controller controls the flow of current to the batteries, preventing the batteries from damage due to excessive overcharge [11]. From the battery the direct current flows through the inverter connecting to alternating current (AC) loads [11]. The system in Figure 1 is an off-grid system. Grid tied systems use the grid as well as PV modules to charge the battery and provide power to household appliances should the PV-generated power be insufficient.

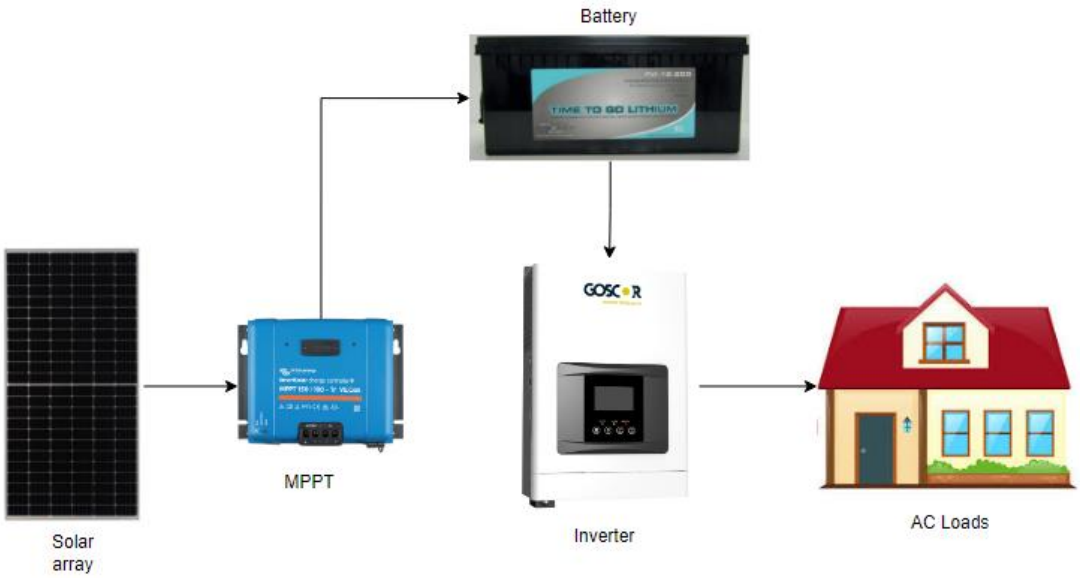

Figure 1: Convectional stand-alone PV system for power generation and storage

2.1.2 PV system for water heating

Figure 2 illustrates the main components of a PV water heating system. The PV array generates direct current (DC), that flows to the controller which feeds the resistive heating element of the geyser (storage tank) [12]. The system in Figure 2 is known as a grid-tied PV system, which means the controller can use the grid to heat the water should the PV array be insufficient. The system is not capable of feeding electricity back into the national grid and therefore any electricity which is generated after the water is already heated to the setpoint temperature is not used [12].

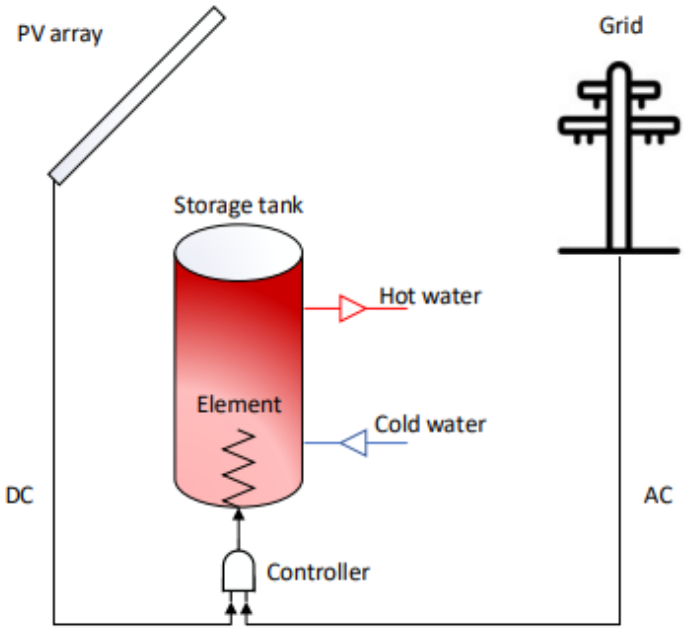

Figure 2: Conventional solar PV water heating system [12]

The success of a combined system depends on whether the different components within the system can work together through the parallel connection. PV modules, controllers and batteries are especially relevant to the success of the study and are discussed in the following sections.

2.2 PV modules

2.2.1 Trend in price of solar photovoltaic modules

There has been a large decline [13] in solar PV module prices over the past few decades, illustrated by Figure 3. The global solar PV market has developed rapidly and multiple factors contribute to this reduction in price [13]. Along with the rapid technological development of PV modules, the giant push for sustainable energy by leading countries has improved international trade of PV modules and led governments to implement policies that benefit commercial and residential users [14].

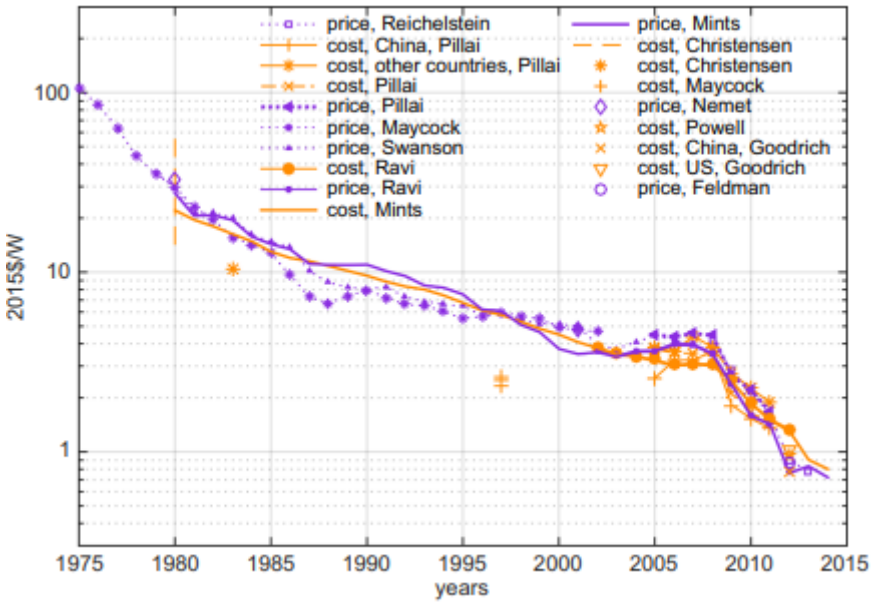

Figure 3: Module costs and prices since 1975 [13]

2.2.2 State of technology

A PV module is a grouping of solar cells joined in series to increase the voltage to a useful value compared to a single cell [15]. A solar cell is described as an electrical device, that uses a chemical/physical phenomenon, known as the photovoltaic effect, to convert the energy of photons into direct current. Three generations of solar cell technology exist today [15].

The first generation (Gen I) consists of wafer-based cells, usually crystalline silicon [15]. The second generation (Gen II) refers to “conventional” thin film technologies such as cadmium telluride (CdTe), copper-indium/gallium-diselenide/sulfide (CIGS), amorphous silicon (a-Si), and single-junction gallium arsenide (GaAs) cells [15]. The first two generation cells cannot

exceed the Shockly-Queisser (SQ) limit for single bandgap devices [15]. Gen I usually has higher efficiency but also higher cost per m^2 than Gen II cells [16]. Advanced thin films, the third generation (Gen III), include emerging cell technologies that can exceed the SQ limit. The Gen III cells include cells of organic materials as well as stacked multi-junction cells [15, 16]. Thin-film and crystalline-silicon cells are the focus of companies that develop new solar cell technology [15]. Once Gen III technologies are more developed as a cell technology, PV modules are expected to have higher efficiencies at a lower unit cost, as shown in Figure 4.

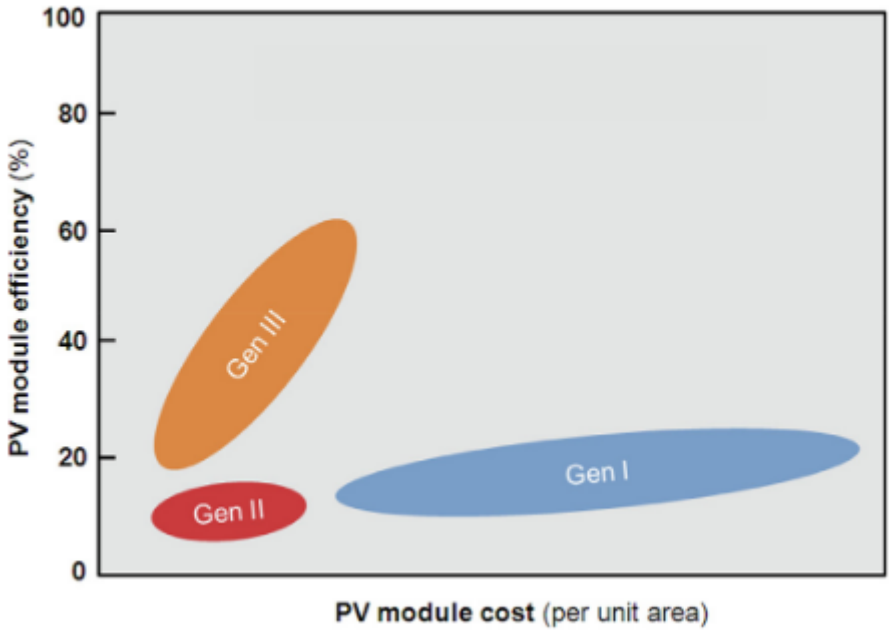

Figure 4: PV generations technologies [16]

Although there is rapid development in new PV cell technologies, there are still a couple of drawbacks that need to be overcome before large-scale production can commence [17]. As a result, single junction c-Si cell (Gen I) is still the dominant technology with a market share of 90% in 2022 [17], slightly less than the market share of 95% in 2017 [16], showing the steady growth of new technologies and their use in the market. Four main types of the traditional wafer-based cells exist and are classified as: mono-crystalline, poly-crystalline, heterojunction and microcrystalline [15]. Mohanty *et al*. [11] did a comprehensive review on the different module technologies available today. The findings agree with other studies [18, 19] that Mono-crystalline modules are currently the best for residential power generation.

2.2.3 Operational characteristics of PV modules

A PV module's operational characteristics is illustrated by an I-V (current-voltage) curve, at any given solar irradiance and operating temperature [20, 21]. When PV modules are connected directly to the geyser element, the operating point is determined by the load connected to the modules, i.e. the resistance of the element [21]. In Figure 5 the P-V (power-

voltage) curve is represented by the orange line and the maximum power point by the yellow dot. The blue line represents the I-V curve and the grey line the load curve. The point where these two lines intersect is known as the operating point.

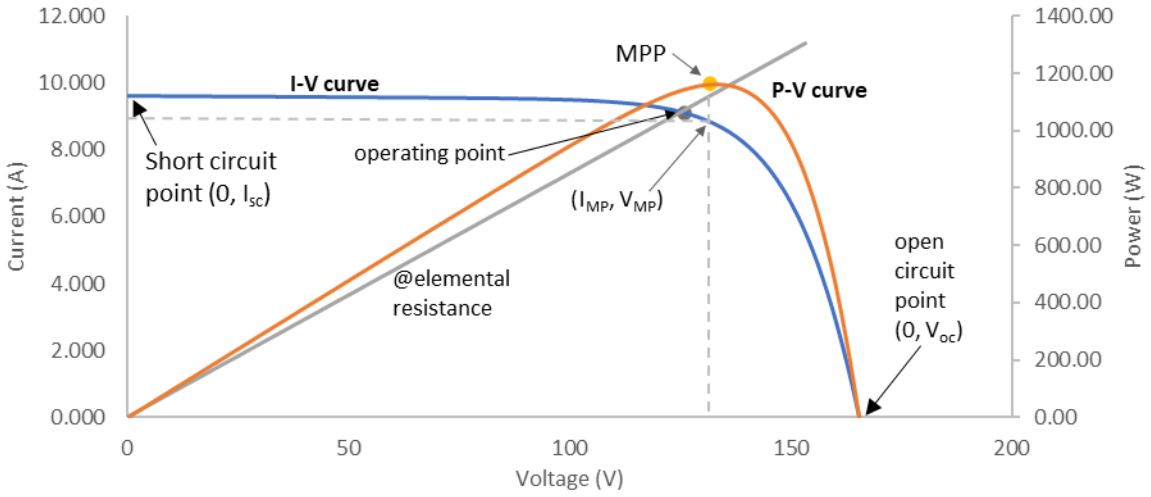

Figure 5: Operational characteristics of a PV module

The maximum power point (MPP) is the point on the P-V curve where the module generates the maximum possible power. The power is calculated as the voltage multiplied by the current for every voltage increment from the short circuit to open circuit voltage of the module. The MPP will always occur in area called the “knee” of the I-V curve [22-24] .

When the power that is generated by the modules is determined by the load curve, it is important to optimise the system in such a way that the operating point is as close as possible to the I_{MP} and V_{MP} on the I-V curve. This is achieved by adjusting the configuration of the modules, i.e. the number of modules in the system and how they are wired together.

2.2.4 Effect of module configurations for a resistive load

The number of modules in the PV configuration and the method of their wiring determines the voltage and current output of the PV array. Within a PV array, modules can either be connected in series or parallel. To increase the voltage of the array, modules are connected in series [11]. To increase the generation current, the modules are connected in parallel [11]. In Figure 6, different array wiring combinations can be seen as well as the load curve of different resistive loads (element sizes). Depending on the size of the resistive load used in the system, the number and wiring of the PV modules in the array will change to get the operating point and MPP to converge [21].

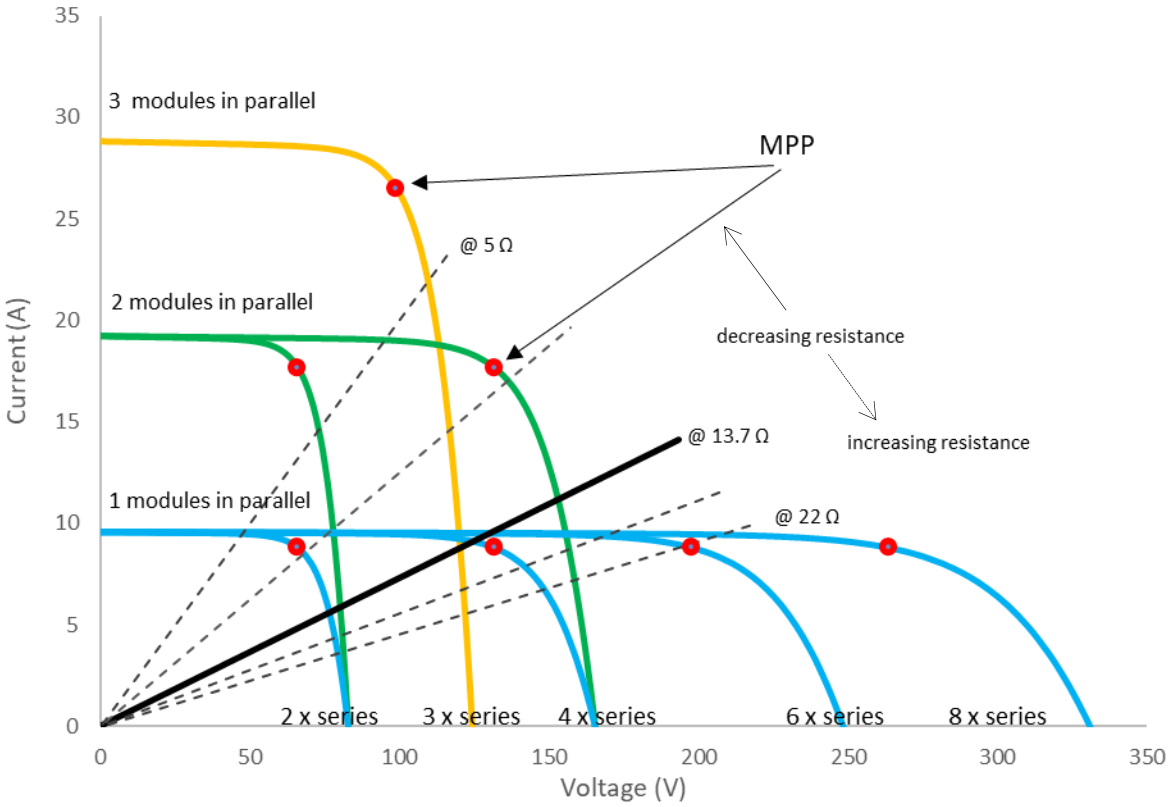

Figure 6: Load curve of a geyser element

The main drawback to PV modules connected directly to the heating element is their efficiency in less optimal weather conditions [25]. With low radiation, cloud cover or any disturbance in solar radiation (shade or soiling on the modules) the current of the PV array drops. This also causes the operating point to move away from the MPP. Charge controllers and geyser controllers with MPPT capabilities can maximise the generation efficiency of PV modules during non-optimal weather conditions.

2.3 Charge and geyser controllers

A charge controller regulates the current and voltage delivered to the loads. Various charge controllers exist that operate with different mechanisms [26]. Shunt controllers disconnect the battery once it is fully charged by converting the excess power to heat [26]. Series controllers disconnects the batteries when they reach a predetermined charge termination set point [26]. When the battery reaches a predetermined minimum discharge set point, it reconnects the power [26, 27].

PWM controllers are like series controllers, using transistors instead of a relay to regulate the flow of power [11, 26]. MPPT controllers can control the array voltage of the modules through maximum power point tracking [11, 26]. Maximum power point tracking is electronic tracking

that monitors the output of the PV modules and compares it to the required input voltage of the load. It calculates the optimal power that the module can generate to power the load and adjusts the voltage accordingly. Most MPPTs are 93-97% efficient in the conversion [11, 26]. Multiple sources [28-30], after review, state that Victron [9] produces the best MPPT charge controllers on the market. They are easy to install, have Bluetooth connection with great customisability and produce the highest load output at MPP compared to the other MPPT controllers.

Three readily available geyser controllers in South Africa today are the ECO MPPT from Geyserwise, the GEYSER ROBOT and the ELON 100 from Power Optimal. With the exception of the Geyserwise solution, these controllers are able to feed the geyser electrical element with DC power from PV modules as well as AC power from the grid [31-33].

The GEYSER ROBOT uses MPPT technology, while the ELON 100 does not. Both controllers are capable of intelligent switching between DC and AC input and can switch according to predetermined temperature settings. The ELON 100 controller has an input PV voltage of 20 - 250V DC and an input current of 20A DC, while the GEYSER ROBOT has an input of 90 – 240V DC and 16A. The MPPT controller from Geyserwise is also able to control the DC power based on predetermined temperature set points. It cannot, however, feed the element with AC power from the grid if the PV generated power is insufficient to heat the water [31-33].

In a PV array, the voltage of the array will often differ from the voltage at the optimal operating point due to ever-changing weather conditions [25]. The element therefore only receives a fraction of the power it received during Standard Test Conditions (STC). The use of a controller with MPPT capabilities can minimise the loss experienced during less optimal weather conditions by heating the water to the desired temperature earlier in the day. When the water is up to temperature, the excess PV-generated electricity can then be stored in batteries to be used as emergency power.

2.4 Batteries

2.4.1 State of technology

Battery technology has made rapid advances in the past century. Lead-acid batteries came on the market in the 1800s [11, 34]. Due to their low manufacturing cost, good performance and long life, they are still popular today [11, 34]. Nickel-cadmium batteries are a matured technology and are being phased out in some countries due to their environmental impact [11, 34]. Lithium-ion batteries have steadily risen in market share since the start of the 21st century [11, 34]. Their high energy density, relatively high voltages and low weight to volume ratio make them very popular [11, 34]. Bandyopadhyay *et al*. [35] compared three different battery technologies used in PV systems. Among the battery technologies considered in their study,

lithium-ion battery-based PV household systems performed the best, followed closely by vanadium redox flow batteries in all metrics. The study also found that, for a small lithium-ion battery capacity (< 5kWh), the depth of discharge (DoD) should be 50% - 60%. For larger battery capacity (>10 kWh), the optimal DoD is 65%-85% [35]. Batteries used in a PV system have to be of the same type, same manufacture, same age, at equal temperature, and have the same charge and discharge properties [11] while the size of the batteries used in the system is dependent on the required emergency load to be powered from the batteries. It should be noted that lithium batteries are able to discharge up to 2 C or more, which means that a 100 ah battery can discharge 200 A while gel batteries cannot discharge more than 1 C.

2.4.2 Trend in price of batteries

Ziegler and Trancik [36] investigated the technology improvement and cost decline rates of lithium-ion batteries. Their study found that lithium-ion cell prices have decreased, scaled by their energy capacity, by 91% since 1991 [36]. Although battery prices have declined, batteries still have high investment costs relative to the other components of a PV system. It is, therefore, important to assess depth of discharge and the capacity of the battery to be used in the PV system to ensure economic feasibility of the system [34].

2.5 Factors considered during model development

This section reviews the different environmental and operating conditions that affect modelling. The use of weather data and water consumption profiles in the simulation model is also studied. Lastly, the modelling techniques for PV modules and the different economic indicators used for solar PV systems are investigated.

2.5.1 Environmental and operating conditions

Environmental and operating conditions such as air temperature, wind speeds, soiling, and maintenance affect the system efficiency [37]. In this section the different factors that affect modelling are investigated. The effect they have on the accuracy of the model will also be evaluated.

Soiling can be a vital factor that influences a PV system's performance. Dust on the module can block the transmission of solar radiation through the module and cause hot spots, resulting in permanent module damage [25]. Acid rain can also damage the model through corrosion and decrease its efficiency and lifespan. The effect of soiling and acid rain can be prevented with regular maintenance, and was therefore not included in the simulation model [38].

Wind helps the ventilation of a PV system and has a cooling effect. A study by Gökmen *et al*. [39] showed that wind speed can affect the operating performance of a PV system. However,

Gaglia *et al*. [40] claimed that wind has a relatively small effect on PV efficiency compared to the effect of temperature and solar radiation. Due to the small effect of wind on the efficiency of the system [40], the effect of wind was not simulated.

Apart from the solar irradiance and incidence angle, the operating temperature of a PV module has the greatest effect on PV efficiency [40]. Module efficiency decreases when the module temperature exceeds 25°C and there is a considerable loss in power at higher module temperatures [25, 41]. Although the change in temperature was not simulated within this study, the modules were modelled at an operating temperature of 55°C to accommodate for the decreased performance [42], which was the typical operating temperature found during experimentation.

From literature it is evident that solar irradiance and tilt angle are the most important factors that influence accuracy when simulating PV power generation [11, 21, 22, 43]. While temperature, wind speed, and soiling do affect the power generation of PV modules, a study by Botes [12] provided very accurate results when simulating PV power generation with only irradiance and tilt angle. The tilt angle of the PV modules and the solar irradiance will be discussed in more detail in their own sections.

2.5.2 Degradation of PV modules

The PV modules and balance of system performance reduce year by year, but most module manufacturers guarantee 80% performance after 25 years by assuming an efficiency loss of 0.5% per year [1]. This claim is supported by the National Renewable Energy Laboratory (NREL) research that shows the mean degradation rate of modules to be 0.5% per year, but claim that it could be higher in hotter climates and for rooftop systems [44]. Pan *et al*. [45] and Ngure *et al*. [46] agree that the climate of different locations across the globe dramatically affects the degradation of solar modules. Ngure *et al*. [46] investigated the degradation mechanism and rates of solar PV modules in eastern Africa under two different climatic conditions. The results indicated power degradation rates of 0.99% per year for monocrystalline modules and 1.15% per year for polycrystalline modules over a period of 6 years under tropical savanna conditions. In semiarid conditions, the degradation for monocrystalline and polycrystalline modules were 1.44% and 1.22% per year, respectively [46]. For this study, degradation of the PV modules will be taken as 1% per year as most applications are in cities.

2.5.3 Climatic design year

A climatic design year is the weather data recorded on every day of the year. Weather data is critical for measuring the feasibility of a solar system and are usually depicted in an hourly format [43]. Figure 7 shows the change in irradiation across South Africa depending on the

area of residence. Areas with lower irradiance will require more PV modules compared to higher irradiance areas to produce equal amounts of electricity.

Weather data sets usually include the wind temperature, air temperature and some form of irradiation measurement [47, 48]. Most studies [11, 12, 21, 49] use the hourly variation of temperature and irradiation to model the I-V curve of the PV module for that hour. This allows the simulation of PV-generated power from the modelled I-V curve for every hourly variation in weather conditions.

There are powerful weather data tools available today like PVGIS, PVWatts and RETScreen that use multiple satellites to measure irradiance across the globe [48]. Out of the above mentioned, PVGIS has the most accurate simulation results with an annual deviation of -2% to real measured data, followed by PVWatts with -9.2% [50]. This is most likely due to the weakness of the programs to forecast the actual climate conditions as they use historical data. PVGIS can calculate the optimal tilt angle and azimuth angle, as well as the generated PV power for any solar system across the globe. While the simulation program calculated the annual PV generated power, PVGIS was used to verify the simulation program.

Weather conditions change over time, and it is therefore important to use the most recent data available to ensure the most accurate simulation possible. The weather data collected in the study by Van Deventer [47], used by Botes, is from 1971 and only provides data for the five largest cities in South Africa at the time, of which Johannesburg is the closest geographical location to Potchefstroom. PVGIS was therefore used to obtain the most recent available weather data for Potchefstroom. The weather data from PVGIS is for 2020. This ensured that the simulation used the most accurate weather data available and could be verified as accurately as possible with experimental data from Potchefstroom.

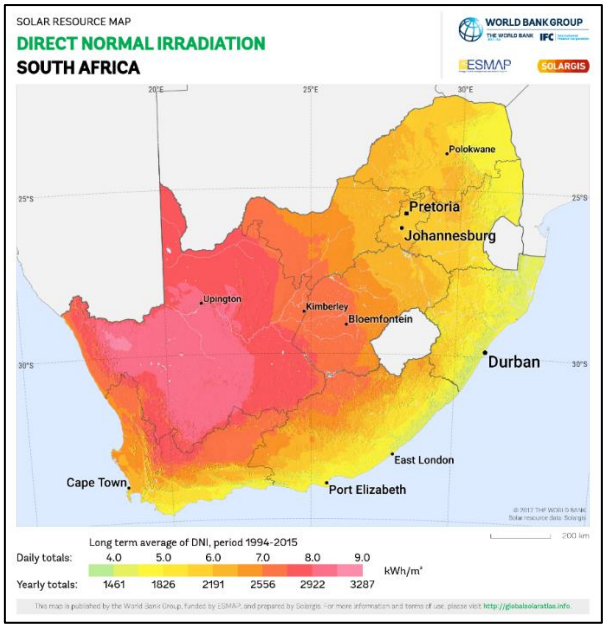

Figure 7: Direct normal irradiation across South Africa [51]

2.5.4 Water consumption profile

To accurately simulate the total PV power consumption of the entire residential system, the electricity consumption of the resistive element needs to be calculated with an energy balance over the geyser [12]. The energy balance uses a set of equations that calculates the energy in and out of the geyser according to the amount of water that flows into and out of the geyser at predetermined temperatures.

A normalised water consumption profile shows how much hot water is consumed by the occupants of a residential household. Multiple studies agree that the profile of a residential house in South Africa has twin peaks. These peaks occur at 9:00 in the morning and 21:00 in the evening, as seen in Figure 8 below. While there is variation in the total consumption of hot water per person per day, 50 litres pp/day in the summer and 70 litres pp/day in the winter is generally accepted [43, 52-54].

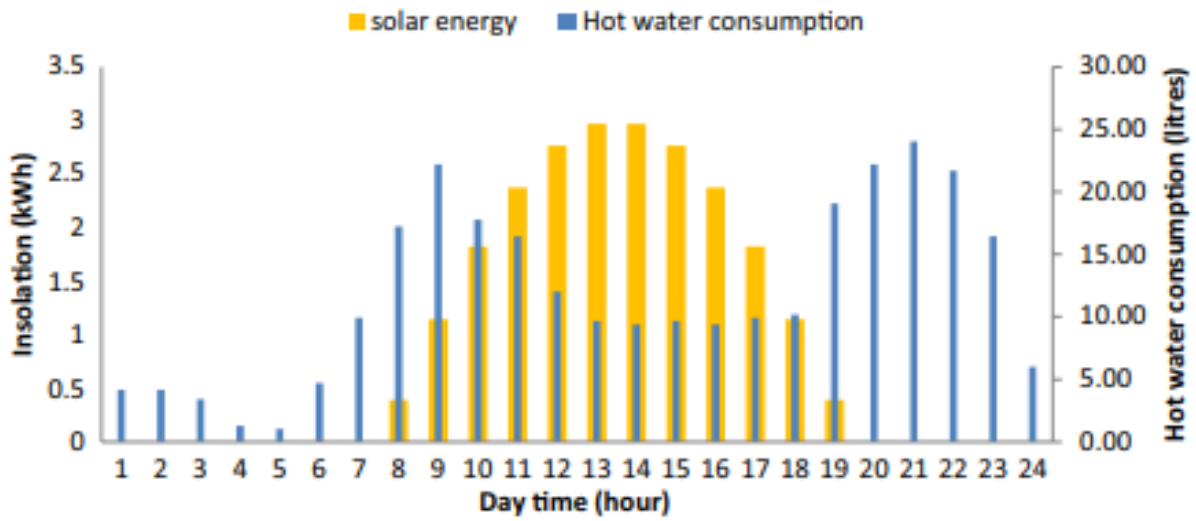

Figure 8: Water consumption profile matched with the hourly generated PV energy [55]

The water consumption profiles used in the reviewed literature matched the hourly water consumption to the hourly PV-generated electricity [12, 55]. With some studies, water stratification within the geyser was neglected [12] while others included the effect of stratification [56]. All studies used the basic equation of $q = mc\Delta T$, calculating the change in energy of the water based on the outflow of hot water and the inflow of cold water [55-57].

A report by Lutz *et al*. [58] investigated different water profiles for elderly households and households with washing appliances that run during the day. While water consumption profiles differ from household to household, this study actively focuses on the average household in South Africa for which a normalised consumption profile with twin peaks is a good representation [52].

2.5.5 Photovoltaic models

Due to the high investment cost of PV systems, it is important to design a system that uses the available solar energy optimally. This necessitates an accurate simulation of the designed system prior to installation [23] to assess the performance of the solar PV system to be used as a power source. A PV module is modelled to optimise the performance, efficiency and cost effectiveness of the module [10]. Important parameters of the solar cell that affect the I-V characteristics are determined during the modelling process [1].

There are many different models that have been proposed by researchers [1, 20, 21, 59]. To model a PV cell, important parameters of the cell are estimated, which are in turn used to model the P-V and I-V characteristic curves of the cell. This imitates the solar cell under various environmental conditions that are changed during simulations. The use of the electrical equivalent circuit, which is primary-based on a diode, is the most popular approach to modelling. Two methods of modelling exist, numerical or analytical. Numerical methods use a

set of equations which can be solved using numerical or iterative algorithms. Analytical methods make use of fast parameter extraction procedures through approximations or assumptions without sacrificing accuracy [59].

The starting point of most models uses the Shockley theory for a p-n junction which is exposed to solar radiation [20]. The Shockley theorem allows for the equivalent circuit of the solar cell to be described at different levels of approximations [12]. An ideal solar cell is modelled where the current source is in parallel with the diode [1]. The current source or light-generated current source is proportional to the solar radiation falling on the solar cell [1]. The PV cell can be modelled as a one-, two- or three-diode model. The number of diodes present in the model are linked to the number of characteristic parameters, the mathematical complexity and the accuracy of the model [1, 12].

2.5.5.1 Different diode models

As illustrated in Figure 9, the one-diode model has five unknown parameters, while the two-diode model has seven and the three-diode model has nine, which all increase in complexity as the number of unknown parameters increase [1]. The diffusion and recombination in the quasi-neutral regions of the solar cell are responsible for the diode current (I_d) in the one-diode model [1]. The one-diode model assumes that there is no recombination loss in the depletion region. The current in the second diode (I_{d2}) is due to the recombination loss that is modelled in the depletion region [1, 12, 23]. Due to the implicit form and exponential terms of the current source equation, it is difficult to determine the parameters in the two-diode model. The two-diode model also requires specific parameters of the semiconductor, not commonly supplied by commercial PV datasheets [10, 23]. The connection of the third diode is to represent the diode current caused by recombination in the defect regions, grain sites etc. [1]. The three-diode model has been proposed for larger crystalline solar cells and acts as a superior model to characterise the large-size industrial solar cells. The mathematical equations applied in the model determines the number of parameters that are extracted [12].

Solar cell model	Equivalent circuit	Mathematical equation	Unknown Parameters
One-diode model	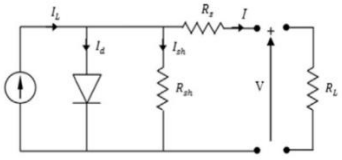	$I = I_L - I_o[e^{(\frac{q(V+IR_s)}{aKT})}-1]-\frac{V+IR_s}{R_{sh}}$	I_L, I_o, a, R_s and R_{sh}
Two-diode model	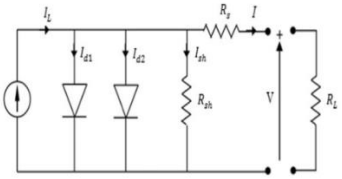	$I = I_L - I_{o1}[e^{\left(\frac{q(V+IR_s)}{a_1KT}\right)}-1]-I_{o2}\left[e^{\left(\frac{q(V+IR_s)}{a_2KT}\right)}-1\right]-\frac{V+IR_s}{R_{sh}}$	I_L, I_{o1}, I_{o2}, a_1, a_2, $R_s$and R_{sh}
Three-diode model	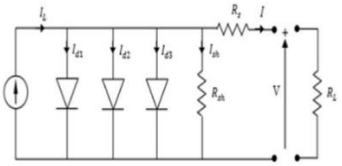	$I = I_L - I_{o1}[e^{\left(\frac{q(V+IR_s)}{a_1KT}\right)}-1]-I_{o2}\left[e^{\left(\frac{q(V+IR_s)}{a_2KT}\right)}-1\right]-I_{o3}[e^{\left(\frac{q(V+IR_s)}{a_3KT}\right)}-1]-\frac{V+IR_s}{R_{sh}}$	I_L, I_{o1}, I_{o2}, I_{o3}, a_1, a_2, a_3, R_s and R_{sh}

Figure 9: Different diode models [1]

The single-diode model (SDM) is favoured due to its simplicity and the lower computational effort required to extract the parameters [1]. Lo Brano *et al*. [10] stated that the one-diode model is an adequate representation of the I-V characteristic curves at STC [12]. It is mostly agreed upon that the one-diode model is, in practice, a good trade-off between accuracy and simplicity [12]. Although the three- and two-diode models are superior in accuracy, the single-diode method is by no means inaccurate [10]. The increased complexity of the two- and three-diode models with diminishing returns in their accuracy compared to the one-diode model, make them undesirable for this study.

2.5.5.2 Five parameter one-diode model

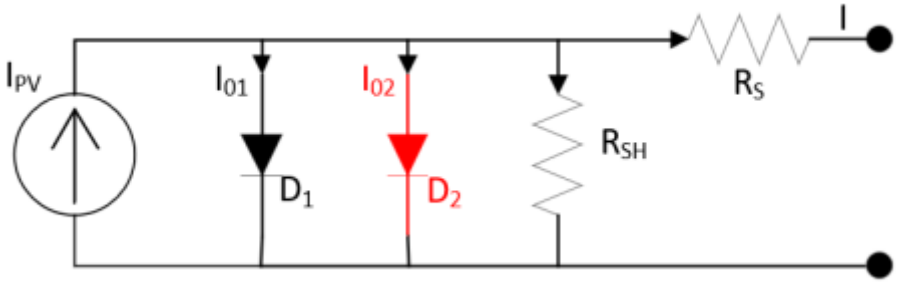

Figure 10: Equivalent electrical circuit used in SDM (black) with an additional red diode [12]

As seen in Figure 10, a solar cell model typically depends on five parameters. These parameters are not provided by manufacturers but can be determined by using the I-V characteristics and analysing their equivalent electric circuit. These parameters are the

photogenerated current (I_{PV}), the reverse saturation current (I_0), the shunt resistance (R_{SH}), the series resistance (R_S) and the diode ideality factor (a) [60]. The values that are provided by manufacturers are the nominal open-circuit voltage (V_{OC}), the nominal short-circuit current (I_{SC}), the voltage and current at maximum power point (V_{MP}) and (I_{MP}), and the maximum power (P_M) [61].

Humada *et al*. [62] compared the effect of the five parameters and found that the diode ideality factor, as well as the series-and shunt resistances, influences the I-V curve significantly. Therefore, many of the models used today focus on solving these three parameters, but other studies have concentrated on either four, three, two or even just one parameter [62].

There is much ambiguity in selecting the values of the ideality factor. According to Lo Brano *et al*. [10], most inaccuracies in modelling occur due to the diode ideality factor being interdependent. Multiple studies [20-22, 59] found the ideality factor to be between 1 and 1.5 in the one-diode model. The ideality factor can change depending on other cell parameters, and can be changed throughout the modelling process to improve the accuracy of the model and of the generated I-V curve [12].

Ibrahim and Anani [59] stated that the shunt and series resistances do not have a significant effect on the I-V characteristic curve at STC, which is not the case under other operating conditions. Lo Bran *et al*. [10] concluded that both resistances influence the slope of the I-V characteristic curve, before and after the curve “knee”. The resistances R_S and R_{SH} do not physically exist in the cell. They are electrical representations of the energy losses and voltage drops found within the semiconductor in the presence of the photocurrent [10]. The values of both resistances can be graphically determined from the I-V curves provided by the manufacturers [12]. This method restricts the model to PV modules whose manufacturers provide I-V graphs. The accuracy of the graphical approach relies heavily on choosing the points to be evaluated on the I-V curve correctly [12, 20].

Lo Brano *et al*. [10] proposed a new five-parameter model capable of analytically describing the I-V characteristics of a PV module for different environmental conditions. Data from manufacturers and standard rating conditions are used to solve a system of equations that extracts the parameters of the equivalent electrical circuit. Ayodele *et al*. [61] compared different numeric algorithms used in solving the five-parameter model [12]. The results indicated that no single algorithm performed increasingly better than the other. The focus area of the user determines the success of the algorithm, as each algorithm is best suited for a given metric [12]. Ibrahim and Anani [59] compared different analytical techniques used for parameter extraction. Although analytical algorithms require some degree of approximation,

they performed on par with popular numeric algorithms. Most studies make use of numerical algorithms.

After a review of different means to model a solar cell and extract the parameters needed, the one-diode model was chosen for this study. The simulation model made use of various five-parameter model techniques.

2.5.6 Analysis of economic indicators used for PV systems

When conducting technical or performance studies, it is important to include financial impacts for the benefit of the consumer. Although PV systems make use of a renewable energy source, the upfront investment of harvesting this energy comes at a cost. There are still capital and operational costs, and as with any project, financial indicators are used to gauge the success of the project [63].

There are multiple studies that have investigated the economic feasibility of residential PV systems [34, 64-69]. Many input parameters exist that can be used for economic analysis. Some of the parameters used in these studies include cost of electricity, PV system costs, government policies, operational and maintenance cost, replacement cost of components, discount rates, inflation, feed-back tariffs and more. While some of these input parameters are essential to the economic analysis, like PV system costs and electricity prices, others may not be. Depending on the country or size of the installed system, feed-back tariffs, government policies and maintenance cost may not exist or be negligible and will not affect the analysis. Similarly, many output-economic indicators exist. Hoppmann *et al*. [64] used a 'Self-consumption module', which was then used in the 'Net present value module'. The 'Storage and PV system size optimisation module' then drew on both the 'Self-consumption calculation module' and the 'Net present value calculation module' to find the optimal PV system size for the household [64]. Litjens *et al*. [65] made use of the Profitability Index and Payback Period as economic indicators while Akter *et al*. [70] used Levelised Cost of Energy (LCOE), Net Present Value (NPV), Internal Rate of Return (IRR), Discounted Payback Period (DPBP), and Payback Period (PBP) in their study conducting economic analyses of residential households with PV systems in Australia. A study by Han *et al*. [34] listed 26 different techno-economic studies of PV systems with batteries. The most used economic indicators, for those studies that focused on simulation, were NPV, LCOE and PBP.

This study therefore also made use of the NPV, LCOE and PBP as financial indicators to evaluate the different systems in terms of their economic feasibility. The NPV of the system is used to compare the system with other alternative power generation systems. The LCOE is used to compare the cost of energy of the PV system with the cost of energy with the national grid. Lastly, the payback period is used to determine when the system will start to be profitable.

These three indicators cover the costs, value and profitability of a system during its lifetime. Usually, a single indicator is sufficient to determine the economic viability of a system, however, multiple indicators give a more in depth look at different aspects of economic viability. Each of the financial indicators used are thoroughly explained in the modelling section.

2.6 Conclusions

The working principles of a stand-alone PV system for power generation and a PV system for water heating were introduced and discussed. This included the components of each system and how they work together to form the system. With a clear understanding of both systems, a combined system can be designed for simultaneous water heating and emergency power.

The study also investigated the current state of technology and the trend in price of PV modules, charge controllers and batteries. From the literature, monocrystalline PV modules were found to be the best for power generation. While the wiring of the modules is important to find the optimal operating point, charge controllers with MPPT tracking maximise the generation and use of the generated electricity from the modules. The ELON 100 controller from PowerOptimal and the GEYSER ROBOT were both tested to determine if the MPPT capabilities of the GEYSER ROBOT outperform the ELON 100 controller in power generation. The SmartSolar MPPT from Victron was used in combination with lithium-ion batteries.

The weather data and water consumption profile was used in an hourly format as input for the one-diode, five parameter PV model. Compared to the other modelling techniques, the one-diode model was found to be the best compromise in both accuracy and simplicity. Lastly, after a review of various different economic indicators used in previous techno-economic studies of PV systems, the NPV, LCOE and PBP methods were used to analyse the economic feasibility of the PV system.

3 Combined PV system experiment

The aim of this chapter is to discuss the experimental goal, setup, procedure and results used to verify parts of the simulation model. Section 3.1 covers the experimental goal and Section 3.2 the setup with the equipment used during testing. Section 3.3 discusses the experimental procedure of the experiment and how each controller was tested as well as the results obtained for each controller and the observed charging behaviour of the MPPT charge controller.

3.1 Experimental goal

The goal of the experiment was to validate the assumptions made, and the modelling methods used within the simulation program. Firstly, the SDM PV power generation model needed to be validated with PV modules and captured irradiation data. Secondly, the efficiency or power loss over the geyser controller needed to be tested and validated to ensure that it was within the manufacturer specifications. The simulation program used the recorded experimental data as a baseline to create the simulation. Thirdly, the MPPT function of the geyser controller needed to be tested and compared to the normal operating condition of the controller. The result of the experiment determined whether the controller would be simulated with the MPPT setting turned on or whether it would only be used to operate on the load curve. Lastly, the viability of using two controllers with a single PV array to charge a battery and heat water simultaneously was tested. The efficiency of the MPPT charge controller was also tested in this stage of the experiment.

3.2 Experimental setup

In Figure 11 below, a schematic of the experimental setup is shown. PV modules were connected to a 13.7-ohm electric resistive element through a geyser controller. Two controllers were tested. The GEYSER ROBOT has an input voltage range of 90-240 VDC while the ELON 100 has an input range of 20-250 VDC. Four PV modules were connected in series, resulting in a maximum operating voltage of 150V at the MPP. The PV modules were mounted on a movable frame at an angle of 30 degrees to the horizontal. A Pyranometer SP-215 was also mounted on the frame, at the same angle as the PV modules, to measure the incoming radiation. The PV modules were positioned at different angles relative to the sun, to emulate different levels of irradiation, for which all the measurements were recorded. The PV modules were then also connected to a 12V 100 Ah gel battery. Two controllers were set up, in a parallel connection, to supply power to the resistive load of the element and the battery simultaneously. The Victron SmartSolar MPPT 150/35 was used to charge the battery, while the ELON 100 was used as the geyser controller.

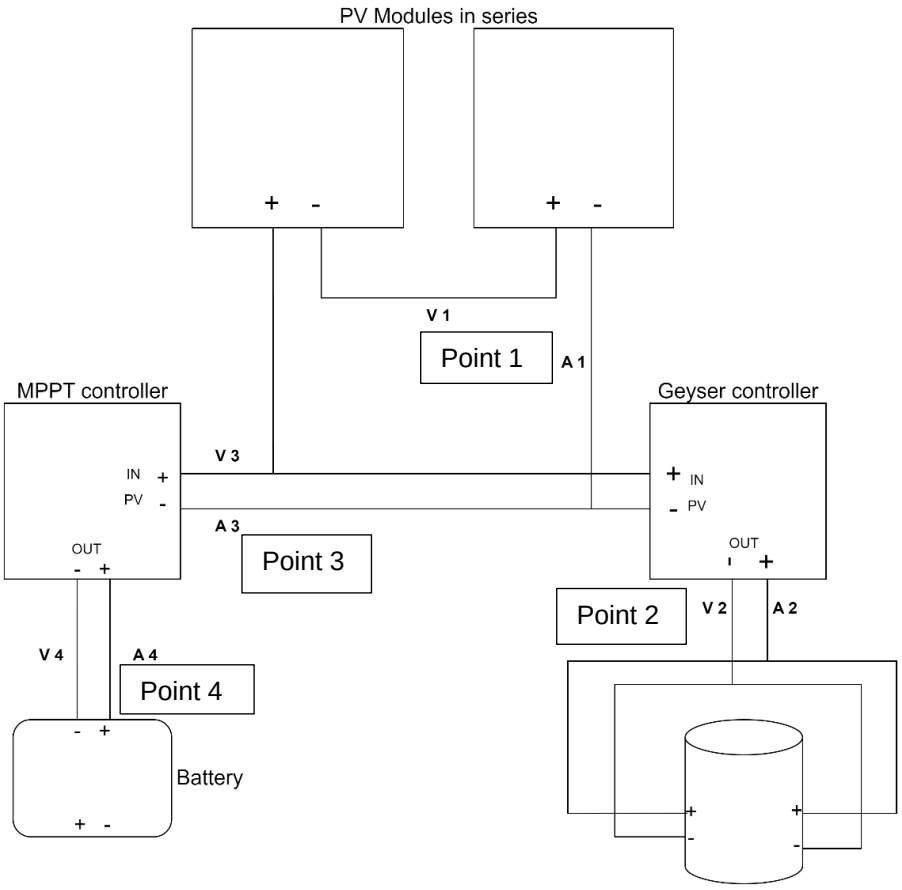

Figure 11: Combined PV system, with the various points for data recordings

3.3 Experimental procedure and results

3.3.1 PV generation

To validate the SDM model for the PV module generation, the output of the PV modules was measured at short-circuit, open-circuit and various other operating points along the “knee” of the I-V curve. The different operating points were created by connecting the PV modules to a load bank, which can change its connected resistance and therefore the load on the PV modules. Two multimeters were used to measure the current and voltage for the different operating points at different levels of irradiation. In Figure 12, the results of the experiment can be seen. The data captured during the experiment was taken with varying panel operating temperatures between 50°C and 60°C, while the SDM model was modelled at a constant 55°C. From Figure 12, the difference between simulated temperature and actual operating temperature is the reason for the slight difference in the operating voltage and current between the SDM simulated I-V curves and the experimental data at open-circuit and short-circuit conditions. Importantly, the shape of the I-V curve at the “knee” is similar for the SDM model

and the experiment data. The SDM model is also verified with the manufacturer provided data, which are discussed in Chapter 5.

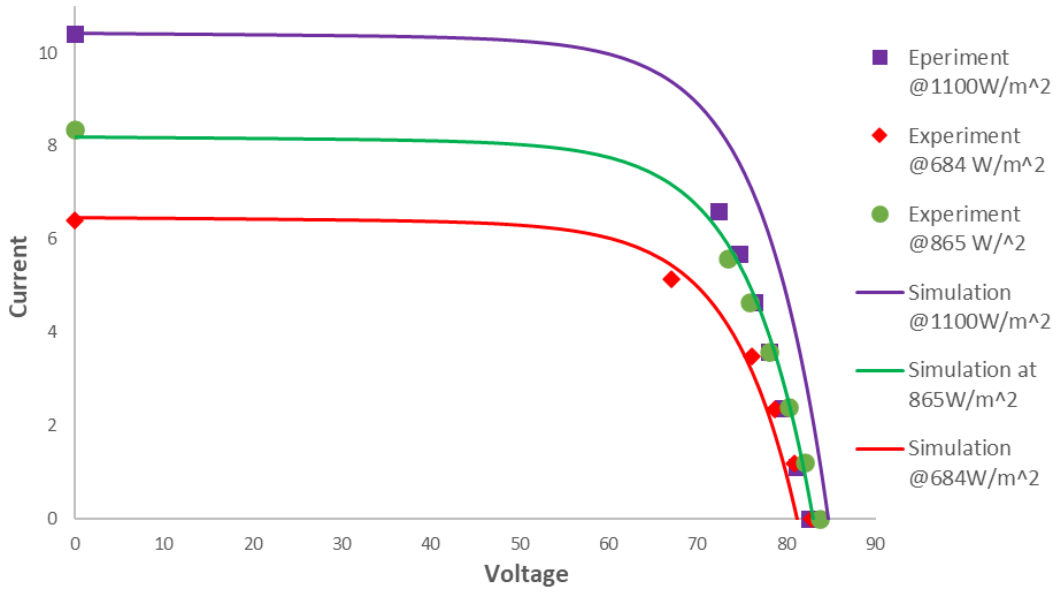

Figure 12: PV SDM validation results

3.3.2 Geyser controller losses

With the MPPT charger disconnected initially, the controller losses as well as the MPPT function of the GEYSER ROBOT were tested. This was accomplished by only connecting the geyser controller and geyser to the PV modules, ensuring that all generated energy was delivered through the controller. The input and output current and voltage of the controller was recorded and analysed to calculate the losses over the controller. The GEYSER ROBOT was only tested with its MPPT function turned on. Botes [12] conducted a similar study with the MPPT function switched off, resulting in the GEYSER ROBOT functioning as a normal controller similar to the ELON 100. The input and output current and voltage of the GEYSER ROBOT was recorded and compared for the MPPT setting and the normal operating setting. The ELON 100 and GEYSER ROBOT were both tested under identical conditions and a final selection was made on which geyser controller to use.

3.3.2.1 GEYSER ROBOT

Table 2 below shows an extract of the experimental results for the GEYSER ROBOT. Each data set in the table represents a voltage and current measurement taken at different solar radiation levels. The data sets recorded at Point 1 (Panels) were measured before the controller and the data sets recorded at Point 2 (Geyser) after the controller. From the recorded data, a clear pattern is evident with the voltage and current measurements over the controller. There was a large voltage drop over the controller, with only a marginal increase in

current. This resulted in an average power loss of 26% over the controller, with a maximum power loss of up to 52%. The large voltage drop was the result of the MPPT function on the GEYSER ROBOT.

Table 2: GEYSER ROBOT experimental results

	Panels				Geyser						
Irradiation (W/m^2)	V1 (V)	I1 (A)	R1 (Ω)	P1 (W)	V2 (V)	I2 (A)	R2 (Ω)	P2 (W)	Voltage drop	Current increase	Power loss
946	148	7.52	19.7	1116	108	7.91	13.6	853	27%	5%	24%
926	146	7.45	19.6	1088	106	7.8	13.6	827	27%	4%	24%
926	146	7.45	19.6	1085	106	7.85	13.5	832	27%	5%	23%
926	146	7.44	19.7	1088	107	7.82	13.6	834	27%	5%	23%
785	145	5.94	24.4	860	89.2	6.55	13.6	584	38%	9%	32%
684	141	4.93	28.6	695	73.8	5.37	13.7	396	48%	8%	43%
584	139	3.87	35.9	538	59.2	4.34	13.6	257	57%	11%	52%

Figure 13 visually represents the recorded data from the table above. The data for Points 1 and 2 at 946 W/m^2 irradiation were plotted as well as the simulated I-V, P-V and load curves of the modules for the same level of irradiation. The voltage and current produced by the panels at Point 1 fell on the I-V curve, but not on the intercept point of the load curve. The voltage and current recorded at Point 2, after the controller, fell on the load curve, but slightly below the expected intercept point on the I-V curve for 946 W/m^2. The same was observed for the power output recorded at Points 1 and 2.

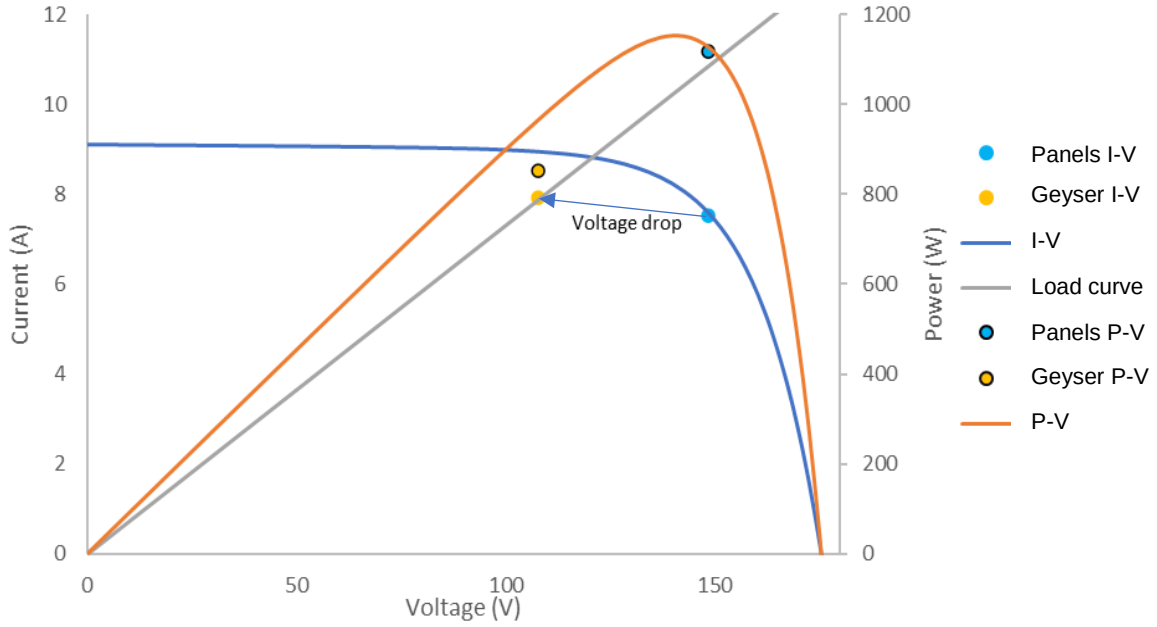

Figure 13: GEYSER ROBOT operating behaviour

3.3.2.2 ELON 100

Unlike at the GEYSER ROBOT, there was a negligible voltage drop over the ELON 100 controller. Table 3 shows the results of the ELON 100. The current and voltage measurements before and after the controller were within 1% of each other. This resulted in a power loss of between 0% and 1%.

Table 3: ELON 100 experimental results

	Panels				Geyser						
Irradiation (W/m^2)	V1 (V)	I1 (A)	R1 (Ω)	P1 (W)	V2 (V)	I2 (A)	R2 (Ω)	P2 (W)	Voltage drop	Current increase	Power loss
926	124	9	14	1109	123	9	14	1100	1%	0%	1%
946	121	9	14	1069	120	9	14	1060	1%	0%	1%
946	125	9	14	1128	123	9	14	1118	1%	0%	1%
946	119	9	14	1030	118	9	14	1023	1%	0%	1%
946	125	9	14	1132	124	9	14	1121	1%	0%	1%
926	124	9	14	1108	122	9	14	1099	1%	0%	1%
905	113	8	14	931	112	8	14	924	1%	0%	1%
825	100	7	14	731	99	7	14	727	1%	0%	1%
744	81	6	14	476	80	6	14	472	1%	0%	1%
664	68	5	14	331	67	5	14	328	1%	0%	1%
604	61	4	14	270	61	4	14	269	1%	0%	0%
523	45	3	14	148	45	3	14	146	1%	0%	1%
463	37	3	14	99	36	3	14	98	1%	0%	1%

Figure 14 visually represents the recorded data from the table above. The data for Points 1 and 2 at 905 W/m^2 irradiation were plotted, as well as the simulated I-V, P-V and load curves of the modules for the same level of irradiation. The voltage and current produced by the panels at Point 1 fell on the I-V curve at the intercept point of the load curve. The voltage and current recorded at Point 2 also fell on the I-V curve at the intercept point, unlike for the GEYSER ROBOT. The same operating behaviour was observed for the power output recorded at Points 1 and 2.

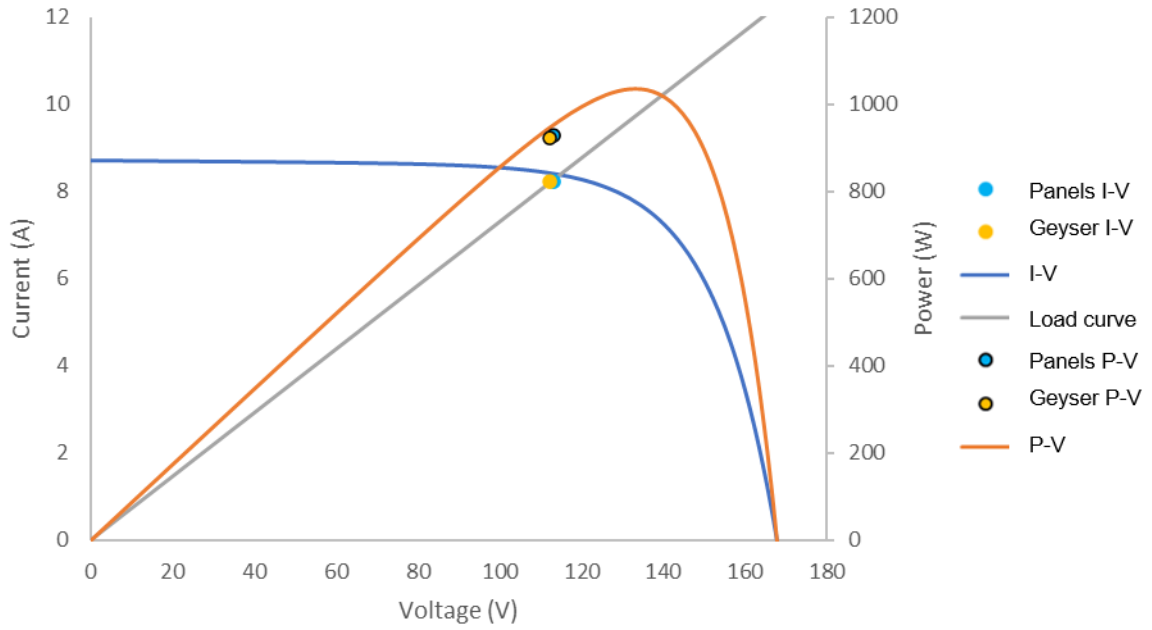

Figure 14: ELON 100 operating behaviour

3.3.2.3 ELON vs GEYSER ROBOT

Figure 15 below compares the input (P1) and output (P2) power for the two geyser controllers. The GEYSER ROBOT maximizes the power that is fed into the element, and for lower irradiation levels, the geyser robot supplies more power to the element than the ELON 100 controller. Therefore, in coastal cities where irradiation is lower, it might be advantageous to use a GEYSER ROBOT with MPPT functionality. The GEYSER ROBOT will also function better with all element types.

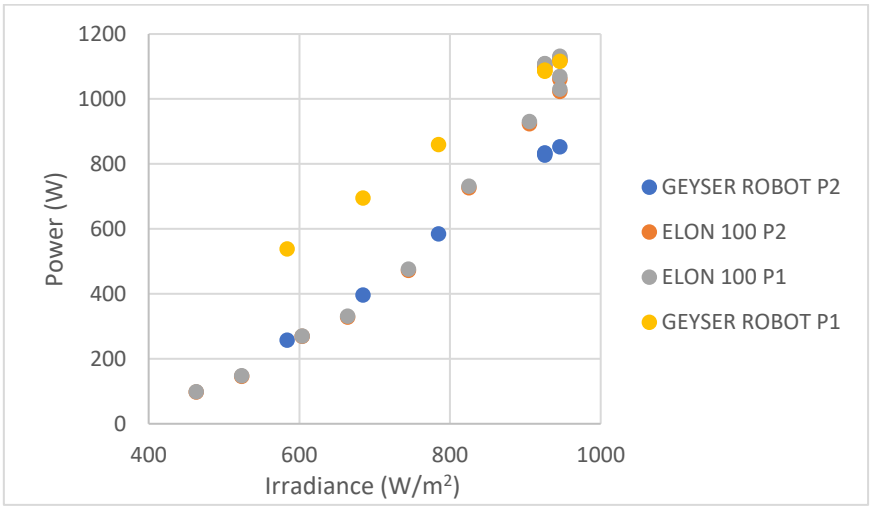

Figure 15: ELON 100 vs GEYSER ROBOT Power output

The minimal power loss over the ELON 100 controller and the higher power output makes it a superior controller to the GEYSER ROBOT in high irradiation areas. The consistent behaviour of the ELON 100, where it operates on the intercept point between the I-V curve and the load curve makes it easier to model accurately, whereas the unpredictable operating behaviour of the GEYSER ROBOT due to its MPPT function makes it very difficult to model. Therefore, the ELON 100 was used as the geyser controller in combination with the MPPT charger during the next stage of the experimental testing.

3.3.3 Parallel connection with the ELON 100 and MPPT charge controller

To test the viability of two controllers working simultaneously, four multimeters were used to measure the voltage and current before and after each controller in the parallel connection. The voltage and current measurements of the two controllers were compared with each other and the power loss over each controller was also calculated. Finally, the input power for the geyser controller in the parallel connection was compared with the input power for the geyser controller without the parallel connection to the MPPT charge controller and the battery.

3.3.3.1 ELON 100 and MPPT charger in parallel

Table 4 below shows the results of the parallel connection in the combined system. The voltage, current and power recorded at each point (1-4) in the combined system is colour coded in the table. With the parallel connection, there was a reduction in the current before the ELON 100 controller. At higher irradiance levels, with a higher operating voltage, the reduction in current was smaller compared with the reduction at lower voltages. Since the total power was split between the MPPT charger and the ELON 100 controller, the initial total power (P1) is the sum of the power to the ELON 100 (P2) and the power to the MPPT charger (P3). The data recorded at Point 3 represents the power consumed by the MPPT controller (P3) while the data recorded at Point 4 represents the power to the battery (P4).

Table 4: Results of the ELON 100 and MPPT controllers in the combined system

	Panels				Geyser				MPPT				Battery			
Irradiation (W/m^2)	V1 (V)	I1 (A)	R1 (Ω)	P1 (W)	V2 (V)	I2 (A)	R2 (Ω)	P2 (W)	V3 (V)	I3 (A)	R3 (Ω)	P3 (W)	V4 (V)	I4 (A)	R4 (Ω)	P4 (W)
845	98	8.3	11.8	813	98	7.1	13.8	698	95	1.2	76.4	118	13.9	8.0	2	111
825	95	8.2	11.7	779	95	6.9	13.7	659	98	1.2	81.7	118	13.9	8.0	2	111
724	80	7.3	11.0	579	79	5.8	13.6	459	79	1.5	54.2	115	13.8	8.0	2	110
624	60	6.3	9.5	377	59	4.3	13.6	256	59	2.0	29.9	116	14.1	8.0	2	113
483	32	4.8	6.6	151	32	2.3	13.7	72	32	2.4	13.1	76	13.7	5.3	3	72

The first observation made was that the power produced by the PV modules at Point 1 was higher than what the modules produced with only the ELON 100 connection for the same level of radiation. With only the ELON 100 controller, the resistance of the system is higher and

therefore the intercept power is lower. With the ELON 100 and MPPT the resistance in parallel is lower and therefore the intercept power is higher. This indicates that the PV modules delivered more power to the systems, than when only the ELON 100 controller is used.

The second observation was that the MPPT charger performed as expected, with an average power loss of 7% over the controller. The MPPT charger has a multitude of charging settings. For this experiment, the charger was set to charge the battery in bulk mode, ensuring the fastest possible charge with the available generated power. Furthermore, the charge current can be set to anything between 0 A and 35 A, which is the maximum rated current of the charger. For this experiment, due to the maximum rated current of the multimeter (10 A), the maximum charging current was set to 8 A. Note that the voltage and current measured at Point 4 (red) are a result of the charging setting chosen for the MPPT controller and not dependent on the I-V curve of the PV modules.

3.3.3.2 MPPT charging behaviour

The MPPT regulated the charging voltage, which oscillated between 13 V and 14.1 V. The power required by the MPPT charger depended on the charging setting. If the MPPT was set to charge at 8 A, the MPPT required more power (8 A x 14 V = 112 W) compared to a charge setting of 4 A (4 A x 14 V = 56 W). Figure 16 below describes the charging behaviour observed during the experimental testing. When the total power required (P 3 = A3 x V3) by the MPPT was less than 40% of the total power produced (P 1 = A1 x V1) by the PV modules, the MPPT charged the battery at the set output current and only consumed the required power (P3) to charge the battery. The remaining power (P2 = A2 x V2) was then available to the ELON 100 controller to heat the water. When the required power by the MPPT exceeded 40% of the available total power from the PV modules (P3 > 0.4P1), the power was split evenly between the two controllers, 50% to the ELON 100 for water heating and 50% to the MPPT for charging. The MPPT then charged the battery at the maximum possible current with the available power.

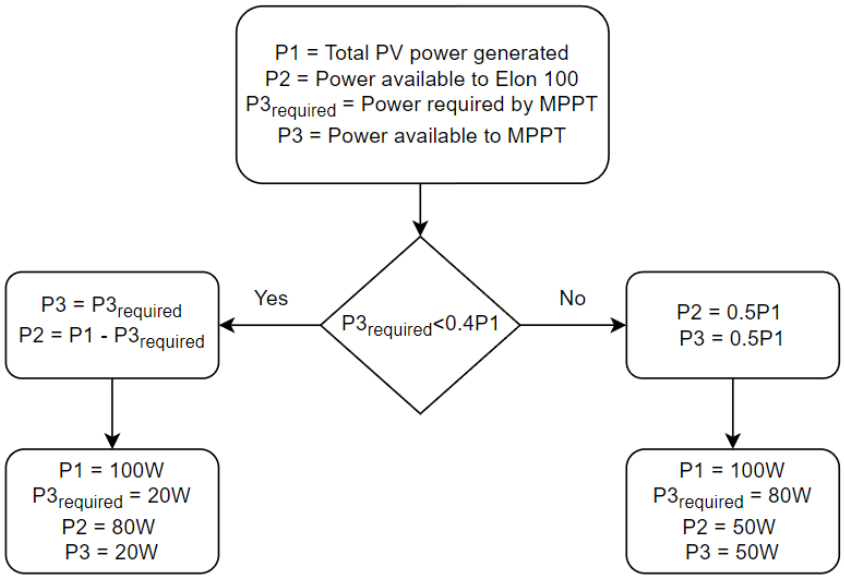

Figure 16: Charging behaviour of MPPT charge controller

Chapter 3 discussed the goal, setup, procedure, and results of the experiment conducted for this study. The experiment served to verify the various assumptions made in the simulation model, confirm the operational output of the PV modules and the geyser controller, and lastly, obtain results from the MPPT charge controller to determine its charging behaviour. The results and insights gained in Chapter 3 were used to develop the simulation model, as described in Chapter 4.

4 Model development

The aim of this chapter is to develop a simulation model in Microsoft Excel that can simulate the parallel connection shown in Figure 11. Section 4.1 discusses the different scenarios which were to be simulated. Section 4.2 discusses the inputs for the model and Section 4.3 the modelling methodology of the simulation model. Sections 4.4 and 4.5 describe the equations used for the PV power generation, water heating and provisioning of emergency power, with the parallel connection of the two controllers. Lastly, Section 4.6 concludes with the economic indicators used for the analysis of the PV system under simulation.

4.1 Scenarios for simulation

As the size of a PV system increases, the capital cost of the system increases, but so does the level of comfort from not being affected by loadshedding. Three scenarios, each with a different electric load to be powered during loadshedding, were investigated. The scenarios ranged from a small load, to a large electrical load to be powered during loadshedding, with water heating included for every scenario.

4.1.1 Appliance usage in an average South African household

4.1.1.1 Large appliance usage in a household

To accurately estimate the power demand for each scenario, the average electrical load of a South African household was needed. A study completed by Hughes and Larmour [71] investigated the appliance ownership, monthly income, and electricity spending of low, middle and high-income households across South Africa. The ownership of different appliances can be seen in Table 5:

Table 5: Selected large appliance ownership levels for different income categories [71]

Appliance	Fridge	TV	Washing machine	Geyser	Deep freeze	Tumble dryer	Dish-washer	Aircon	Pool pump
All	98%	92%	76%	66%	35%	19%	14%	14%	8%
Low	94%	84%	52%	33%	21%	11%	5%	6%	4%
Middle	99%	93%	76%	65%	35%	18%	10%	11%	5%
High	100%	95%	91%	87%	45%	27%	26%	23%	17%

Accordingly, the data could be used to simulate the power demand of the household. In high income households, 100% have a fridge, Hughes and Lamour were not clear on whether it was just a fridge or a double door fridge with a freezer, 95% have at least one TV, 91% have a washing machine, and 87% have a geyser. Therefore, an assumption could be made that the average high-income household has at least these four appliances. By adding the

electrical load of all four appliances, the power demand of these appliances could be calculated. The size of the inverter required to supply power to these appliances also changes as the power demand increases and therefore affects the capital costs of the system.

4.1.1.2 Small appliance usage in a household

Smaller appliances commonly found in households include computers (laptop and desktop), tablets, Wi-Fi routers, cell phones, gaming consoles, DSTV decoders (including PVR), DVD players, home theatre systems, and audio systems [71]. As with the larger appliances, the number of smaller appliances increase per household as the gross monthly income of the household increases [71].

4.1.1.3 Lighting

An average household has around two lights per room. The number of lights used in a household is dependent on the household's income level. Although some people were not able to tell the difference between a LED and CFL bulb, data collected by Hughes and Larmour [71] indicated that more households use CFL bulbs, compared to LEDs [71]. Lastly, most households indicated that they have between 1 and 3 lights on for more than four hours a day.

4.1.2 Power demand for each scenario

For each scenario, the appliances, that needed to be powered during loadshedding were chosen as:

Table 6: Appliances ownership for each scenario

	Scenario A	**Scenario B**	**Scenario C**
Wi-Fi	1	1	1
Lights	2	2	2
Fridge	0	1	1
Microwave	0	0	1

The rated wattage of each appliance is listed as: [72] [73]

Table 7: Rated wattage of different appliances

Appliance	**Rated (Running) Watts**
Light Bulb (CFL)	20 W
Fridge	700 W
WIFI	5 W
Microwave	1500 W

With the known list off appliances in each scenario and their rated wattage, the power demand for each scenario could be calculated as:

	System A	System B	System C
Maximum Load	45 W	745 W	2245 W

4.2 Input for simulation model

4.2.1 Input for all scenarios

The input data for the simulation model are discussed in this section. To avoid repetition, the input parameters for all modelling sections are also discussed and listed in this section.

4.2.1.1 Battery capacity per scenario

As mentioned in Chapter 1, the battery capacity for each system will scale according to the load requirement of the scenario. The power demand increased from Scenario A to Scenario C, and the number of appliances with low running wattages formed a decreasing percentage of the total power demand. The main difference between the scenarios was whether there was a fridge or microwave that needed to be powered during loadshedding. Appliances with high loads are often used for short periods of time (less than an hour), while appliances with low loads are used for extended periods of time. In Scenario A, the lights and Wi-Fi run constantly for 4 hours during loadshedding, which results in the load of the appliance being equal to the consumption of that appliance per hour. The battery in System A is only expected to power the lights and the Wi-Fi for a period of up to 4 hours. Therefore, a 12V, 20Ah battery with a capacity of 240 Wh should be sufficient. For Scenario B, although a fridge has a relatively high load, the constant on and off cycling results in a lower consumption per hour than the load requirement of the appliance. Therefore, a battery capacity of 1000 Wh should be sufficient. The same concept applies for Scenario C. Although the load requirement for a microwave is extremely high, the consumption of the appliance is relatively low. Therefore, a battery capacity of 1500 Wh should be sufficient for System C.

Table 8: 12 V battery capacity for each scenario

	Scenario A	Scenario B	Scenario C
Battery capacity	240 Wh	1000 Wh	1500 Wh

4.2.1.2 Load profile input

Figure 17 illustrates the load profile for Scenario C. While appliances like a microwave are only used in the morning and evening for a few minutes, they have a high load, which is seen in the spikes in the load profile. A fridge constantly cycles on and off during the day, but only consumes a fraction of the load of a microwave. The lights are all used during the evening, which adds to the total power demand in the evening. It is assumed that the majority of the power demand takes place in the evening. This matches with the load profile used in another

study by Toussaint and Moodley [74]. Similar load profiles were used for Scenario A and B as input for the simulation model.

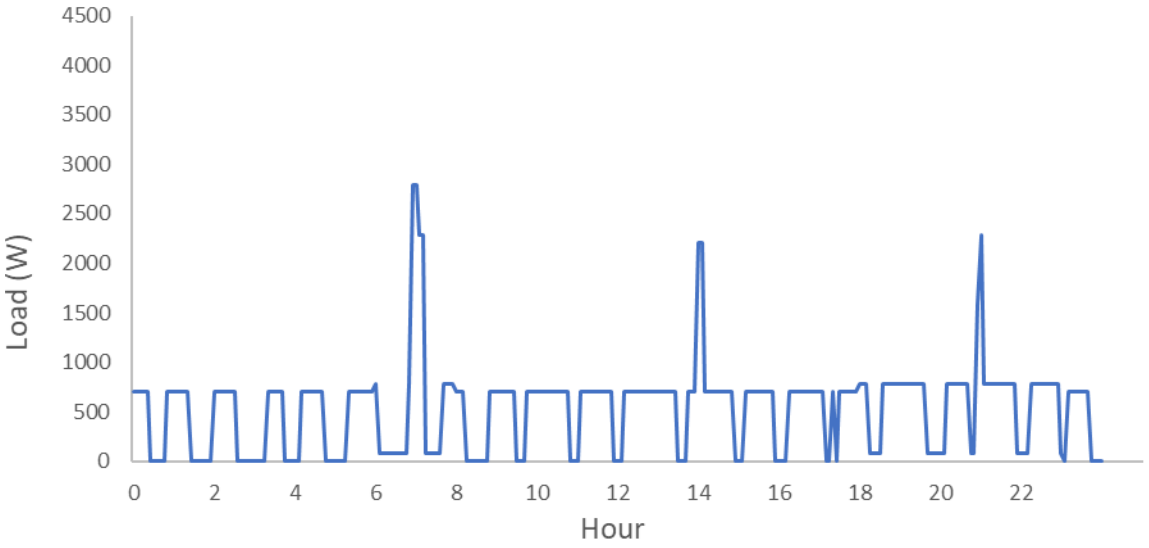

Figure 17: Load profile for Scenario C appliances

4.2.1.3 Weather data

Table 9 below shows an extract of the weather data [48] used in the study; the table contains the hourly irradiation measurements for Potchefstroom. Month 1 represents the first month of the year, January. Similarly, Day 1 represents the first day of the corresponding month. The global total radiation on a horizontal surface was used as the climatic input for the model. The model then converts the horizontal radiation to tilted ration to predict the PV modules' power generation.

Table 9: Extract of climatic year data

Month	Day	Hour	Total horizontal radiation (W/m^2)
1	1	7	533
1	1	8	762
1	1	9	924

4.2.1.4 Water heating and consumption

Figure 18 shows the water consumption profile, obtained from literature [52], which was used for the simulation. The profile is for a household of four people with each person consuming 45 and 65 L/day during the summer and winter months, respectively. The same profile will be used for every day of the year to match the climatic design year.

The geyser has both a higher electric load and total load consumption compared with the household appliances. This is due to the 4 kW resistive element and the time it takes to heat the constant inflow of cold water during the day. Figure 18 also shows the load requirement of the geyser to heat the constant inflow of cold water. Note that the geyser has a timer which switches the geyser on and uses grid electricity if the water temperature in the geyser is not at the desired temperature. This timer was set to switch on between 4:00 and 6:00 in the morning and between 18:00 and 20:00 in the evening, before heavy water consumption takes place. The geyser was also set to heat the water to 65°C using PV power during the day, while it was set to heat the water to 55°C with grid power. This is a conscious design choice to heat the water as much as possible in the day to lower the need for grid power between 18:00 and 20:00 in the evening.

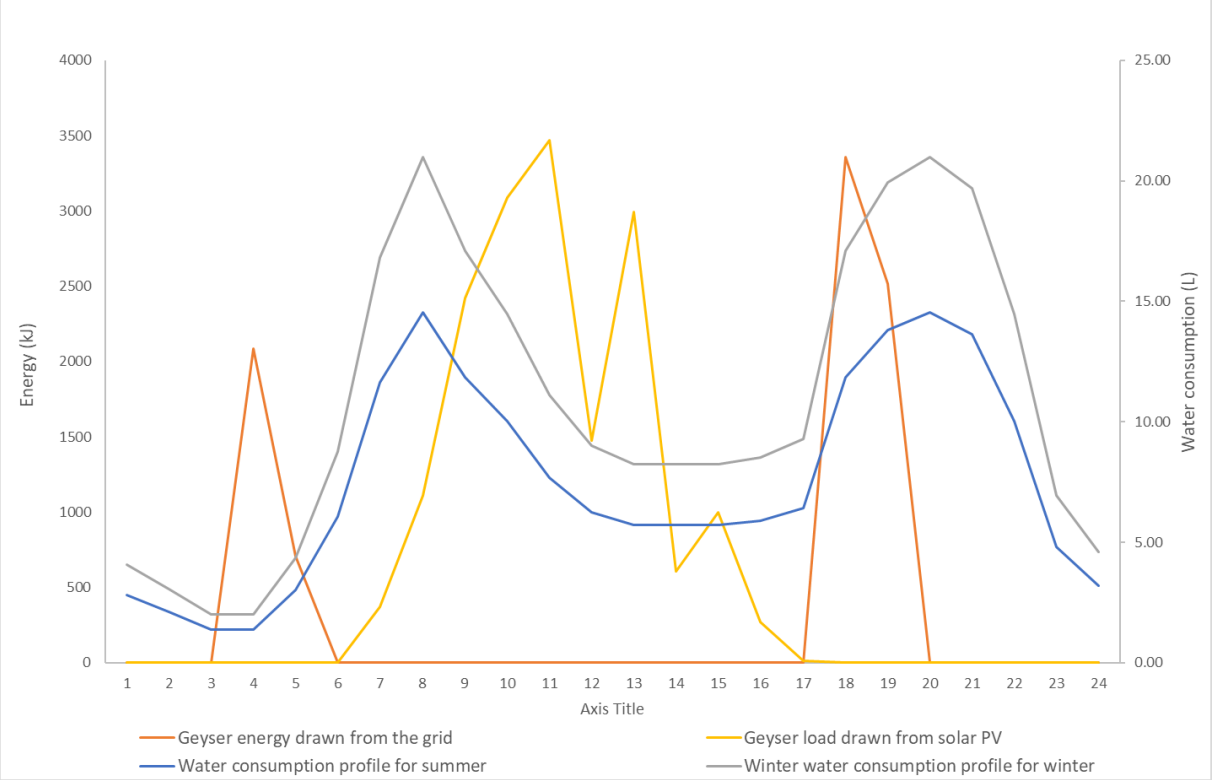

Figure 18: Geyser load requirement with the water consumption profile

4.2.2 PV module simulation input

In Table 10 the parameters V_{oc_STC}, I_{sc_STC}, V_{mp}, I_{mp}, K_V, K_I, N_s and P_m are all obtained from the manufacturer data sheet of the PV module [75]. Through experimental testing it was found that the temperature of the solar cell rises significantly when exposed to direct sunlight. As the change in operating temperature was neglected in this study to accommodate for the loss in performance of the PV module, compared to STC conditions, the cell temperature at operating conditions was chosen as a constant 328.15 K (55°C). Lastly, the slope of the I-V curve at

open-circuit and short-circuit conditions was entered after obtaining them from WebPlotDigitizer.

Table 10: Input for PV module simulation

Parameter Name	Symbol	Value	Unit
STC open circuit voltage	V_{oc_STC}	45.5	V
Short circuit current	I_{sc_STC}	9.34	A
Maximum power voltage	V_{mp}	37.00	V
Maximum power current	I_{mp}	8.78	A
Thermal coefficient of V_{OC}	K_V	-0.3%	V/K
Thermal coefficient of I_{SC}	K_I	0.05%	A/K
Number of cells connected in series	N_s	72.00	-
Cell temperature	T	328.15	K
Rated power	P_m	335.00	W
Slope at short circuit	dI/dV_{sc}	-0.003	-
Slope at open circuit	dI/dV_{oc}	-2.50	-

4.2.3 Water heating simulation input

Table 11 above shows the morning and evening hours when the geyser uses grid electricity to heat the water if it is not at the predetermined temperature. A normal household consumes more hot water during the winter compared to the summer months. The hot water consumption is therefore given as two separate values, mS_{water}, for the summer and mW_{water}, for the winter. The inlet water temperature (T_{inlet}) of the geyser was chosen as 15°C and it was assumed that the geyser (Tt_0) was already heated to 55°C. The temperature setpoint for PV-generated energy was set as 65°C to maximise the use of solar energy and store as much energy in the water tank as possible. The temperature setpoint for grid energy water heating was set at 55°C. The volume (Vt) of the geyser was 200 L and it was assumed that the temperature distribution through the water in the geyser was uniform [12]. The geyser had a B-rated efficiency, indicating a standing loss of 1.37 kWh/day. The element is also rated at 4 kW total heating capacity with 13.7 Ω resistance. Finally, the latitude of Potchefstroom is -26.2 degrees, but a tilt angle of 30 degrees was used for simplicity.

Table 11: Input for water heating model for a household of four people

Parameter Name	Symbol	Value	Unit
Grid supply to geyser on	$Grid_{morning1}$	4:00	time
Grid supply to geyser on	$Grid_{morning2}$	5:00	time
Grid supply to geyser on	$Grid_{evening1}$	18:00	time
Grid supply to geyser on	$Grid_{evening2}$	19:00	time
Hot water consumption in the summer	mS_{water}	180	L/day
Hot water consumption in the winter	mW_{water}	260	L/day
Water temperature in	T_{inlet}	15	°C
Initial geyser temperature	Tt_0	55	°C
Temperature setpoint when using PV-generated energy	$Tmax_{PV}$	65	°C
Temperature setpoint when using grid energy	$Tmax_{GRID}$	55	°C
v	Vt	200	L
Standing loss of water in the geyser	Q_{LOSS}	1.37	kWh/day
Heating capacity of the geyser	E_{AUX}	4	kW
Resistance of water heating element	R_{geyser}	13.7	Ω
Latitude of Potchefstroom	ϕ	-26.7	°
Tilt angle	β	30	°

4.3 Modelling methodology

Figure 19 gives an overview of the main modelling methodology, showing the order in which the model was developed. The model was divided into three main sections. Section 1 revolved around the modelling of the PV modules and their power generation. Section 2 used the results of Section 1, i.e. the power generated by the modules, to model the water heating and powering of household appliances. Section 3 used the results of Section 1 and 2 to perform an economic analysis of the PV system.

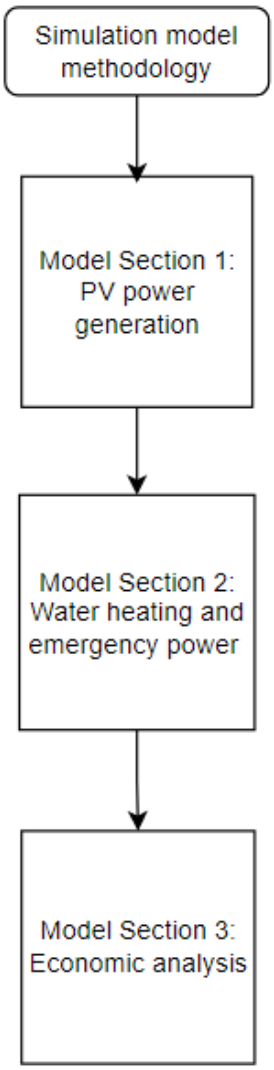

Figure 19: Model development process

4.4 Model section 1: PV power generation

This section explains the modelling methodology behind the PV power generation. This includes the equivalent electrical circuit of the PV cell, which was used in the single diode model (SDM) simulation. The extraction of the five parameters that were used to model the I-V curve of the PV cell, is also discussed. Lastly, the operating point of the PV modules and the power generation was calculated. Figure 20 shows the detailed modelling methodology followed for Section 1 of the simulation model.

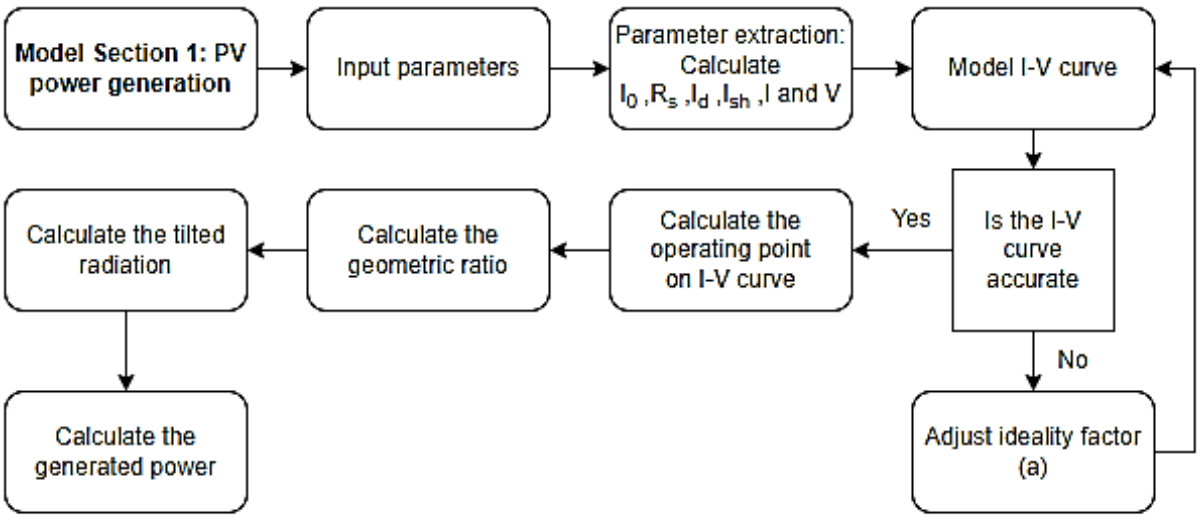

Figure 20: Detailed methodology of Model Section 1

4.4.1 Analysis of the single-diode equivalent circuit

A lumped circuit parameter model of the PV generator was required for the simulation. A PV generator delivers the rated power at the required voltage and current levels [76]. A PV cell, module, or array of modules arranged in series or parallel are all seen as a PV generator. Figure 21 shows the SDM used for the simulation of a typical PV generator [76]. With a simulation program, it was possible to extract the five parameters required for this modelling method. The parameters were then used to calculate the MPP and intercept point on the I-V curve. This could be repeated for every possible change in temperature and irradiance.

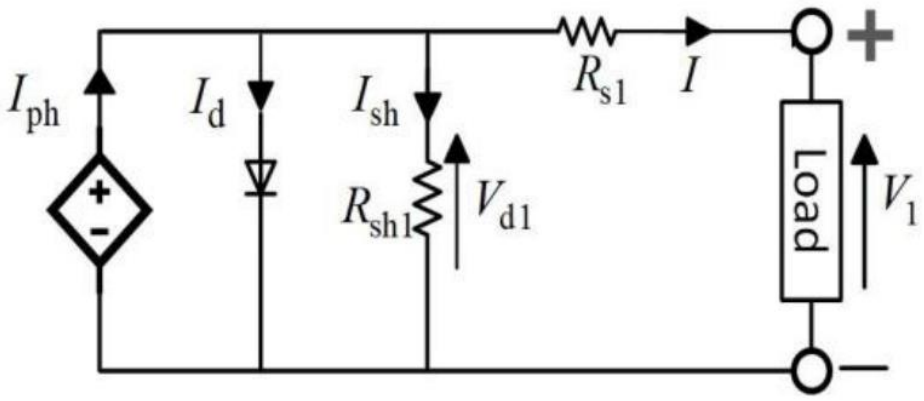

Figure 21: Single-diode equivalent circuit model of a PV cell [76]

The circuit in Figure 21 consists of a current source I_{ph}, a diode with its diode current I_d, the series resistance R_{s1}, the shunt resistance R_{sh1} and the shunt resistance current I_{sh}. The terminal current of a single diode PV cell is given by

$$I = I_{ph} - I_d - I_{sh} \quad (1)$$

The diode current is given as

$$I_d = I_0[\exp\left(\frac{V_{d1}}{aV_t}\right) - 1] \quad (2)$$

where I_0 is the reverse saturation current, V_{d1} the diode voltage, a the ideality factor of the diode and V_t the thermal voltage. The thermal voltage is given by the operating temperature of the cell T, the electronic charge $q = 1.602\,E - 19$ (C) and the Boltzmann constant $k = 1.38E - 23$ (J.k^{-1}) as:

$$V_t = \frac{kT}{q} \quad (3)$$

The shunt resistance current is given as

$$I_{sh} = \frac{V_{d1}}{R_{sh1}} \quad (4)$$

Note that the Subscript 1 is an indication of a single cell. The diode voltage is expressed as

$$V_{d1} = V_1 + IR_{s1} \quad (5)$$

After substitution, Equation 1 can be fully expressed as

$$I = I_{ph} - I_0\left[\exp\left(\frac{V_1 + IR_{s1}}{aV_t}\right) - 1\right] - \frac{V_1 + IR_{s1}}{R_{sh1}} \quad (6)$$

The method of modelling allows the single-diode model to be easily adjusted according to the number of identical cells connected in series within the PV module (N_s) [12]. The terminal current, photocurrent and diode current do not change, regardless of a single cell or multiple cells connected in series within the module. The diode voltage of the cell changes according to the number of cells connected in series, and is given by

$$V_{d1} = \frac{V}{N_s} + IR_{s1} \quad (7)$$

which simplifies to

$$V_{d1} = \frac{V + IN_sR_{s1}}{N_s} \quad (8)$$

Accordingly, the module current, which is equal to the single-cell current, now becomes

$$I = I_{ph} - I_0 \left[\exp\left(\frac{V + IN_sR_{s1}}{aN_sV_t}\right) - 1\right] - \frac{V + IN_sR_{s1}}{N_sR_{sh1}} \quad (9)$$

The series resistance can be expressed as

$$R_s = N_sR_{s1} \quad (10)$$

Similarly, the shunt resistance is

$$R_{sh} = N_sR_{sh1} \quad (11)$$

Therefore, Equation 1 can now be written as

$$I = I_{ph} - I_0 \left[\exp\left(\frac{V + IR_s}{aN_sV_t}\right) - 1\right] - \frac{V + IR_s}{R_{sh}} \quad (12)$$

4.4.2 Parameter extraction

Five parameters, R_s, R_{sh}, a, I_0, and I_{ph}, must be known to model a PV module. The simulation model used the data provided by the manufacturer to extract these parameters with the single-diode model method. Manufacturers typically provide datasheets with the I-V data at three key points: the maximum power point, the open-circuit point, and the short-circuit point [76]. Usually, the temperature coefficients and module efficiency are also included within the data sheets. When shorting the external terminal of the equivalent electrical circuit, maximum current is reached, and this is the short-circuit current I_{sc}. With the terminal fully opened, the maximum voltage is delivered, resulting in the open-circuit voltage. As the open-circuit voltage increases, the terminal current decreases [12]. The maximum power point is reached when the product of the open-circuit voltage and the terminal current is at its highest point.

The data provided by manufacturers is recorded at STC. At STC, $T = 298.15\ K,\ G = 1000\frac{W}{m^2}$ and $Air\ Mass = 1.5$. The data extracted at STC can only be used for STC conditions, therefore, for any other operating conditions, the parameters need to be adjusted [76].

For any change in temperature, the voltage at open circuit can be calculated with

$$V_{oc} = V_{ocSTC} + (\alpha_{V,STC} \times V_{ocSTC} \times (T - T_{STC}) \quad (13)$$

where V_{ocSTC} and $\alpha_{V,STC}$, the temperature coefficient, are given by the manufacturer and $T_{STC} = 298.15\ K$. T is the operating temperature of the cell where V_{oc} is being calculated.

4.4.2.1 Photocurrent extraction:

During short-circuit conditions, $V = 0$ and $I = I_{sc}$ and Equation 12 becomes

$$I_{sc} = I_{ph} - I_0 \left[\exp\left(\frac{I_{sc}R_s}{aN_sV_t}\right) - 1\right] - \frac{I_{sc}R_s}{R_{sh}} \quad (14)$$

The diode and shunt resistance currents are very small compared to the short-circuit current, and are therefore neglected [10, 76]. Equation 12 then reduces to $I_{ph} = I_{sc}$. However, I_{sc} is dependent on the cell area, material, temperature and the irradiance level. According to Humada *et al*. [62] I_{sc} is linearly proportional to irradiance and at any given irradiance the photocurrent, I_{ph}, can be expressed as

$$I_{ph} = [I_{sc,STC} + \alpha_{I,STC}\,(T - T_{STC})]\frac{G}{G_{STC}} \quad (15)$$

where $I_{sc,STC}$ is the short-circuit current at STC, $\alpha_{I,STC}$ the temperature coefficient of the short-circuit current at STC, T the cell operating temperature, T_{STC} = 298.15 K, G the measured irradiance, and $G_{STC} = 1000\ W/m^2$.

4.4.2.2 Shunt resistance extraction:

At short-circuit conditions, where the current is higher, the shunt resistance has the greatest effect. The derivative of the I-V curve at the short-circuit point is therefore used to estimate the shunt resistance. Since $R_s \ll R_{sh}$ Equation 12 can be approximated as [76]

$$R_{sh} = -\frac{dV}{dI}\bigg|_{sc} \quad (16)$$

4.4.2.3 Series resistance extraction:

At open-circuit conditions, where the voltage is higher, the effect of the series resistance is more dominant. The derivative of the I-V curve at the open-circuit point is therefore used to estimate the series resistance [76]. The same derivation is used as with the shunt resistance extraction- the open-circuit point is now substituted into the general expression of the derivative and the equation becomes [76]

$$R_s = -\frac{dV}{dI}\bigg|_{oc} - \frac{aN_sV_t}{I_{sc}} \quad (17)$$

The slope can be graphically estimated or calculated from the I-V curve.

4.4.2.4 Reverse saturation current extraction:

The reverse saturation current are determined at the open-circuit point, and easily obtained by writing Equation 12 as an expression of I_0 [76]. At open-circuit conditions $I = 0, I_{ph} = I_{sc}$ and $V_{oc} = V$:

$$I_0 = \left(I_{sc} - \frac{V_{oc}}{R_{sh}}\right) / (\exp\left(\frac{V_{oc}}{aN_sV_t}\right) - 1) \quad (18)$$

The open-circuit voltage V_{oc} and N_s is available on the manufacturer's data sheet. The ideality factor a still needs to be determined.

4.4.2.5 Ideality Factor Extraction:

The diode ideality factor can range from 1 to 2 [59], but it is generally accepted to be between 1 and 1.5 [12, 77]. The effect of the diode ideality factor is the most dominant at the MPP [62]. Substituting the data of the MPP point into Equation 12 supplies a final equation to solve for three unknowns (I_0, R_s, a) with three non-linear equations (Eq. 17,18,19):

$$I_{mp} = I_{sc} - I_0\left[\exp\left(\frac{V_{mp} + I_{mp}R_s}{aN_sV_t}\right) - 1\right] - \frac{V_{mp} + I_{mp}R_s}{R_{sh}} \quad (19)$$

with $V_{mp}\ and\ I_{mp}$ being the voltage and current at MPP. The three equations above can be solved simultaneously within MATLAB or Excel solver. However, this method is very sensitive to the initial guess values and requires a lot of computing power. To simplify the modelling process, a model that increments the voltage and ideality factor of the cell and calculates the parameters for each increment can be developed.

4.4.3 Parameter extraction procedure

The ideality factor was swept from 1 to 2 with increments of 0.05 within Microsoft Excel [76]. For each increment the reverse saturation current (I_0) and series resistance (R_s) was calculated using Equations 17 and 18. To find the I-V curve of the module, the diode voltage was swept from 0 to 0.7 V with 0.01 V increments and for each increment, I_d, I_{sh}, I and V were calculated with

$$I_d = I_0\left(exp\left(\frac{qV_{d1}}{akT}\right) - 1\right) \quad (20)$$

and

$$I_{sh} = \frac{V_{d1}}{\frac{R_{sh}}{N_s}} \quad (21)$$

It follows then that, with I_{sc} provided by the manufacturer, the module current can be calculated with

$$I = I_{sc} - I_d - I_{sh} \quad (22)$$

Finally, the module voltage is calculated with

$$V = N_s \left[V_{d1} - I \left(\frac{R_s}{N_s} \right) \right] \tag{23}$$

As a was adjusted, the calculations were performed iteratively to find the new values of I_0, R_s, I_d, I_{sh}, I, and V. With the module current (I) and voltage (V) obtained, the I-V curve could be plotted for every ideality factor between 1 and 2. The ideality factor has the greatest affect in the "knee" of the I-V curve. This is the area where the MPP occurs. The ideality factor could then be adjusted to visually match the I-V curve shape from the manufacturer data sheets. Figure 22 shows the process of matching the I-V curves for different ideality factors to the I-V curve from the manufacturer.

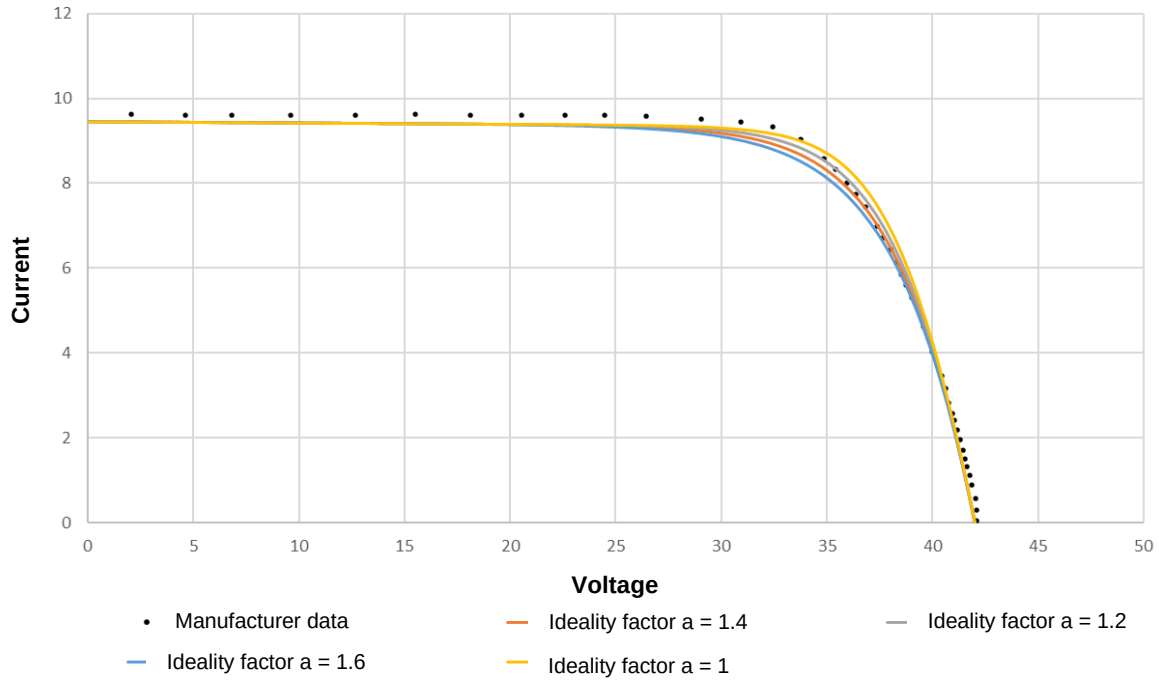

Figure 22: Ideality factor validation with I-V curves

4.4.4 Operating point on I-V curve

Without the use of an MPPT controller, the PV modules operate at the intersect point between the load curve and the I-V curve (refer to Figure 5). A 13.7 Ω resistive element was used in the model. To plot the load curve, Ohm's law $\left(I_R = \frac{V}{R}\right)$ was used to determine the load current at every voltage increment. The intersect point closest to the load curve, with the available voltage increments, was selected as the operating point. The absolute difference between the module current (I) and the load current (I_R) was determined, and the intersecting point closest to zero is the operating point. To find the voltage and current at the smallest intersecting point, the SMALL function was used. The MATCH function was then used to find the corresponding voltage and current cells, and their values displayed with the INDEX function. Similarly, the voltage and current at maximum power point were determined with the MAX function and the

corresponding voltage and current displayed with the MATCH and INDEX functions. The operating power was then calculated with $P = VI$.

To plot the I-V curve for the given irradiance, Equation 15 was used to recalculate the photocurrent for the requested irradiance. The module current and voltage is then calculated for the arbitrary irradiance. As the module current and voltage is updated, the maximum power point and intersecting point is recalculated. The data table function within Excel's What-If Analysis was used to calculate the I-V curve, MPP and Intersecting point for every arbitrary irradiance in the climatic design year [12]. Annexure A.2 gives a detailed explanation of the What-If Analysis.

4.4.5 Panel tilt

Solar modules have a surface from which they collect solar radiation. To optimise the orientation and tilt of the module, it is essential to estimate how differently orientated surfaces collect solar energy. Due to various factors such as the movement of the sun, different radiation components, and varying weather conditions, this is a complex calculation that aims to convert hourly solar radiation data on a horizontal surface to radiation on a sloped surface of the solar module [78].

The geometric relationship between the plane (solar module) and the incoming beam solar radiation at any instant in time is used to convert the radiation on a horizontal plane to a tilted plane. The constant angles that define the location and orientation of the tilted plane are:

- Slope: β, the tilt of the plane and the horizontal, $0° \leq \beta \leq 180°$
- Surface azimuth angle: γ, azimuth angle of the tilted plane, east negative, zero due south, and west positive, $-180° \leq \gamma \leq 180°$
- Latitude: ϕ, angular location, north positive, $-90° \leq \phi \leq 90°$

Next are the angles that vary according to the time of day. They define the position of the sun relative to the celestial sphere and Earth:

- Declination: δ, the angular position of the sun when it is on the local meridian, measured in degrees above or below the celestial equator, $-23.45° \leq \delta \leq 23.45°$
- Hour angle: ω, the angular displacement of the sun relative to the local meridian due to the rotation of the earth on its axis, $-180° \leq \omega \leq 180°$

The declination angle can be calculated as a function of the day of the year d:

$$\delta = 23.45 \sin\left(360 \frac{284+d}{365}\right) \tag{24}$$

The hour angle is calculated from the time of the day- the earth rotates 15° every hour around its polar axis, displacing the sun westward 15° every hour. The hour angle is zero at solar noon and can be calculated with

$$\omega = 15\left(\frac{t_s}{60} - 12\right) \tag{25}$$

where t_s is the solar time of the day in minutes [43, 78]. The local solar time in Potchefstroom differs by just a couple of minutes from the standard local time and therefore it is assumed as equal to the standard local time [12].

It is generally accepted that modules are placed in the optimal position for winter conditions, as to maximize the generating capabilities during the colder months when more electricity is used [7]. In South Africa, the optimal tilt angle and orientation of the modules are due north at the latitude plus 10 degrees [79].

Beam radiation is the radiation received from the sun without being scattered by the atmosphere. To calculate the angle of incidence, θ, of beam radiation on the surface of the tilted plane, one can use location- and time-varying angles in an equation that shows the relationship between the angle of incidences and these angles [43]

$$\begin{aligned} cos\theta = {} & sin\delta\ sin\phi\ cos\beta - sin\delta\ cos\phi\ sin\beta\ cos\gamma + cos\delta\ cos\phi\ cos\beta\ cos\omega \\ & + cos\delta\ sin\phi\ sin\beta\ cos\gamma\ cos\omega + cos\delta\ sin\beta\ sin\gamma\ sin\omega \end{aligned} \tag{26}$$

For horizontal planes, the tilt of the plane is β = 0. The zenith angle is the result of the simplification of the relationship above when β = 0:

$$cos\theta_z = cos\phi\ cos\delta\ cos\omega + sin\phi\ sin\delta \tag{27}$$

The angle of incidence may be greater than 90° when the sun is behind the surface, but Equation 27 can only be used when the hour angle is between sunrise and sunset, so that the earth is not blocking the sun, which can lead to incorrect radiation calculations [43].

For surfaces sloped due north or due south, useful relationships can be derived from the fact that surfaces with slope β to the north or south, and horizontal surfaces with an artificial latitude of ϕ - β, have the same angular relationship to beam radiation [43]. For the northern hemisphere, Equation 27 can be modified to

$$cos\theta = \cos(\phi - \beta)\ cos\delta\ cos\omega + \sin(\phi - \beta)\ sin\delta \tag{28}$$

By replacing $\phi - \beta$ with $\phi + \beta$ for the southern hemisphere, the equation becomes

$$cos\theta = \cos(\phi + \beta)\ cos\delta\ cos\omega + \sin(\phi + \beta)\ sin\delta \tag{29}$$

The geometric factor R_b, describing the ratio of beam radiation on the tilted surface to that on a horizontal surface is referenced from Duffie and Beckman [43]. The equation uses $cos\theta$ and $cos\theta_z$, which are both derived from Equation 27. In the southern hemisphere, the optimum azimuth angle for PV modules is usually γ = 180°. In this case, the equations above can be used to calculate $cos\theta$ and $cos\theta_z$, resulting in [43]

$$R_b = \frac{cos\theta}{cos\theta_z} \tag{30}$$

$$R_b = \frac{\cos(\phi+\beta)\, cos\delta\, cos\omega + \sin(\phi+\beta)\, sin\delta}{cos\phi\, cos\delta\, cos\omega + sin\phi\, sin\delta} \tag{31}$$

To eliminate any unrealistic radiation peaks, the ratio can only be used when the sun is above the horizon, i.e. the numerator and denominator of Equation 31 must be positive numbers [12].

4.5 Model section 2: Water heating and emergency power

This section explains the modelling methodology for Section 2 of the simulation model. Figure 23 gives a detailed overview of the modelling methodology followed for Section 2. Geyserwise [33] recommends 1005 W (3 x 335 W) of PV modules for a 200 L water heating PV system in high irradiation areas and 1340 W (4 x 335 W) of PV modules in low irradiation areas. The relationship between the power generated by the recommended modules and what is available for water heating and emergency power within each system was simulated. Modules can be added to increase the power available for household application should the base system fall short in generating capability.

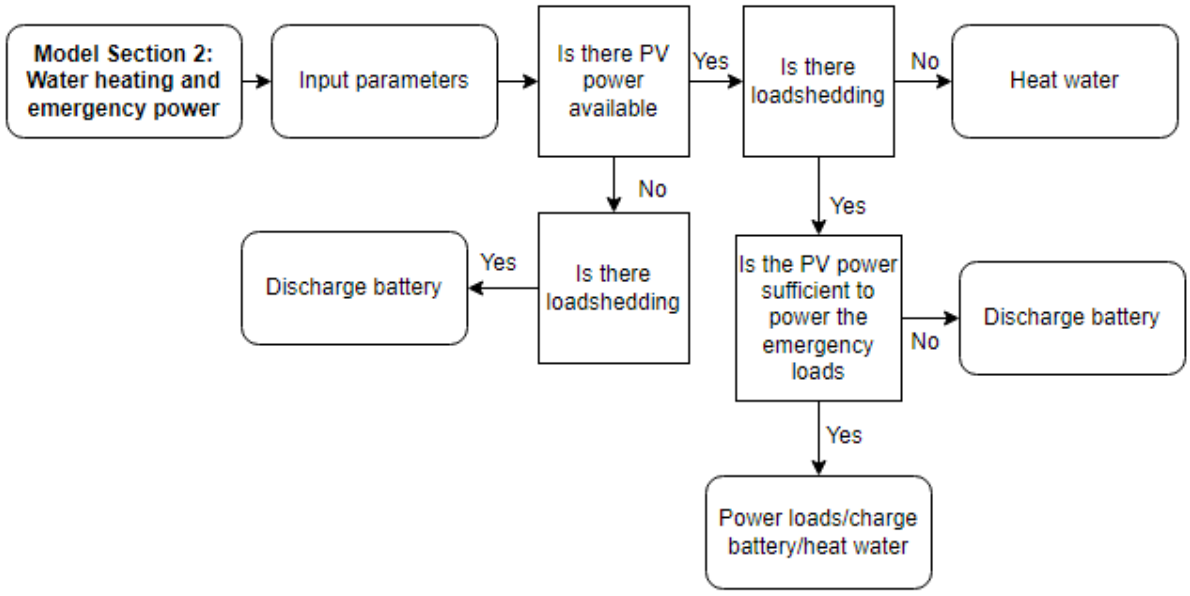

Figure 23: Detailed modelling methodology of Model section 2

4.5.1 Element losses and heating capacity of the geyser

The simulation was done in an hourly format. According to the manufacturer [80], the standing loss of the geyser is 1.37 kWh/day which is equivalent to 205.5 kJ/hour. A 4 kW element will heat the water at a rate of 14400 kJ/hour (4×3600).

4.5.2 Energy balance for water heating

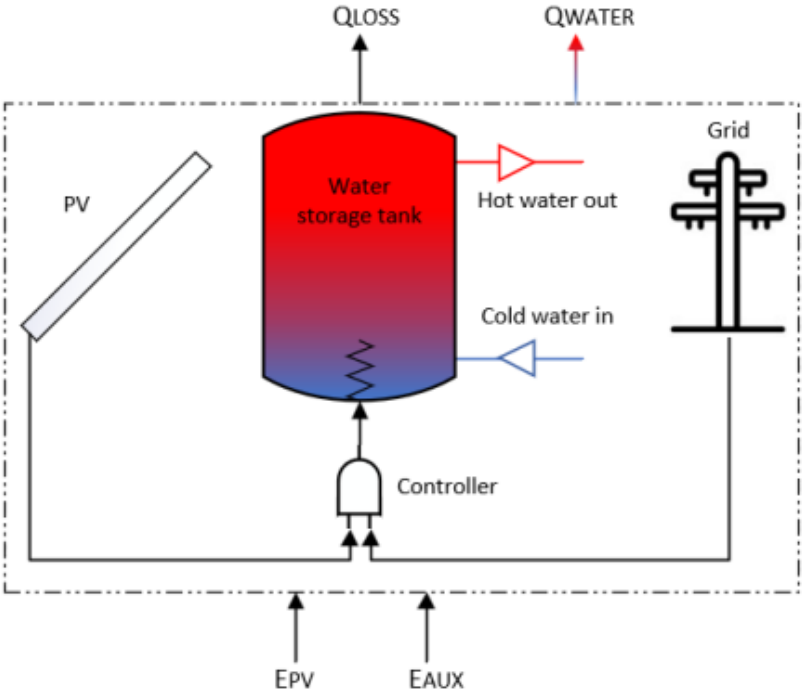

Figure 24: Water heating setup for simulation [12]

Figure 24 depicts the energy balance used to simulate the water heating within the geyser,

$$U_{i-1} + E_{PV} + E_{AUX} = U_i + Q_W + Q_{LOSS} \tag{32}$$

where U_{i-1} is the initial internal energy, in kJ, of the geyser at the end of the previous hour i-1 [12]. E_{PV} represents the electrical energy supplied by the PV modules. E_{AUX} is the electrical energy supplied by the grid when PV energy is insufficient to heat the water to the predetermined temperature set point [12]. The internal energy at the current hour is represented by U_i. Q_W is the change in thermal energy in the geyser due to the outflow of hot water and the inflow of cold water. Finally, the standing energy loss of the geyser is represented by Q_{LOSS}.

The internal energy of the geyser at the end of the previous hour is calculated with

$$U_{i-1} = Vt \times c_p \times Tt_{i-1} \tag{33}$$

where Vt is the mass volume of the water. Water has a density of 1kg/L, and therefore a 200L tank has a mass of 200kg. c_p is the specific heat of water and Tt_{i-1} the temperature of the water at the end of the previous hour i-1.

$$E_{PV} = P \times \frac{3600}{1000} \tag{34}$$

E_{PV} is calculated by converting the electrical power (P) calculated in Section 1 of the model from (W) to (kJ). E_{AUX} needs to be determined and is dependent on the energy needed (Q_W) to heat the water after the energy input of E_{PV} and energy loss due to the standing loss of the geyser (Q_{LOSS}) [12].

The internal energy of the geyser at the current hour is calculated with

$$U_i = Vt \times c_p \times Tt_i \tag{35}$$

while Q_W is calculated with

$$Q_W = Vt \times c_p(T_{out} - T_{inlet}) \tag{36}$$

Accordingly, Equation 32 can be re-written as

$$Vtc_pTt_{i-1} + E_{PV} + E_{AUX} = Vtc_pTt_i + Vtc_p(T_{out} - T_{inlet}) + Q_{LOSS} \tag{37}$$

T_{out} is equal to the water inside the geyser at the current hour (Tt_i). The equation can then be written as

$$Tt_{i-1} + \frac{E_{PV}}{Vtc_p} + \frac{E_{AUX}}{Vtc_p} = Tt_i + (Tt_i - T_{inlet}) + \frac{Q_{LOSS}}{Vtc_p} \tag{38}$$

This allows E_{PV}, E_{AUX} and Q_{LOSS} to be expressed in terms of their temperature difference and the substitution of $(Tt_i - T_{inlet})$ to $\Delta T_{\dot{m}}$ as the change in temperature due to consumption [12]

$$Tt_{i-1} + \Delta T_{PV} + \Delta T_{AUX} = Tt_i + \Delta T_{\dot{m}} + \Delta T_{LOSS} \tag{39}$$

The above equation can then be re-written as

$$Tt_i = Tt_{i-1} + \Delta T_{PV} + \Delta T_{AUX} - \Delta T_{\dot{m}} - \Delta T_{LOSS} \tag{40}$$

where the change in temperature due to PV energy can be calculated with

$$\Delta T_{PV} = \frac{E_{PV}}{Vtc_p} \tag{41}$$

and the change in temperature due to auxiliary grid energy can be calculated with

$$\Delta T_{AUX} = \frac{E_{AUX}}{Vtc_p} \tag{42}$$

The change in temperature due to consumption is a result of the inflow of cold water to replace the outflow of hot water. The term $Tt_{i-1}(Vt - V_i)$ is the volume of water remaining in the geyser at the temperature Tt_{i-1} after consumption [12]. The volume of water that refills the geyser is represented by $T_{inlet}V_i$ at the inlet temperature T_{inlet}. The new geyser temperature is then calculated by adding these two terms and dividing by the volume of the geyser Vt. The new geyser temperature is then subtracted from the previous geyser temperature Tt_{i-1} to find the change in geyser temperature [12].

$$\Delta T_{\dot{m}} = Tt_{i-1} - \frac{Tt_{i-1}(Vt - V_i) + T_{inlet}V_i}{Vt} \tag{43}$$

4.5.3 Charge and discharge of the battery

The model developed for the charging of the battery incorporates the charging behaviour observed during the experiment. The MPPT charger was connected in parallel with the ELON 100 and set to different charging currents to observe the change in charging behaviour according to the generated power that is available from the PV modules. Battery charging is always in bulk mode and not absorption, with a maximum charging voltage specific to the type of battery set to 14.6 V and a maximum charging current set to 20 A in the simulation model. The model was developed with a set of charging and discharging conditions which can be seen in Figures 25 and 26. Note that the battery is always in a state of absorption charging unless there is discharge required, after which it will be in bulk charging until it is recharged and reverts back to absorption charging.

The discharge conditions state that if there is loadshedding and there is no PV energy available to sustain the household emergency loads, the battery should discharge to power the household emergency loads. Should there be PV energy available, and there is enough PV energy to fully power the household emergency loads, the battery stays charged. However, if the PV energy is insufficient to power all the loads, the battery discharges to supply the shorfall in power required to power the household emergency loads.

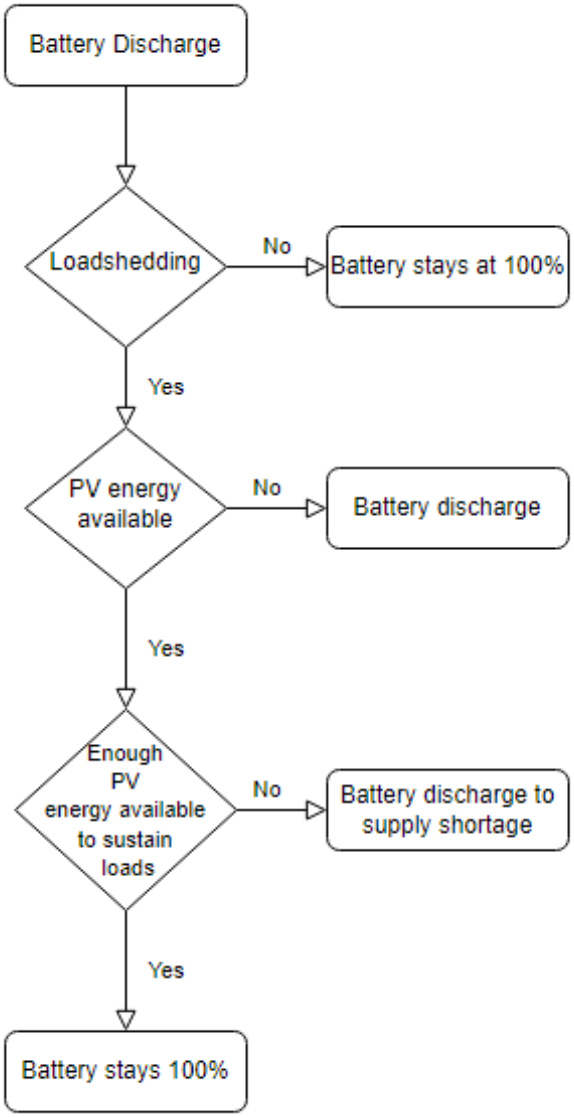

Figure 25: Discharge conditions for the battery

The charge conditions state that if there is PV energy available, the battery should charge with the available energy. Should the generated PV energy be enough to charge the battery at the maximum rate of charge (20A), it should. However, if the available energy is insufficient to charge the battery at the maximum rate of charge, the maximum possible charging current should be used that adheres to the 40% rule observed in the experiment. If there is no PV energy available while the battery is discharged, the battery should charge to 100% with grid power. The charging of the battery with grid power is only used should the battery be at less than 100% charge between 0:00 and 6:00 and there is no loadshedding during that time. This is an intentional design choice to ensure that there is battery backup power available if loadshedding occurs during the morning when the family wakes up.

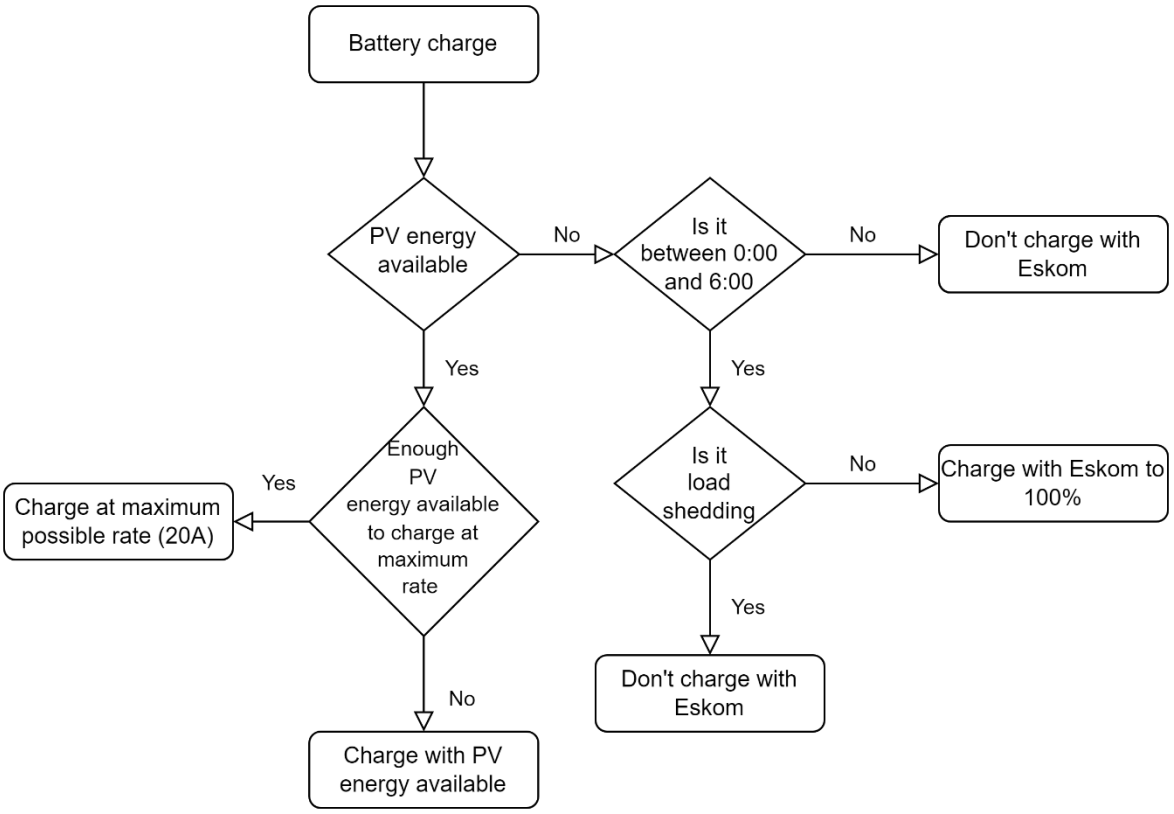

Figure 26: Charge conditions for the battery

4.6 Model section 3: Economic analysis

This section covers the economic indicators used within the simulation model and the input used for each indicator. As discussed in the literature study, three indicators are considered.

4.6.1 Levelised cost of energy

The LCOE of a system is defined as the annualised expenditures relative to the annual energy production, i.e. [81]

$$LCOE = \frac{Net\ Present\ Value\ of\ Lifetime\ Generation\ Costs}{Net\ Present\ Value\ of\ Lifetime\ Energy\ Production} \tag{44}$$

$$LCOE = \frac{[(CAPEX + BOS + OPEX)/(1+d)^n]}{NAEP/(1+d)^n} \tag{45}$$

where d is the discount rate of the system and n the lifetime of the system in years, with the other elements of the expression as follows:

- CAPEX Capital expenditure for the system
- BOS Balance of system costs
- OPEX Annual operating expenditure of the system
- NAEP Net annual energy production of the system

The Balance of System cost include the assembly, installation and the connection to electrical infrastructure. The discount rate of the system is typically between 6% and 8% for a 20-year lifetime [81, 82].

4.6.2 Net present value

The NPV of the system is calculated as

$$NPV = \sum_{n=0} \frac{C_t}{(1+d)^n} \tag{46}$$

where C_t is the net cash flow of the system.

4.6.3 Payback period

Lastly, the PBP indicates the time in years for the system to recover the initial cash investment and is calculated as

$$PBP = \frac{(C_{system} + \sum_1^n C_{maintenance})/(1+d)^n}{Annual\ savings/(1+d)^n} \tag{47}$$

where C_{system} is the initial cost of the system, and $C_{maintenance}$ is the yearly maintenance cost [83].

Chapter 4 covered the input and modelling methodology used for the development of the simulation program. The chapter started by listing the input parameters, data and profiles used for the development of the model. The three main sections of the model were each discussed in detail in the rest of the chapter. This included the equations used for each section, the assumptions made as a result of the experimental testing and the operating behaviour of the different components. The following chapter covers the verification and validation of the simulation model developed in Chapter 4.

4.7 Power saving model

This section explains the calculations used to determine the power saved for each system.

The PV power used per year was calculated by adding the total power used for water heating, with the PV power used to charge the battery. The total grid power used per year is calculated by adding the grid power used to heat the water, charge the battery and power the appliances in the system.

The amount of PV power that is available, to charge the battery, depends on the time of day and whether there was any loadshedding that discharged the battery. As seen in Chapter 3.3.3.1, for any arbitrary time of day, the system will generate the maximum possible amount of power with the PV panels. The model then calculates the intercept point, as shown in Figure

16, and the power generated at the intercept point, which is solely available for water heating. Should the water be below the set temperature and all the PV power, generated at the intercept point, can be used to heat the water, all of the PV power will be used. As for the battery charging, referring back to Figure 16, the maximum PV power minus the PV power at the intercept point is available for battery charging. Should the battery be depleted when the PV power is available, it will use the PV power to charge. However, if the battery is not fully charged at the end of the day, grid power will be used to charge the battery.

An example of the calculations will be provided in the annexures.

5. Validation and Verification

This chapter covers the verification and validation of the simulation program. The equations used within the program were verified with hand calculation by means of a spot check on a random date of the year. The simulation program, which simulates the PV module, and its power generation were validated by comparing the program results with that of the manufacturer data and recorded data from PVGIS.

5.1 Validation of simulation program

5.1.1 Simulated power of the PV system

In Figure 27, the generated power of the simulation program is compared with the generated power from PVGIS for the same solar PV system. On days with high levels of generated power, the error between the simulation program and PVGIS was very small. On days with low levels of generated power, the error increased. The average error for this illustrated month was 3% and for the entire year it was 2%, which is acceptable for this study.

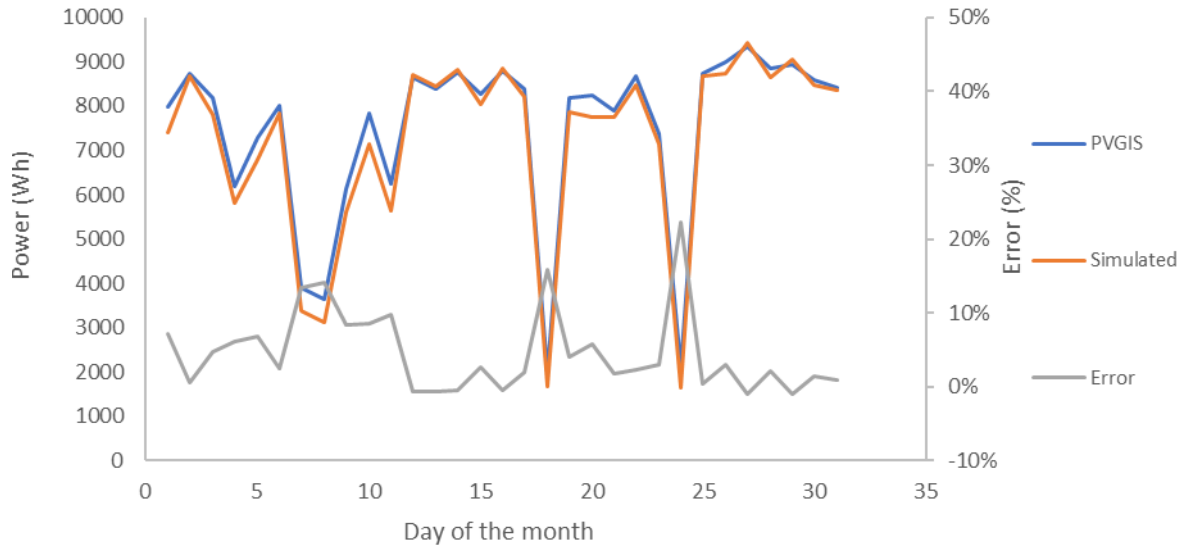

Figure 27: PVGIS vs Simulated power generated

5.1.2 PV module simulation with SDM

To validate the SDM model, the I-V curves of the PV module were simulated at the various irradiance levels and compared to the I-V curves provided by the manufacturer, as shown in Figure 28. The biggest differences between the curves occurred at the MPPT region and for the higher irradiance levels. The accuracy of the data extracted from WebPlotDigitizer may seem questionable since it is only able to capture data per corresponding pixel. Excel, on the

other hand, is a very powerful software tool that can plot data in very small increments. The validation aligned with comments made by Mares *et al*. [20] with regard to graphical models.

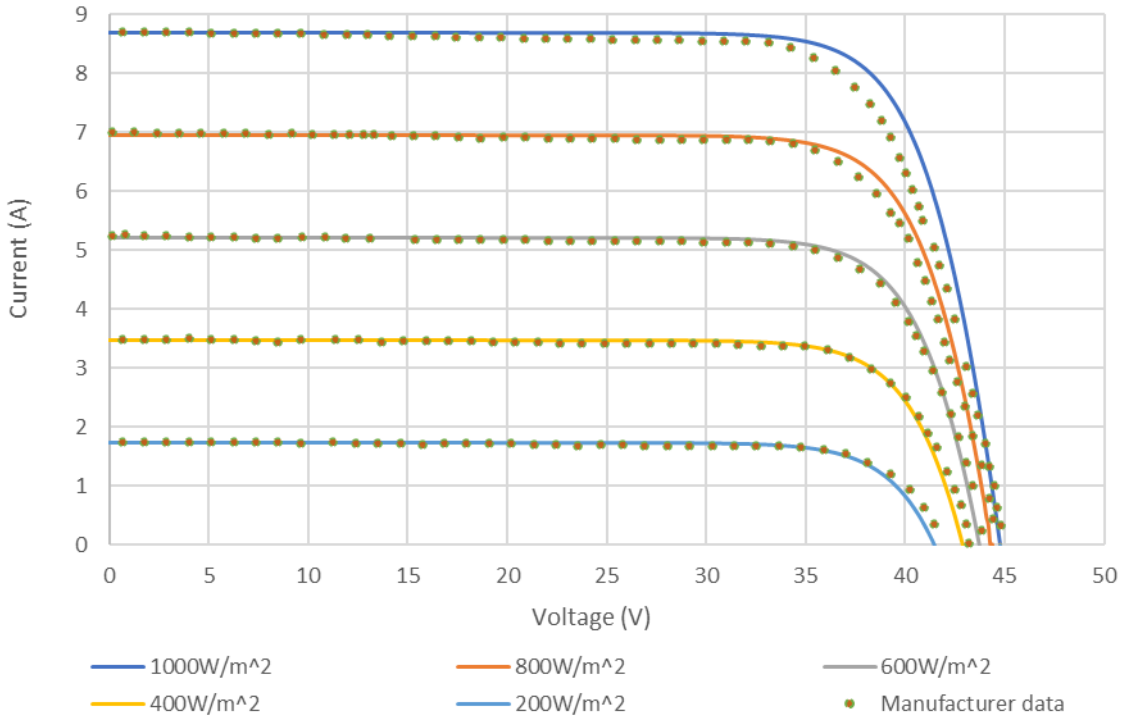

Figure 28: Validation of I-V curves of model

5.1.3 Experimental validation of the simulation program

Figure 29 shows the results of the simulation program compared to that of the experiment. Two sets of data are represented in Figure 29. The first set of four operating points (green and red) are for an irradiance level of 845 W/m^2 (blue I-V curve). The second set of four operating points (blue and purple) are for an irradiance of 624 W/m^2 (green I-V curve). Note that for both sets of data, Point 4 (battery) falls on the same point on the graph, since the output is pre-determined by the MPPT controller. There is a slight difference in voltage and current, but this can be attributed to the changing conditions of the weather during the experiment, which change the panel operating temperature, whereas the simulation results are obtained at a constant temperature of 55°C.

Unlike with the operating behaviour with just the ELON 100 and the geyser element, where the output current and voltage were determined by just the geyser element, and therefore the operating point fell on the intercept point, i.e. Point 1 and Point 2 lay on the same point. With the addition of the battery and MPPT controller, the panels need to generate additional power. Therefore, for the same voltage, the panels are producing more power, by increasing the output current, to also provide power to the MPPT controller (P1 = P2+P3).

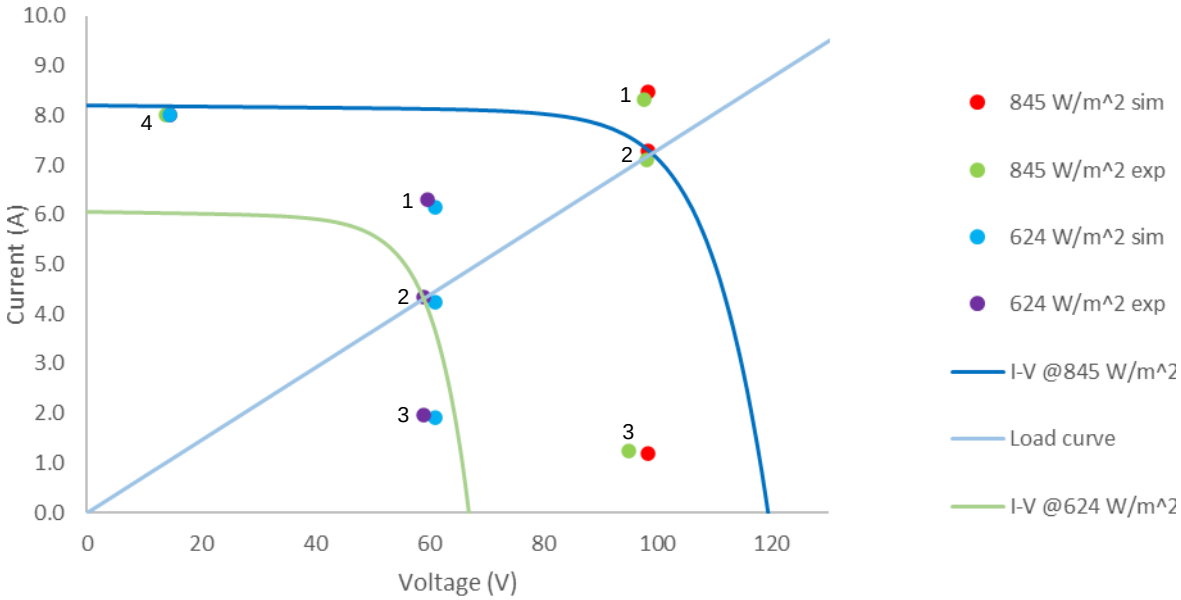

Figure 29: Validation of the simulation program

Table 12 shows the simulated results for each component in the system compared to the experimental results for different irradiation measurements. The average error is between 0,5% and 3,9%, any errors larger than the average error can be attributed to the difference in panel temperature for the experiment and the simulation.

Table 12: Simulated vs experimental results

	845 W/m²			724 W/m²			624 W/m²		
	exp	**sim**	**error**	**exp**	**sim**	**error**	**exp**	**sim**	**error**
V1	98	98	0.6%	83	80	4.0%	61	60	2.2%
A1	8	8	2.0%	8	7	3.6%	6	6	-2.6%
P1	826	813	1.6%	618	579	6.2%	367	377	-2.5%
V2	98	98	0.2%	83	79	5.0%	61	59	3.3%
A2	7	7	2.5%	6	6	5.1%	4	4	-2.4%
P2	717	698	2.7%	509	459	9.8%	259	256	1.0%
V3	98	95	3.4%	83	79	5.0%	61	59	3.3%
A3	1	1	-4.7%	1	1	-3.7%	2	2	-3.2%
P3	117	118	-1.1%	117	115	1.5%	117	116	0.3%
V4	15	14	4.8%	15	14	5.5%	15	14	3.4%
A4	8	8	0.0%	8	8	0.0%	8	8	0.0%
P4	117	111	4.8%	117	110	5.5%	117	113	3.4%
			1.4%			3.9%			0.5%

5.2 Verification of simulation program

5.2.1 Parameter extraction

For chosen values of $a = 1.45$, $V_d = 0.15$ with the data provided by the manufacturer $I_{sc} = 9.54$, $V_{ocSTC} = 45.8$, $N_s = 72$, $\alpha_{V,STC} = -0.031\%$, $T_{STC} = 298.15$ and an operating temperature of $T = 323.15$

$$V_{oc} = V_{ocSTC} + (\alpha_{V,STC} \times V_{ocSTC} \times (T - T_{STC})$$

$$V_{oc} = 45.8 + (-0.0031 \times 45.8 \times (323.15 - 298.15)$$

$$V_{oc} = 42.2505 \text{ V}$$

V_t was calculated with Equation 2

$$V_t = \frac{kT}{q}$$

$$V_t = \frac{1.38E-23 \times 323.15}{1.602E-19}$$

$$V_t = 0.02785 \text{ V}$$

with V_{oc} and V_t determined and where R_{sh} is the inverse of the slope at short circuit conditions, (the slope is determined in WebPlotDigitizer and given as -0.003), the reverse saturation current could be calculated as

$$I_0 = \left(I_{sc} - \frac{V_{oc}}{R_{sh}}\right) / (\exp\left(\frac{V_{oc}}{aN_sV_t}\right) - 1)$$

$$I_0 = \left(9.54 - \frac{42.2505}{333.33}\right) / (\exp\left(\frac{42.2505}{1.45 \times 72 \times 0.02785}\right) - 1)$$

$$I_0 = 4.59\text{E} - 06 \text{ A}$$

The series resistance was then calculated with Equation 15

$$R_s = -\left.\frac{dV}{dI}\right|_{oc} - \frac{aN_sV_t}{I_{sc}}$$

$$R_s = -(-0.4) - \frac{1.45 \times 72 \times 0.02785}{9.54}$$

$$R_s = 0.095226\ \Omega$$

Next, the diode current was calculated for every diode voltage (V_d) increment- in this example

$$V_d = 0.15$$

$$I_d = I_0\left(exp\left(\frac{qV_{d1}}{akT}\right) - 1\right)$$

$$I_d = 4.59E-06\left(exp\left(\frac{1.602E-19 \times 0.15}{1.45 \times 1.38E-23 \times 323.15}\right) - 1\right)$$

$$I_d = 0.0001841 \text{ A}$$

The shunt resistance current was then

$$I_{sh} = \frac{V_{d1}}{\frac{R_{sh}}{N_s}}$$

$$I_{sh} = \frac{0.15}{\frac{333.33}{72}}$$

$$I_{sh} = 0.0324 \text{ A}$$

It followed then that the module current was calculated with

$$I = I_{sc} - I_d - I_{sh}$$

$$I = 9.54 - 0.0001841 - 0.0324$$

$$I = 9.507415 \text{ A}$$

and the module voltage was

$$V = N_s\left[V_{d1} - I\left(\frac{R_s}{N_s}\right)\right]$$

$$V = 72\left[0.15 - 9.507415\left(\frac{0.095226}{72}\right)\right]$$

$$V = 9.89465 \text{ V}$$

5.2.2 Power generation

For the 12th hour on the first day of the first month, the recorded horizontal radiation was 764 W/m^2. The hour angle was then calculated as

$$\omega = 15\left(\frac{t_s}{60} - 12\right)$$

$$\omega = 15\left(\frac{720}{60} - 12\right)$$

$$\omega = 0$$

The declination was calculated next with

$$\delta = 23.45\sin\left(360\frac{284+d}{365}\right)$$

$$\delta = 23.45\sin\left(360\frac{284+1}{365}\right)$$

$$\delta = -23.0116$$

With the optimal tilt angle taken as $\beta = 36.2$ and the latitude of Johannesburg being $\phi = -26.2$, the geometric factor ratio could be calculated with Equation 31

$$R_b = \frac{\cos(\phi+\beta)\cos\delta\cos\omega+\sin(\phi+\beta)\sin\delta}{\cos\phi\cos\delta\cos\omega+\sin\phi\sin\delta}$$

$$R_b = \frac{\cos(-26.2+36.2)\cos-23.0116\cos0+\sin(-26.2+36.2)\sin-23.0116}{\cos-26.2\cos-23.0116\cos0+\sin-26.2\sin-23.0116}$$

$$R_b = 0.8398603$$

The tilted radiation could then be calculated by multiplying the ratio with the horizontal radiation, and the PV-generated power was then calculated with the data table as explained in Chapter 3.

5.2.3 Water heating

For the 9th hour of the first day, with the previous hour geyser temperature $Tt_{i-1} = 53.67°C$, the energy from the PV modules $E_{PV} = 121.230993$ kJ, the volume of the geyser $Vt = 200$ L, the water consumption $V_i = 6.3$ L, the standing loss of the geyser $Q_{LOSS} = 205.5$ kJ, the inlet water temperature $T_{inlet} = 15°C$ and the specific heat of water $c_p = 4.184$ kJ/kgK, the current hour geyser temperature could be calculated with

$$Tt_i = Tt_{i-1} + \Delta T_{PV} + \Delta T_{AUX} - \Delta T_{\dot{m}} - \Delta T_{LOSS}$$

$$Tt_i = Tt_{i-1} + \frac{E_{PV}}{Vtc_p} + \frac{E_{AUX}}{Vtc_p} - \left(Tt_{i-1} - \frac{Tt_{i-1}(Vt - V_i) + T_{inlet}V_i}{Vt}\right) - \frac{Q_{LOSS}}{Vtc_p}$$

$$Tt_i = 53.6744 + \frac{121.23099}{200 \times 4.184} + \frac{0}{200 \times 4.184} - \left(53.6744 - \frac{53.6744(200 - 6.3) + 15 \times 6.3}{200}\right) - \frac{205.5}{200 \times 4.184}$$

$$Tt_i = 52.35°C$$

Note that $E_{AUX} = 0$, since the time is during the day when the sun is shining, and the simulation was set up so that during sunshine only the modules heat the geyser.

To calculate the auxiliary energy used during the timed grid hours, Equation 32 was used. For the 4th hour of the 1st day, the previous hour geyser temperature was $Tt_{i-1} = 53.01751$°C, the energy from the PV modules was $E_{PV} = 0$ kJ, the volume of the geyser was $Vt = 200$ L, the water consumption was $V_i = 1.3875$ L, the standing loss of the geyser was $Q_{LOSS} = 205.5$ kJ, the inlet water temperature was $T_{inlet} = 15°C$, the specific heat of water is $c_p = 4.184$ kJ/kgK, and the current hour geyser temperature was $Tt_i = 55$°C

$$\Delta T_{AUX} = Tt_i - Tt_{i-1} - \Delta T_{PV} + \Delta T_{\dot{m}} + \Delta T_{LOSS}$$

$$\Delta T_{AUX} = 55 - 53.01751 - 0 + \left(53.0175 - \frac{53.0175(200 - 1.3875) + 15 \times 1.3875}{200}\right) + \frac{205.5}{200 \times 4.184}$$

$$\Delta T_{AUX} = 2.4922°C$$

The energy used was then calculated with

$$\Delta T_{AUX} = \frac{E_{AUX}}{Vtc_p}$$

$$E_{AUX} = 2.4922 \times 200 \times 4.184$$

$$E_{AUX} = 2085.47296 \text{ kJ}$$

This concludes the chapter on verification and validation. The next chapter discusses the results obtained with the validated simulation program.

6. Results and Discussion

This chapter discusses the results obtained from the simulation program. Section 1 gives an overview of the techno-economic results from the study. Section 2 discusses the various criteria used to evaluate and compare the different systems. Finally, a scoring table compares the three systems.

6.1 Techno-economic results

In Table 13 below, an overview of the techno-economic results of the study are shown. The baseline system, used for comparison, consisted of only a PV array with four modules and the geyser controller used for water heating, with no battery for emergency power. System A added a small battery with a MPPT charge controller to the baseline system through a parallel connection to the PV array (refer to Figure 11). The battery capacity was then increased for Systems B and C. The methodology behind the power saving calculations is explained in Chapter 4.The savings for system A, B and C is the same percentage wise because, as the battery size increases for each system, the load consumption of the system increases i.e, the number of appliances powered by the battery. Therefore, as there is enough PV power to charge the battery, when it is available during the day, the fraction of the power used to charge the battery from PV and to charge it with grid power stays the same. The difference is that for system C, the surplus power i.e., the power generated from the PV not used for charging or water heating is less than for system A. Essentially meaning that system C utilized more of the potential PV power than system A, as seen in the figure below.

Table 13: Techno-economic results

Location	System	PV potential power (kWh/year)	PV power used (kWh/year)	Grid power used (kWh/year)	Total power saved	PBP
Upington	**Baseline**	**2721**	**2159**	**1745**	**55%**	**4**
	A	2721	2195	1846	54%	6
	B	2721	2280	1931	54%	11
	C	2721	2369	2025	54%	12
Durban	**Baseline**	**1981**	**1574**	**2135**	**42%**	**5**
	A	1981	1610	2234	42%	8
	B	1981	1687	2327	42%	15
	C	1981	1760	2436	42%	18
Pretoria	**Baseline**	**2506**	**1934**	**1916**	**50%**	**4**
	A	2506	1971	2016	49%	6
	B	2506	2052	2105	49%	12
	C	2506	2133	2206	49%	14
Cape Town	**Baseline**	**1789**	**1418**	**2253**	**39%**	**6**
	A	1789	1455	2345	38%	12
	B	1789	1533	2437	39%	17
	C	1789	1605	2547	39%	20+

Table 13 shows the financial and technical results for each system in various high and low irradiation cities across South Africa. From the left, the PV potential power is the total possible annual power that the system could generate according to the solar radiation in the area. The next two columns show the total PV power used as well as the total grid power used. The final technical column shows the total power saved, which is the PV power used divided by the sum of the grid and PV power used. The last column shows the payback period for each system.

The results obtained from the baseline system were similar to the results obtained from PowerOptimal's own case studies [84]. Comparing the baseline with System A, the main difference lay with the financial benefit. Due to the absence of an MPPT and battery, the payback period of the baseline system was only four years. This is due to the fact that 90% of the power savings came from the water heating and not the emergency power. The small batteries used in this study only provide emergency power to the household appliances during loadshedding and were therefore included as a convenience factor and not as a way to save money.

Ultimately all the system sizes and locations tested in this study would provide some level of savings and added convenience during loadshedding. The rest of the chapter focuses on the criteria used to evaluate and compare the technical and economic feasibility of the various

systems as well as the level of convenience they provide to the homeowner during loadshedding.

6.2 Criteria for utility and convenience evaluation

The technical, financial and convenience factor criteria used to evaluate the different systems for each scenario are discussed in this section. Potchefstroom was used for this evaluation. Each system was then compared with the other and given a score out of 3. Finally, the scores were added for each criterion and the system with the highest overall score was determined.

6.2.1 Technical criteria for system evaluation

6.2.1.1 Water heating

Arguably the most important criterion for the system evaluation was the amount of electricity saved due to PV water heating. As water heating is the single largest consumer of power within most South African households, the amount of power saved with PV water heating is an important indication of the success of the system.

6.2.1.2 Backup power

A prerequisite of the system was whether or not the battery capacity for the system would be capable of powering the required backup loads of the system during 4 hours of loadshedding. The level of discharge of the battery was then evaluated. A battery with a lower DoD will have a shorter lifespan than a battery with a higher DoD. Lastly, the amount of power saved by charging the battery with PV modules during the day was evaluated.

6.2.2 Financial criteria for system evaluation

The payback period of each system was used as the criterion to gauge the viability of the system. A short payback period means that the system has a low LCOE and a high NPV. Payback period also shows the homeowner exactly when the system will start to be profitable and is also the easiest financial indicator to understand.

6.2.3 Convenience factor of backup power

This is the level of convenience that the system provides. A larger system with a bigger battery is able to power more appliances during loadshedding compared to a system with a smaller battery, and therefore provides a higher level of convenience to the homeowner during loadshedding.

6.2.4 Systems comparison

Table 14 shows the final comparison between the three systems. Each system is scored out of 3 for each criterion mentioned above. The system is awarded a 3 if it performs the best compared to the other two systems and a 1 if it performs the worst. A 0 is awarded if all three

systems perform equally for any of the criterion. Systems A and B scored the same number of 13 points, while system C only score 10.

Table 14: Systems comparison for Potchefstroom

	System		
Criteria	**A**	**B**	**C**
Power saved: PV water heating	0	0	0
Battery Depth of Discharge	2	3	1
Power saved: PV battery charging	1	2	3
Financial benefit	3	2	1
Level of Convenience	1	2	3
Total	13	13	10

In the following chapter, the results are interpreted, and a conclusion is made about each of the systems. The last chapter will conclude with a brief summary of the entire study and provide recommendation for further research.

7. Conclusion

In the final chapter, conclusions will be drawn based on the results observed in Chapter 6 and recommendations will be given for future studies.

7.1 Conclusion

In this study, a PV system that generates electricity for water heating and emergency power was investigated. The PV system consisted of a PV array with two controllers working in parallel, supplying power to the geyser element and the battery. Three systems were evaluated, each having a different battery and inverter capacity to power larger emergency loads during loadshedding. A baseline system was also used for comparison with each system. A system level simulation model, which used environmental and operating factors as input, was developed for the PV system. Furthermore, the model used climatic design year data with hourly horizontal radiation as input. The PV system was simulated as if retrofitted to an already existing electric geyser. The model was experimentally verified.

The study found that the PV systems generated close to 60% of the power needed for water heating in in-land cities, while only producing 44% of the water-heating power in coastal cities. The savings, with regard to emergency power, for each system increased as the system size increased. The PV system saved on average 40% of the power needed for emergency power, with 26% of the power being saved in Cape Town with system A and 50% saved in Upington with system C. The combined system saved on average, 52.5% of the total power required for the connected appliances and electric resistive heater, for in-land cities. In coastal cities the PV system saved 40.5% of the total power required.

The PV systems performed the best financially in the in-land cities with an average payback period of 6 years for System A and 13 years for system C. In coastal cities the payback period was significantly longer, with system A having a payback period of 10 years and system C close to 20 years.

The three systems were then scored according to the criteria set out in Chapter 6. Although System A and B both scored the same and System C slightly worse, the system which will best suit the homeowner is determined by what the homeowner expects from the system. Should the homeowner just want the best system to save money while still having warm water and the bare minimum of emergency power, System A is clearly the best option. Should the homeowner want the highest level of convenience, where they can continue with their daily lives without feeling the impact of loadshedding, System C is the best. However, if the homeowner wants to save as much money as possible while having a relatively useful amount of emergency power available during loadshedding, System B is the best suited.

Due to the various factors that determine the success of the system, it is difficult to determine which system is the best overall. Every system tested in this study will heat water equally and provide some level of emergency power. The study concluded that: Firstly, the proposed combined system worked, providing reliable emergency power and financial benefit through savings in water heating. Secondly, the factors which the homeowner values more, convenience through emergency power or financial benefit through water heating, determine which system is better suited to the household.

7.2 Recommendations

First and foremost, the recommendations for additional research involve refining the assumptions that were established in this study. Stratification was ignored in favour of the assumption that the temperature distribution inside the water storage tank was uniform. It is possible to examine the impact of stratification in a subsequent study. Also, the water storage tank's hourly standing loss was taken to be constant at its rated loss. More in-depth modelling is possible to determine how the surrounding ambient temperature affects the standing losses around the water storage tank. Solar time was assumed to be equal to local time, due to it only being a couple minutes of difference.

Secondly, it is possible to use more accurate modelling techniques like the two- or three-diode models. The modelling can also be in more detail. Future studies can make use of a component level simulation model, whereas the PV system was only modelled on a system level in this study.

It is recommended that various load, water consumption profiles and PV array sizes are investigated in a future study. The model created in this study could simulate all of the mentioned above, each would however necessitate a different sensitivity study, which fell outside the main scope of this study. These profiles affect the results of the study greatly. The effect of loadshedding during different times of the day and longer and shorter stages can also be investigated.

Lastly, different weightings could be used for the criteria used to determine the success of the systems for different income groups.

Reference list

[1] M. Kumar and A. Kumar, "Performance assessment and degradation analysis of solar photovoltaic technologies: A review," *Renewable and Sustainable Energy Reviews,* vol. 78, pp. 554-587, 2017/10/01/ 2017, doi: https://doi.org/10.1016/j.rser.2017.04.083.

[2] Deloitte Consulting Pty (Ltd), "An overview of electricity consumption and pricing in South Africa.," 2017. [Online]. Available: https://vdocuments.site/download/and-pricing-in-south-africa-an-overview-of-electricity-consumption-and-pricing

[3] Department of Minerals and Energy, *White Paper on the Energy Policy of the Republic of South Africa*, Department of Minerals and Energy, ed., 1998.

[4] MINMET. "Eskom corruption scandal and its implications." https://min-met.com/blog/eskom-corruption-scandal-and-its-implications/?msclkid=0dd963a2c16411ec9d916eddf26d45f3 (accessed April, 2022).

[5] T. Niselow. "Load shedding through the years and how Eskom has struggled to keep the lights on." News24. https://www.news24.com/fin24/Economy/Eskom/sunday-read-load-shedding-through-the-years-and-how-eskom-has-struggled-to-keep-the-lights-on-20190324 (accessed May, 2022).

[6] S. Grootes, "Twelve years of load shedding – written, starring & directed by the ANC," in *dailymaverick*, ed, 2019.

[7] P. A. Hohne, K. Kusakana, and B. P. Numbi, "A review of water heating technologies: An application to the South African context," *Energy Reports,* vol. 5, pp. 1-19, 2019, doi: 10.1016/j.seta.2018.12.027.

[8] Geyserwise, "Lifespan of solar system components," ed, 2022.

[9] victronenergy. "Victron energy." https://www.victronenergy.com (accessed.

[10] V. Lo Brano, A. Orioli, G. Ciulla, and A. Di Gangi, "An improved five-parameter model for photovoltaic modules," *Solar Energy Materials & Solar Cells,* vol. 94, no. 8, pp. 1358-1370, 2010/08/01/ 2010, doi: https://doi.org/10.1016/j.solmat.2010.04.003.

[11] P. Mohanty, T. Muneer, and M. Kolhe, *Solar photovoltaic system applications : a guidebook for off-grid electrification* (Green energy and technology). Springer, 2015.

[12] C. W. Botes, "Techno-economical evaluation of domestic water heating technologies," M.Eng Mechanical, Engineering, North-West University, 2021.

[13] G. Kavlak, J. McNerney, and J. E. Trancik, "Evaluating the causes of cost reduction in photovoltaic modules," *Energy Policy,* vol. 123, pp. 700-710, 2018, doi: 10.1016/j.enpol.2018.08.015.

[14] I. Hajdukovic, "The impact of international trade on the price of solar photovoltaic modules: empirical evidence," *EconomiA,* vol. 23, no. 1, pp. 88-104, 2022, doi: 10.1108/ECON-05-2022-0007.

[15] M. H. Shubbak, "Advances in solar photovoltaics: Technology review and patent trends," *Renewable and Sustainable Energy Reviews,* vol. 115, 2019, doi: 10.1016/j.rser.2019.109383.

[16] W. C. Sinke, "Development of photovoltaic technologies for global impact," *Renewable Energy,* vol. 138, pp. 911-914, 2019/08/01/ 2019, doi: https://doi.org/10.1016/j.renene.2019.02.030.

[17] K. O. Geoffrey and L. A. Lilian. (2022). A Review of Emerging Photovoltaic Construction Technologies to Increase Efficiencies in Solar as a Renewable Energy Source. Available: http://asrjetsjournal.org/index.php/American_Scientific_Journal/article/view/7407

http://worldcat.org/search?q=on:JOASR+http://asrjetsjournal.org/index.php/American_Scientific_Journal/oai+American_Scientific_Journal+CNTCOLL

[18] M. Huot, L. Kumar, J. Selvaraj, M. Hasanuzzaman, and N. A. Rahim, "Performance Investigation of Tempered Glass-Based Monocrystalline and Polycrystalline Solar Photovoltaic Panels," *International Journal of Photoenergy,* Article pp. 1-8, 2021, doi: 10.1155/2021/2335805.

[19] A. Taşçıoğlu, O. Taşkın, and A. Vardar, "A Power Case Study for Monocrystalline and Polycrystalline Solar Panels in Bursa City, Turkey," *International Journal of Photochemistry,* Article vol. 2016, pp. 1-7, 01// 2016, doi: 10.1155/2016/7324138.

[20] O. Mares, M. Paulescu, and V. Badescu, "A simple but accurate procedure for solving the five-parameter model," *Energy Conversion and Management,* vol. 105, pp. 139-148, 2015/11/15/ 2015, doi: https://doi.org/10.1016/j.enconman.2015.07.046.

[21] M. S. Elias and T. B. Yilma, "Modeling and Analysis of Photo-Voltaic Solar Panel under Constant Electric Load," *Journal of Renewable Energy,* article vol. 2019, 01/01/ 2019, doi: 10.1155/2019/9639480.

[22] M. E. Alaoui, F. Farah, M. Ouremchi, K. El Khadiri, and H. Qjidaa, "Modelling of Photovoltaic Module with POWERSIM," presented at the 6th International Renewable and Sustainable Energy Conference, 2018.

[23] K. Ishaque, Z. Salam, H. Taheri, and Syafaruddin., "Modeling and simulation of photovoltaic (PV) system during partial shading based on a two-diode model," *Simulation Modelling Practice and Theory,* vol. 19, no. 7, pp. 1613-1626, 2011/08/01/ 2011, doi: https://doi.org/10.1016/j.simpat.2011.04.005.

[24] D. A. Alqahtani, *A simplified and accurate photovoltaic module parameters extraction approach using matlab*. 2012, pp. 1748-1753.

[25] Z. Wang, Y. Li, K. Wang, and Z. Huang, "Environment-adjusted operational performance evaluation of solarphotovoltaic power plants: A three stage efficiency analysis," *Renewable and Sustainable Energy Reviews,* vol. 76, pp. 1153-1162, 2017, doi: https://doi.org/10.1016/j.rser.2017.03.119.

[26] SunWize. "Solar Charge Controller Types." https://www.sunwize.com/tech-notes/solar-charge-controller-types/ (accessed.

[27] Y. E. Abu Eldahab, N. H. Saad, and A. Zekry, "Enhancing the design of battery charging controllers for photovoltaic systems," *Renewable and Sustainable Energy Reviews,* vol. 58, pp. 646-655, 2016, doi: 10.1016/j.rser.2015.12.061.

[28] A. Beale. "5 Best MPPT Charge Controllers." https://footprinthero.com/best-mppt-solar-charge-controllers (accessed.

[29] O. Bolt. "6 Best MPPT Solar Charge Controllers." https://energytheory.com/6-best-mppt-solar-charge-controllers/ (accessed.

[30] Nick. "Best MPPT Solar Charge Controller." https://cleversolarpower.com/best-mppt-solar-charge-controller/ (accessed.

[31] POWEROPTIMAL. "Product Specifications." https://poweroptimal.com/specifications/ (accessed.

[32] GEYSERROBOT. https://www.geyserrobot.co.za (accessed.

[33] Geyserwise. "200L PV Water Heating System." https://www.geyserwise.com/products/pv-water-heating-systems/200l-pv-water-heating-system/ (accessed 2023).

[34] X. Han, J. Garrison, and G. Hug, "Techno-economic analysis of PV-battery systems in Switzerland," *Renewable and Sustainable Energy Reviews,* vol. 158, 2022, doi: 10.1016/j.rser.2021.112028.

[35] S. Bandyopadhyay, Z. Qin, L. Ramirez-Elizondo, and P. Bauer, "Comparison of Battery Technologies for DC Microgrids with Integrated PV," ed: IEEE, 2019, pp. 1-9.

[36] M. S. Ziegler and J. E. Trancik, "Re-examining rates of lithium-ion battery technology improvement and cost decline," *Energy & Environmental Science,* 10.1039/D0EE02681F vol. 14, no. 4, pp. 1635-1651, 2021, doi: 10.1039/D0EE02681F.

[37] W. S. Ebhota and P. Y. Tabakov, "Impact of Photovoltaic Panel Orientation and Elevation Operating Temperature on Solar Photovoltaic System Performance," *International Journal of Renewable Energy Development,* vol. 11, no. 2, pp. 591-599, 2022, doi: 10.14710/ijred.2022.43676.

[38] S. A. Kalogirou, R. Agathokleous, and G. Panayiotou, "On-site PV characterization and the effect of soiling on their performance," *Energy,* vol. 51, pp. 439-446, 2013/03/01/ 2013, doi: https://doi.org/10.1016/j.energy.2012.12.018.

[39] N. Gökmen, W. Hu, P. Hou, Z. Chen, D. Sera, and S. Spataru, "Investigation of wind speed cooling effect on PV panels in windy locations," *Renewable Energy,* vol. 90, pp. 283-290, 2016/05/01/ 2016, doi: https://doi.org/10.1016/j.renene.2016.01.017.

[40] A. G. Gaglia, S. Lykoudis, A. A. Argiriou, C. A. Balaras, and E. Dialynas, "Energy efficiency of PV panels under real outdoor conditions–An experimental assessment in Athens, Greece," *Renewable Energy,* vol. 101, pp. 236-243, 2017/02/01/ 2017, doi: https://doi.org/10.1016/j.renene.2016.08.051.

[41] J. K. Kaldellis, M. Kapsali, and K. A. Kavadias, "Temperature and wind speed impact on the efficiency of PV installations. Experience obtained from outdoor measurements in Greece," *Renewable Energy,* vol. 66, pp. 612-624, 2014/06/01/ 2014, doi: https://doi.org/10.1016/j.renene.2013.12.041.

[42] A. Dhouib and S. Filali, "OPERATING TEMPERATURES OF PHOTOVOLTAIC PANELS," in *Energy and the Environment*, A. A. M. Sayigh Ed. Oxford: Pergamon, 1990, pp. 494-498.

[43] J. A. Duffie and W. A. Beckman, *Solar engineering of thermal processes*, 4 ed. Hoboken, N.J.: Wiley, 2013, p. 910.

[44] B. Mow. "STAT FAQs Part 2: Lifetime of PV Panels." https://www.nrel.gov/state-local-tribal/blog/posts/stat-faqs-part2-lifetime-of-pv-panels.html#:~:text=NREL%20research%20has%20shown%20that%20solar%20panels%20have,decrease%20at%20a%20rate%20of%200.5%25%20per%20year. (accessed June 2022).

[45] R. Pan, J. Kuitche, and G. Tamizhmani, "Degradation analysis of solar photovoltaic modules: Influence of environmental factor," in *2011 Proceedings - Annual Reliability and Maintainability Symposium*, 24-27 Jan. 2011 2011, pp. 1-5, doi: 10.1109/RAMS.2011.5754514.

[46] S. M. Ngure, A. B. Makokha, E. O. Ataro, and M. S. Adaramola, "Degradation analysis of Solar photovoltaic module under warm semiarid and tropical savanna climatic conditions of East Africa," *International Journal of Energy and Environmental Engineering,* vol. 13, no. 2, pp. 431-447, 2022/06/01 2022, doi: 10.1007/s40095-021-00454-5.

[47] E. N. V. Deventer, "Climatic and other design data for evaluating heating and cooling requirements of buildings," in "CSIR Research Report " CSIR, Pretoria, 1971.

[48] PVGIS. "PHOTOVOLTAIC GEOGRAPHICAL INFORMATION SYSTEM." https://re.jrc.ec.europa.eu/pvg_tools/en/ (accessed.

[49] M. Mbulelo, F. Donald, and B. Bernard, "COMPARING LONG-TERM ACTUAL VERSUS SIMULATED PV SYSTEM PERFORMANCE: A REVIEW AND CASE STUDY." [Online]. Available: https://www.crses.sun.ac.za/files/research/publications/technical-reports/COMPARING%20LONG-TERM%20ACTUAL%20VERSUS%20SIMULATED%20PV%20SYSTEM%20PERFORMANCE%20-%20A%20REVIEW%20AND%20CASE%20STUDY.pdf

[50] C. S. Psomopoulos, G. C. Ioannidis, S. D. Kaminaris, K. D. Mardikis, and N. G. Katsikas, "A Comparative Evaluation of Photovoltaic Electricity Production Assessment Software (PVGIS, PVWatts and RETScreen)," *Environmental Processes,* vol. 2, no. 1, pp. 175-189, 2015/11/01 2015, doi: 10.1007/s40710-015-0092-4.

[51] SOLAGIS. "Solar resource maps of South Africa." World Bank Group. https://solargis.com/maps-and-gis-data/download/south-africa (accessed 2022).

[52] P. G. Rousseau and G. P. Greyvenstein, "Enhancing the impact of heat pump water heaters in the South African commercial sector," *Energy,* vol. 25, no. 1, pp. 51-70, 2000, doi: 10.1016/S0360-5442(99)00053-5.

[53] J. P. Meyer and M. Tshimankinda, "Domestic hot water consumption in south african townhouses," *Energy Conversion and Management,* vol. 39, no. 7, pp. 679-684, 1998, doi: 10.1016/S0196-8904(97)00048-4.

[54] N. Beute, "Domestic utilisation of electrical grid energy in South Africa," Potchefstroom University for Christian Higher Education, 1993.

[55] P. A. Friedrich Ferrer, "Average economic performance of solar water heaters for low density dwellings across South Africa," *Renewable and Sustainable Energy Reviews,* vol. 76, pp. 507-515, 2017, doi: 10.1016/j.rser.2017.03.074.

[56] T. T. Chow, K. F. Fong, A. L. S. Chan, and Z. Lin, "Potential application of a centralized solar water-heating system for a high-rise residential building in Hong Kong," *Applied Energy,* vol. 83, no. 1, pp. 42-54, 2006, doi: 10.1016/j.apenergy.2005.01.006.

[57] İ. H. Yılmaz, "Residential use of solar water heating in Turkey: A novel thermo-economic optimization for energy savings, cost benefit and ecology," *Journal of Cleaner Production,* vol. 204, pp. 511-524, 2018, doi: 10.1016/j.jclepro.2018.09.060.

[58] J. Lutz, X. Liu, J. McMahon, C. Dunham, L. Shown, and Q. McCure, "Modeling patterns of hot water use in households," Lawrence Berkeley National Laboratory, 1996. [Online]. Available: https://escholarship.org/uc/item/9zh371jz

[59] H. Ibrahim and N. Anani, "Evaluation of Analytical Methods for Parameter Extraction of PV modules," *Energy Procedia,* vol. 134, pp. 69-78, 2017/10/01/ 2017, doi: https://doi.org/10.1016/j.egypro.2017.09.601.

[60] D. T. Cotfas, P. A. Cotfas, and S. Kaplanis, "Methods to determine the dc parameters of solar cells: A critical review," *Renewable and Sustainable Energy Reviews,* vol. 28, pp. 588-596, 2013/12/01/ 2013, doi: https://doi.org/10.1016/j.rser.2013.08.017.

[61] T. R. Ayodele, A. S. O. Ogunjuyigbe, and E. E. Ekoh, "Evaluation of numerical algorithms used in extracting the parameters of a single-diode photovoltaic model," *Sustainable Energy Technologies and Assessments,* vol. 13, pp. 51-59, 2016/02/01/ 2016, doi: https://doi.org/10.1016/j.seta.2015.11.003.

[62] A. M. Humada, M. Hojabri, S. Mekhilef, and H. M. Hamada, "Solar cell parameters extraction based on single and double-diode models: A review," *Renewable and Sustainable Energy Reviews,* vol. 56, pp. 494-509, 2016/04/01/ 2016, doi: https://doi.org/10.1016/j.rser.2015.11.051.

[63] G. A. Thopil, C. E. Sachse, J. r. Lalk, and M. S. Thopil, "Techno-economic performance comparison of crystalline and thin film PV panels under varying meteorological conditions: A high solar resource southern hemisphere case," *Applied Energy,* vol. 275, 2020, doi: 10.1016/j.apenergy.2020.115041.

[64] J. Hoppmann, J. Volland, T. S. Schmidt, and V. H. Hoffmann, "The economic viability of battery storage for residential solar photovoltaic systems - A review and a simulation model," *Renewable and Sustainable Energy Reviews,* vol. 39, pp. 1101-1118, 2014, doi: 10.1016/j.rser.2014.07.068.

[65] G. B. M. A. Litjens, E. Worrell, and W. G. J. H. M. van Sark, "Economic benefits of combining self-consumption enhancement with frequency restoration reserves provision by photovoltaic-battery systems," *Applied Energy,* vol. 223, pp. 172-187, 2018, doi: 10.1016/j.apenergy.2018.04.018.

[66] V. Bertsch, J. Geldermann, and T. Lühn, "What drives the profitability of household PV investments, self-consumption and self-sufficiency?," *Applied Energy,* vol. 204, pp. 1-15, 2017, doi: 10.1016/j.apenergy.2017.06.055.

[67] G. de Oliveira e Silva and P. Hendrick, "Photovoltaic self-sufficiency of Belgian households using lithium-ion batteries, and its impact on the grid," *Applied Energy,* vol. 195, pp. 786-799, 2017, doi: 10.1016/j.apenergy.2017.03.112.

[68] C. Truong, M. Naumann, R. Karl, M. Müller, A. Jossen, and H. Hesse, "Economics of Residential Photovoltaic Battery Systems in Germany: The Case of Tesla's Powerwall," *Batteries,* vol. 2, no. 2, p. 14, 2016, doi: 10.3390/batteries2020014.

[69] A. Chaianong, A. Bangviwat, C. Menke, B. Breitschopf, and W. Eichhammer, "Customer economics of residential PV-battery systems in Thailand," *Renewable Energy,* vol. 146, pp. 297-308, 2020, doi: 10.1016/j.renene.2019.06.159.

[70] M. N. Akter, M. A. Mahmud, and A. M. T. Oo, "Comprehensive economic evaluations of a residential building with solar photovoltaic and battery energy storage systems: An Australian case study," *Energy & Buildings,* vol. 138, pp. 332-346, 2017, doi: 10.1016/j.enbuild.2016.12.065.

[71] A. Hughes and R. Larmour, "Residential electricity consumption in South Africa," University of Cape Town, University of Cape Town, 2021.

[72] M. Gerther. "List of electric appliances and their wattage usage." https://generatorist.com/list-of-electric-appliances-their-wattage-usage (accessed May, 2022).

[73] Energy Rating. "SWIMMING POOL PUMPS." https://www.energyrating.gov.au/products/swimming-pool-pumps#:~:text=single%20speed%20pumps%20with%20a,between%202.6%20and%2015%20amps). (accessed 2023).

[74] W. Toussaint and D. Moodley, "Clustering Residential Electricity Consumption Data to Create Archetypes that Capture Household Behaviour in South Africa," *South African Computer Journal,* vol. 32, no. 2, pp. 1-34, 2020, doi: 10.18489/sacj.v32i2.845.

[75] CanadianSolar. "MAXPOWER CS6U-325|330|335|340P." www.canadiansolar.com/na (accessed.

[76] N. Anani, "A Simple Method for Parameter Extraction of a PV Module," presented at the Energy Sys., Istanbul, Turkey, 2020.

[77] M. G. Villalva, J. R. Gazoli, and E. R. Filho, "Comprehensive approach to modeling and simulation of photovoltaic arrays," *IEEE Transactions on Power Electronics,* vol. 24, no. 5, 2009.

[78] J. Widèn and J. Munkhammar, *Solar Radiation Theory*. Uppsala University, 2019.

[79] R. Page-Shipp, "Basic principles of solar water heating," 09/10 1980.

[80] Electrolux SA. "KWIKOT superline 400 DUAL electric water heaters." https://www.kwikot.com/kwikot/brochures/Superline-Dual-Electric-Water-Heaters-July-2019.pdf (accessed May 27, 2020).

[81] E. Loth, C. Qin, J. G. Simpson, and K. Dykes, "Why we must move beyond LCOE for renewable energy design," *Advances in Applied Energy,* vol. 8, 2022, doi: 10.1016/j.adapen.2022.100112.

[82] N. R. Deevela, B. Singh, and T. C. Kandpal, "Techno-economics of solar PV array-based hybrid systems for powering telecom towers," *Environment, Development and Sustainability : A Multidisciplinary Approach to the Theory and Practice of Sustainable Development,* vol. 23, no. 11, pp. 17003-17029, 2021, doi: 10.1007/s10668-021-01379-z.

[83] D. R. Kiran, *Principles of economics and management for manufacturing engineering*, [S.l.]: Butterworth-Heinemann, 2022. [Online]. Available: https://www.sciencedirect.com/science/book/9780323998628

https://www.vlebooks.com/vleweb/product/openreader?id=none&isbn=9780323998635

https://search.ebscohost.com/login.aspx?direct=true&scope=site&db=nlebk&db=nlabk&AN=2963140.

[84] PowerOptimal. "PowerOptimal Elon® 100 Case Studies." https://poweroptimal.com/case-studies-elon/ (accessed 2023).

Annexure A

A.1 Parameter extraction

Shunt resistance derivation and approximation

At higher currents the effect of the shunt resistance is the greatest, i.e. at short-circuit conditions, which is why the derivative of the I-V curve at the short-circuit point is used to estimate the resistance. The derivative of Eq. 12 along any point on the I-V curve is then derived as [76]

$$\frac{dI}{dV} = -\frac{I_0}{aN_sV_t}\left[\exp\left(\frac{V+IR_s}{aN_sV_t}\right)\left(1+R_s\frac{dI}{dV}\right)\right] - \frac{1}{R_{sh}} - \frac{R_s}{R_{sh}}\left(\frac{dI}{dV}\right) \tag{48}$$

solving for the derivative

$$\frac{dI}{dV} = -\frac{\left[\frac{I_0}{aN_sV_t}\exp\left(\frac{V+IR_s}{aN_sV_t}\right)+\left(\frac{1}{R_{sh}}\right)\right]}{\left[1+\frac{R_s}{R_{sh}}+\frac{I_0R_s}{aN_sV_t}\exp\left(\frac{V+IR_s}{aN_sV_t}\right)\right]} \tag{49}$$

Finally, at short-circuit conditions, the derivative becomes

$$\left.\frac{dI}{dV}\right|_{sc} = -\frac{\left[\frac{I_0}{aN_sV_t}\exp\left(\frac{I_{sc}R_s}{aN_sV_t}\right)+\left(\frac{1}{R_{sh}}\right)\right]}{\left[1+\frac{R_s}{R_{sh}}+\frac{I_0R_s}{aN_sV_t}\exp\left(\frac{I_{sc}R_s}{aN_sV_t}\right)\right]} \tag{50}$$

The diode current is represented by $\mathrm{I}_0\exp\left(\frac{I_{sc}R_s}{aN_sV_t}\right)$, which is neglected due to its small size compared to the short-circuit current [10]. Also, since R_s is smaller than R_{sh}, $\frac{R_s}{R_{sh}}$ is also neglected. The derivation then becomes

$$\left.\frac{dI}{dV}\right|_{sc} = -\frac{1}{R_{sh}} \tag{51}$$

which can be expressed in terms of the shunt resistance as the inverse of the slope at short circuit

$$R_{sh} = -\left.\frac{dV}{dI}\right|_{sc} \tag{52}$$

Series Resistance derivation

At open-circuit conditions, where the voltage is higher, the effect of the series resistance is more dominant. The derivative of the I-V curve at the open-circuit point is therefore used to estimate the series resistance [76]. The same derivation is used as with the shunt resistance

extraction, substituting the open-circuit point $(V_{oc}, 0)$ in the general expression for the derivative in Eq. 49 [76]

$$\left.\frac{dI}{dV}\right|_{oc} = -\frac{\left[\frac{I_0}{aN_sV_t}\exp\left(\frac{V_{oc}}{aN_sV_t}\right) - \left(\frac{1}{R_{sh}}\right)\right]}{\left[1 + \frac{R_s}{R_{sh}} + \frac{I_0R_s}{aN_sV_t}\exp\left(\frac{V_{oc}}{aN_sV_t}\right)\right]} \tag{53}$$

The diode current, represented by $\mathrm{I}_0\exp\left(\frac{V_{oc}}{aN_sV_t}\right)$, is the same as the photon current under open-circuit conditions [76]. Also, since the photon current is equal to the short-circuit current:

$$I_o \exp\left(\frac{V_{oc}}{aN_sV_t}\right) = I_{sc} \tag{54}$$

The derivative becomes

$$\left.\frac{dI}{dV}\right|_{oc} = -\frac{\left(\frac{I_{sc}}{aN_sV_t} + \frac{1}{R_{sh}}\right)}{1 + \frac{R_s}{R_{sh}} + \frac{I_{sc}R_s}{aN_sV_t}} \tag{55}$$

Furthermore, since $\frac{I_{sc}}{aN_sV_t} \gg \frac{R_s}{R_{sh}}$, the terms $\frac{I_{sc}}{aN_sV_t}$ and $\frac{R_s}{R_{sh}}$ may be neglected in practice [76] and the equation becomes

$$R_s = -\left.\frac{dV}{dI}\right|_{oc} - \frac{aN_sV_t}{I_{sc}} \tag{56}$$

The slope can be graphically estimated or calculated from the I-V curve.

A.2 Simulation procedure in Excel

The power generation model makes use of the data table function within Excel. On the power generation sheet, two cells are allocated to the input solar irradiance and the output intercepted power. The input solar radiation is equated to the variating radiation G_{VAR} and the output intercepted power is calculated for every arbitrary irradiance [12]. The inclusion of these two cells makes it easier when working with different sheets in Excel. Instead of selecting the input and output variables directly from the simulation model in a different sheet, it can be selected from within the same sheet as the data table. The data table works as follows:

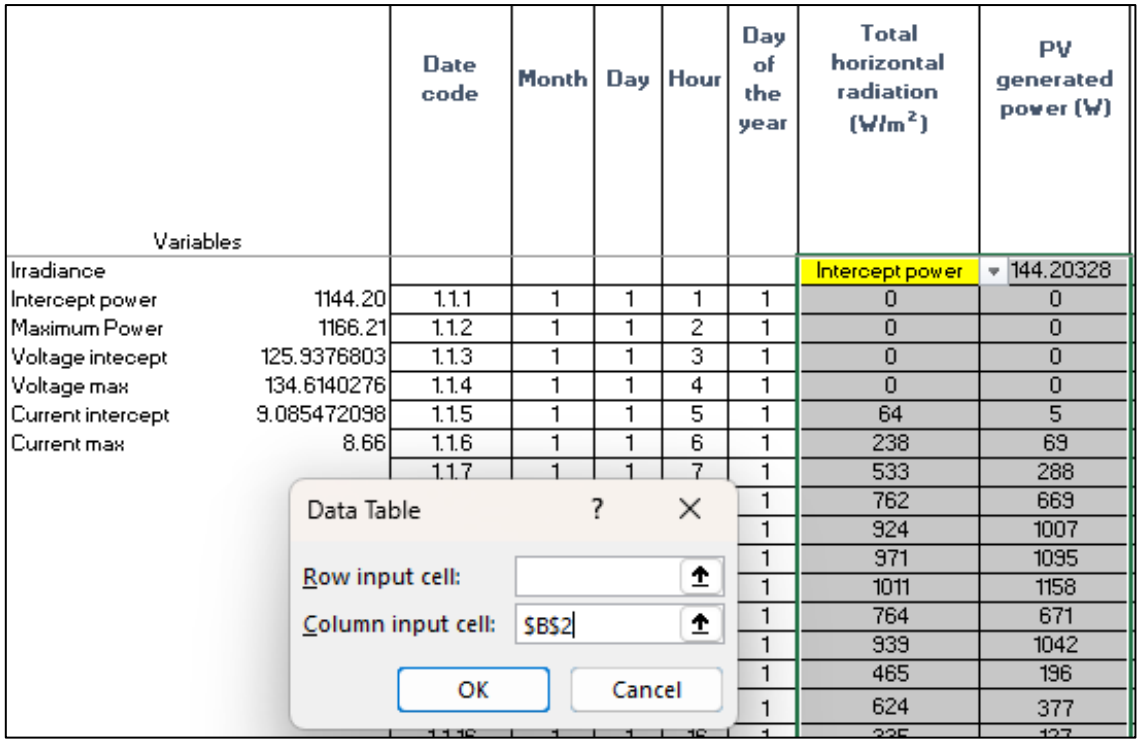

Variables		Date code	Month	Day	Hour	Day of the year	Total horizontal radiation (W/m²)	PV generated power (W)
Irradiance							Intercept power	144.20328
Intercept power	1144.20	1.1.1	1	1	1	1	0	0
Maximum Power	1166.21	1.1.2	1	1	2	1	0	0
Voltage intecept	125.9376803	1.1.3	1	1	3	1	0	0
Voltage max	134.6140276	1.1.4	1	1	4	1	0	0
Current intercept	9.085472098	1.1.5	1	1	5	1	64	5
Current max	8.66	1.1.6	1	1	6	1	238	69
		1.1.7	1	1	7	1	533	288
						1	762	669
						1	924	1007
						1	971	1095
						1	1011	1158
						1	764	671
						1	939	1042
						1	465	196
						1	624	377

Data Table

Row input cell:

Column input cell: B2

OK Cancel

Figure 30: Data table with What-if analysis in Excel

To initiate the what-if analysis, highlight the “Total horizontal radiation” and “PV generated power” columns and select Data Table from the What-if analysis drop down in Excel. The initial value in Row 1 of the intercepted power is P_{INT} (1144.20 in this case). The data table automatically knows that for every arbitrary irradiance in the “Total horizontal radiation” column, the intercepted power needs to be calculated in the “PV generated power” column. Within the data table function, a row input cell or a column input cell can be selected. The variable irradiance data populates the radiation column; therefore, the column input values are selected as G_{VAR}. The model then starts at Row 3 in the Excel sheet and computes the MPP for every irradiance input. As an example:

For a radiation of 924 W/m^2, the input is 924, the variable G_{VAR} is then equated to 924 W/m^2. The program then generates the I-V curve shown in Figure 31. Then the intersect point is calculated and the corresponding voltage and current values are given as 117.34 V and 8.585 A. The output power is then calculated by multiplying the voltage and current at the intersect point, which results in 1007 W. This process is repeated for every arbitrary irradiance in the “Total horizontal radiation” column.

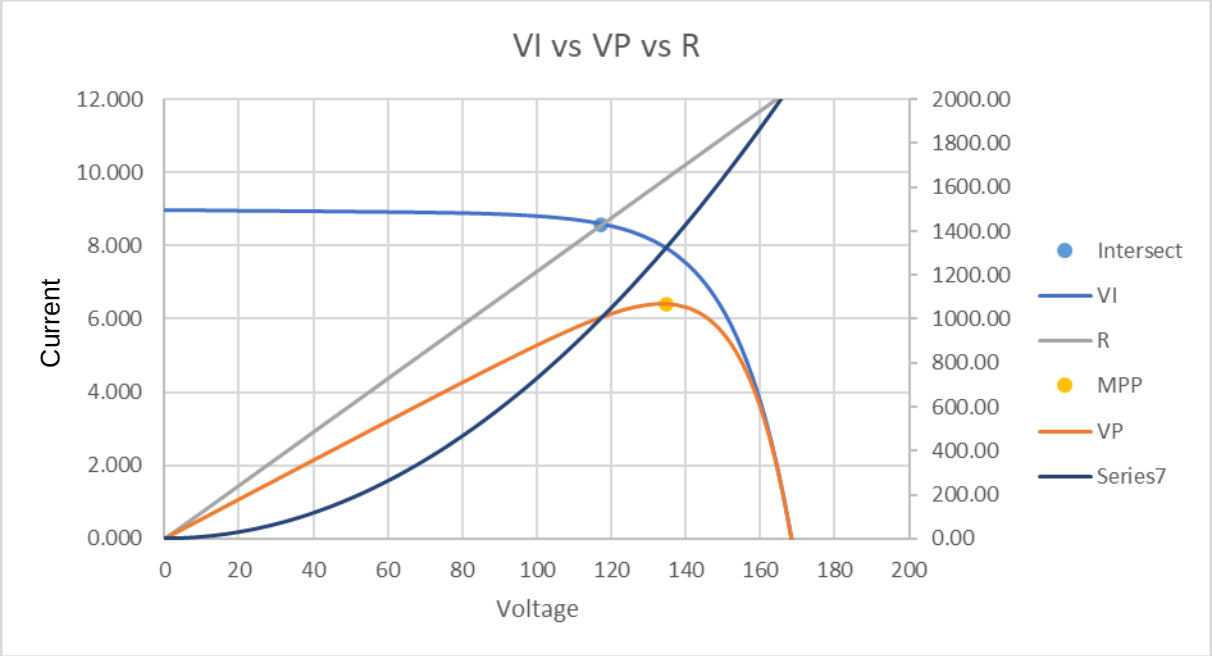

Figure 31: I-V curve for 924 W/m^2

A.3 Water heating model (IF statements)

The geyser temperature is determined by Eq.43. The standard geyser temperature is, however, calculated without the auxiliary grid input

$$Tt_i = Tt_{i-1} + \Delta T_{PV} - \Delta T_{\dot{m}} - \Delta T_{LOSS}$$

The 1st condition states: Should the geyser temperature be below the predetermined temperature setpoint ($Tmax_{GRID}$) when it is 4:00 or 5:00 in the morning and when it is 18:00 or 19:00 at night the new temperature is calculated with auxiliary grid input [12]

$$Tt_i = Tt_{i-1} + \Delta T_{PV} + \Delta T_{AUX} - \Delta T_{\dot{m}} - \Delta T_{LOSS}$$

Note that, during grid input hours, there is no solar radiation as the sun is not fully above the horizon and ΔT_{PV} is therefore equal to zero. The maximum temperature increase, with a heating element capacity of 14400 kJ/h, is 17.2°C. Should the geyser temperature at the end of the first grid input hour not have reached 55°C, it is calculated as such. A second grid hour is allocated to heat the geyser to 55°C, should the first hour be insufficient.

The 2nd condition states: If the geyser temperature is above or equal to the predetermined PV temperature setpoint, the temperature is equal to the setpoint of 65°C [12].

$$Tt_i = Tmax_{PV}$$

With these conditions, the thermal energy (Q_{AUX}) used for water heating can be calculated:

The 1st condition states: If the geyser temperature after an hour of heating is below the predetermined setpoint during the first timed grid input hour in the morning or evening [12]

$$Q_{AUX} = E_{AUX}$$

Eq. 50 states that the maximum heating capacity is used for the whole hour if the difference between Tt_i and Tt_{i-1} is greater than 17.2°C.

The 2nd condition states: If the water reaches the temperature setpoint of 55°C when it is 4:00 or 5:00 in the morning and when it is 18:00 or 19:00 at night

$$Q_{AUX} = Vt \times c_p \times (Tt_i - Tt_{i-1} + \Delta T_{\dot{m}} + \Delta T_{LOSS})$$

The 3rd condition states: If the geyser temperature is above the predetermined set point ($Tmax_{GRID}$) during any grid input hours

$$Q_{AUX} = 0$$

This means that the PV energy was enough to heat the water to the required temperature.

A.4 WebPlotDigitizer procedure

The slopes of the I-V curve at short-circuit and open-circuit conditions are obtained using WebPlotDigitizer, illustrated in Figure 32 and 33. The website allows a Joint Photographic Experts Group (JPEG) of the I-V curve to be imported and analysed. When the I-V curve graph, provided by the manufacturer, is imported as a 2-D graph, the coordinates of $x_1 = 0$, $x_2 = 50, y_1 = 0$ and $y_2 = 10$ are recorded using the computer mouse to click on these points in the picture, after which various points on the two slopes can be made with the cursor of the computer mouse. WebPlotDigitizer then extracts all the points (red dots) made on the graph relative to x_1, x_2, y_1 and y_2 into a comma-separated values (csv) file.

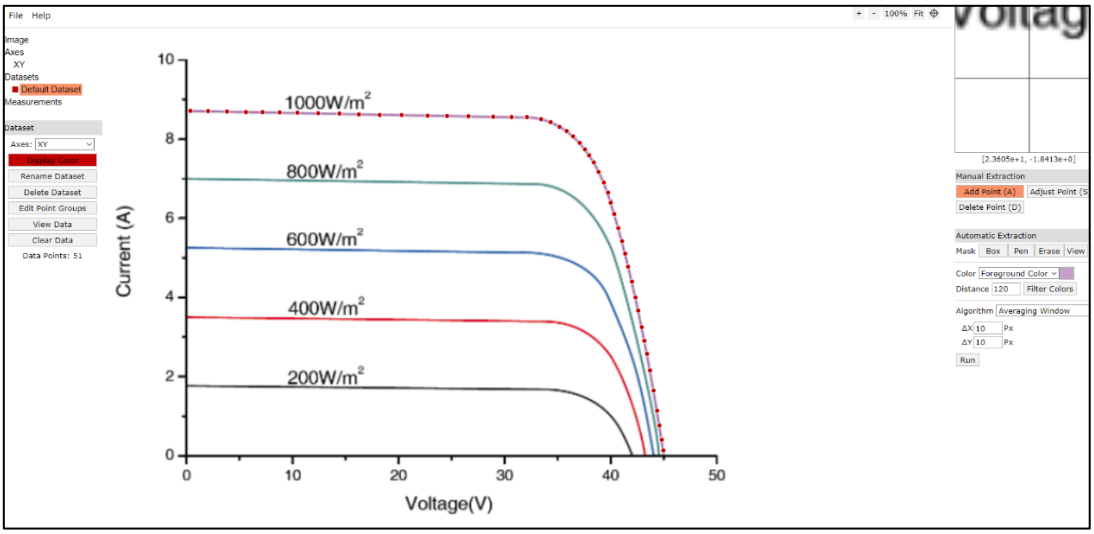

Figure 32: Data points made on the I-V curve using WebPlotDigitizer

The csv file consists of each data point's x and y coordinates, which can be used in a simple calculation to determine the slope at I_{sc} and V_{oc}.

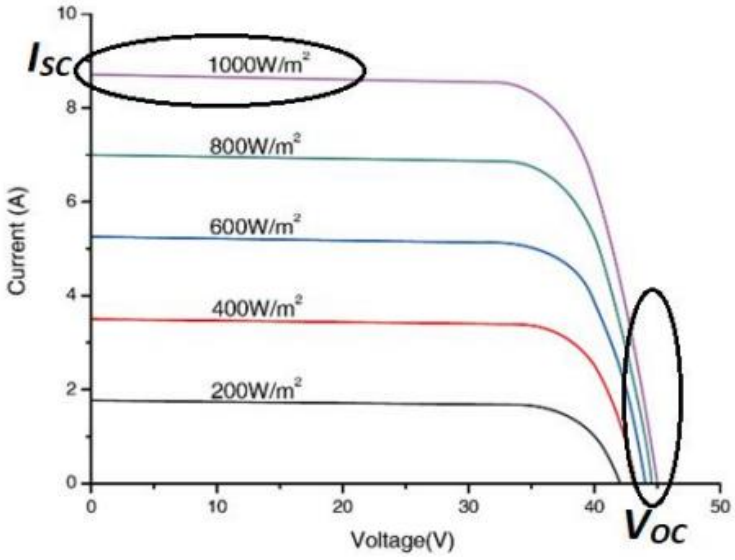

Figure 33: Slopes at open-circuit and short-circuit conditions

A.5 Procedure for water heating

Table 15: Table used in water heating model

Day	Hour	Day of the year	Total tilted radiation (W/m^2)	PV generated power (W)	PV generated energy (kJ)	Normalised consumption	Water consumption (L)	Tank temp	Qeksom
			Maximum Power	577.16057				55	
1	1	1	0	0	0	0.016	2.8275	54.18892	0
1	2	1	0	0	0	0.012	2.1075	53.53039	0
1	3	1	0	0	0	0.008	1.3875	53.01751	0
1	4	1	0	0	0	0.008	1.3875	55	2085.1532
1	5	1	0	0	0	0.017	3.0075	55	708.8352
1	6	1	0	0	0	0.030	5.4	53.67442	0
1	7	1	77.677564	31.149398	112.137831	0.035	6.3	52.34461	0
1	8	1	263.2445114	130.68257	470.457268	0.036	6.48	51.45127	0
1	9	1	454.4780861	241.48118	869.332235	0.035	6.3	51.09636	0
1	10	1	573.4968132	312.72988	1125.82759	0.036	6.48	51.02665	0
1	11	1	632.6132617	348.52601	1254.69365	0.043	7.6875	50.89569	0
1	12	1	747.4753735	419.13318	1508.87943	0.060	10.8	50.5149	0
1	13	1	715.8518488	399.56451	1438.43224	0.060	10.8	50.07049	0
1	14	1	743.1226311	416.4397	1499.1829	0.055	9.9	49.88049	0
1	15	1	636.2693205	350.73983	1262.66337	0.032	5.7075	50.14843	0
1	16	1	427.772331	225.66614	812.398088	0.033	5.8875	49.839	0
1	17	1	129.4626067	57.596805	207.348499	0.046	8.2275	48.40802	0
1	18	1	0	0	0	0.060	10.8	55	7231.281
1	19	1	0	0	0	0.090	16.2	55	2916.732
1	20	1	0	0	0	0.100	18	51.15442	0
1	21	1	0	0	0	0.090	16.2	47.98034	0
1	22	1	0	0	0	0.056	10.0275	46.08121	0
1	23	1	0	0	0	0.027	4.8075	45.08851	0
1	24	1	0	0	0	0.018	3.1875	44.3634	0

The Excel model makes use of various if statements which can be referred to in the Annexure A.3. Firstly, the initial geyser temperature is set to 55°C. Every hour onwards, the new geyser temperature is calculated with Equation 39. At 4:00 and 5:00, as well as at 18:00 and 19:00, the auxiliary grid input is switched on to heat the water to the predetermined set point of 55°C ($Tmax_{GRID}$). During the day, the maximum temperature setpoint is 65°C ($Tmax_{PV}$). There is no minimum temperature setpoint to ensure that only the PV modules are used during the day to heat the water. During the day, the water temperature is affected by the consumption, PV energy and the standing loss of the geyser. When there is less than adequate generated PV energy and the loss of energy due to consumption and standing loss is higher than what the PV modules can replace, there will be a continuous decline in geyser temperature. In the evening at 18:00 and 19:00, if the water is not up to temperature, the auxiliary energy will be used to heat the water up to $Tmax_{GRID}$.

To determine the amount of auxiliary energy required, Equation 38 can be rearranged, making ΔT_{AUX} the subject of the equation which can then be used to calculate E_{AUX}

A.6 PV system saving calculations

Hour	PV generated power intercept point (Wh)	Household load consumption (Wh)	Houeshold emergency load consumption (Wh)	Load shedding	Total load consumed (Wh)	Batter discharge (Wh)	Battery capacity (Wh)	Battery SoC (Wh)	Available power for charging (Wh)	PV used for charging (Wh)	Eskom used for charging (Wh)	Total Generated Power (Wh)	PV Available power for water heating (Wh)	PV energy available for water heating (kJ)	Water consumption profile	Water consumption (L)	Tank temp (°C)	Energy used eksom (kJ)	Temperature with just panels	PV potential energy not used for water heating (Water > 65°C) (kJ)	Energy difference (kJ) (if this sum is negative, the panels are not enough to	Total Energyused to heat water kJ
	1144.20328						500	64%									55		55			
1	0	63	5	N	63	0	500	100%	0	0	0	0	0	0	2%	2.8	54.2	0	54.2	0.0	0	0
2	0	63	5	N	63	0	500	100%	0	0	0	0	0	0	1%	2.1	53.5	0	53.5	0.0	0	0
3	0	63	5	N	63	0	500	100%	0	0	0	0	0	0	1%	1.4	53.0	0	53.0	0.0	0	0
4	0	63	5	N	63	0	500	100%	0	0	0	0	0	0	1%	1.4	55.0	2085	52.5	0.0	-2085	2085
5	0	63	5	N	63	0	500	100%	0	0	0	0	0	0	2%	3.0	55.0	709	51.7	0.0	-709	709
6	0	103	45	Y	45	45	455	91%	0	0	0	0	0	0	3%	6.1	53.5	0	50.3	0.0	0	0
7	104	353	45	Y	45	45	424	85%	14	14	0	117	104	373	6%	11.6	51.5	0	48.5	0.0	0	373
8	308	63	5	Y	5	5	500	100%	81	81	0	390	308	1111	8%	14.5	49.9	0	47.1	0.0	0	1111
9	672	63	5	Y	5	5	500	100%	190	5	0	863	672	2421	7%	11.8	50.5	0	47.9	0.0	0	2421
10	857	63	5	N	63	0	500	100%	258	0	0	1115	857	3086	6%	10.0	52.2	0	49.7	0.0	0	3086
11	964	63	5	N	63	0	500	100%	272	0	0	1236	964	3471	4%	7.7	54.6	0	52.2	0.0	0	3471
12	410	63	5	N	63	0	500	100%	81	0	0	492	410	1477	3%	6.2	54.9	0	52.6	0.0	0	1477
13	832	63	5	N	63	0	500	100%	258	0	0	1090	832	2995	3%	5.7	57.1	0	54.9	0.0	0	2995
14	168	313	5	N	313	0	500	100%	27	0	0	196	168	606	3%	5.7	56.4	0	54.2	0.0	0	606
15	278	63	5	N	63	0	500	100%	81	0	0	359	278	999	3%	5.7	56.2	0	54.0	0.0	0	999
16	75	63	5	N	63	0	500	100%	14	0	0	89	75	271	3%	5.9	55.0	0	53.0	0.0	0	271
17	3	63	5	N	63	0	500	100%	14	0	0	17	3	12	4%	6.4	53.5	0	51.5	0.0	0	12
18	0	103	45	Y	45	45	455	91%	0	0	0	0	0	0	7%	11.8	55.0	3355	49.1	0.0	-3355	3355
19	0	103	45	Y	45	45	410	82%	0	0	0	0	0	0	8%	13.8	55.0	2516	46.5	0.0	-2516	2516
20	0	353	45	Y	45	45	365	73%	0	0	0	0	0	0	8%	14.5	51.8	0	44.0	0.0	0	0
21	0	103	45	Y	45	45	320	64%	0	0	0	0	0	0	8%	13.6	49.1	0	41.8	0.0	0	0
22	0	103	45	N	103	0	320	64%	0	0	0	0	0	0	6%	10.0	47.1	0	40.2	0.0	0	0
23	0	103	45	N	103	0	320	64%	0	0	0	0	0	0	3%	4.8	46.1	0	39.3	0.0	0	0
24	0	63	5	N	63	0	320	64%	0	0	0	0	0	0	2%	3.2	45.4	0	38.7	0.0	0	0
1	0	63	5	N	63	0	500	100%	0	0	180	0	0	0	2%	2.8	44.7	0	38.1	0.0	0	0
2	0	63	5	N	63	0	500	100%	0	0	0	0	0	0	1%	2.1	44.1	0	37.6	0.0	0	0
3	0	63	5	N	63	0	500	100%	0	0	0	0	0	0	1%	1.4	43.7	0	37.2	0.0	0	0

Figure 34: Extract of model calculations for 1 day

The PV generation starts at 7:00 in the morning. For this specific day loadshedding is active from 6:00 to 10:00 and 18:00 to 22:00. Accordingly the battery is not at 100% state of charge when the PV starts generating. Therefore at 7:00, the PV generates 117 Wh at the maximum and 104 Wh at the intercept point, therefore, 14 Wh is available for charging and since the battery is at 85%, all 14 Wh is used to charge the battery. When there is more power available to charge the battery than needed, the surplus power is wasted.

Annexure B

Scenario A: Component Pricing

Component	Specifics	Amount	Total Price
PV modules	Enersol 335W Mono	4	ZAR 8000
Inverter	Not needed	-	ZAR 0
Battery	BlueNova BN13V-22-286Wh MPS	1	ZAR 2 750
BOS	Wiring, support structure etc.	-	ZAR 3 000
Geyser controller	ELON 100	1	ZAR 6 510
MPPT	Victron 150/35	1	ZAR 5 500
Labour	Installation		ZAR 2 000

The capital cost of this system adds to ZAR 27 760 VAT incl.

Scenario B: Component Pricing

Component	Specifics	Amount	Total Price
PV modules	Enersol 335W Mono	4	ZAR 8 000
Inverter	RCT Axpert VM 1K12 1kVA 1kW 12V	1	ZAR 4 650
Battery	BlueNova BN13V-22-286Wh MPS	4	ZAR 9 100
BOS	Wiring, support structure etc.	-	ZAR 3 000
Geyser controller	ELON 100	1	ZAR 6 510
MPPT	Victron 150/35	1	ZAR 5 500
Labour	Installation		ZAR 2 000

The capital cost of this system adds to ZAR 38 760. VAT incl.

Scenario C: Component Pricing

Component	Specifics	Amount	Total Price
PV modules	Enersol 335W Mono	4	ZAR 8 000
Inverter	RCT Axpert VM3 3K24 3kVA 3kW 12V	1	ZAR 10 200
Battery	BlueNova BN13V-22-286Wh MPS	6	ZAR 11 601
BOS	Wiring, support structure etc.	-	ZAR 3 000
Geyser controller	ELON 100	1	ZAR 6 510
MPPT	Victron 150/35	1	ZAR 5 500
Labour	Installation		ZAR 2 000

The capital cost of this system adds to ZAR 46 811 VAT incl.

Component pricing sources

PV modules: 330W-340W

https://solarpanelsonline.co.za ZAR1759

https://www.sustainable.co.za ZAR2367

https://solarwc.co.za	ZAR1899
https://pvstore.co.za	ZAR1990
Average price for a 330W panels is:	ZAR2000
Inverter: 1kW	
https://sinetechstore.co.za	ZAR6250
https://www.sustainable.co.za	ZAR5122
https://solarwarehousesa.com	ZAR2580
Average price for a 1kW inverter is:	ZAR4650
Battery:	
240Wh	
https://www.sustainable.co.za	ZAR2500
https://www.sustainable.co.za	ZAR3000
Average price for 500Wh battery is:	ZAR2750
ELON 100:	
https://www.takeless.co.za	ZAR6500
https://www.unlimitedsolar.co.za	ZAR6234
https://diyshop.co.za	ZAR6795
Average price for ELON 100 is:	ZAR6510
Victron MPPT 150/35	
https://www.solarsmarttechnology.co.za	ZAR5296
https://sunstore.co.za	ZAR5511
https://www.communica.co.za	ZAR5318
https://www.sustainable.co.za	ZAR5698
The average price for the MPPT is:	ZAR5500
Inverter: 3kW	
https://www.sustainable.co.za	ZAR13200

https://www.sustainable.co.za	ZAR9176
https://sinetechstore.co.za	ZAR8995
https://www.solar-shop.co.za	ZAR9400
Average price for a 3kW inverter is:	ZAR10200

Battery: 1000Wh

https://sunstore.co.za	ZAR9325
https://www.sustainable.co.za	ZAR8534
https://www.sustainable.co.za	ZAR9375
Average price for a 1000Wh battery is:	ZAR9100

Battery: 1500Wh

https://www.sustainable.co.za	ZAR10386
https://lifetide.co.za	ZAR11999
https://www.sustainable.co.za	ZAR12420
Average price for a 1500Wh battery is:	ZAR11601

Annexure C: Techno-economic results

Table 16: Complete table of results

Loacation	System	PV power generated (kW)	Grid power used	Total Power used	Total Power saved	LCOE	PBP	NPV	PV used for emergency power	Grid used for emergency power	Power saved with emergency power	PV used for water heating	Grid used for water heating	Power saved with water heating	Maximum Battery DoD
Potchefstroom	**Baseline**	**2502**	**1920**	**3878**	**50%**	**R 1.21**	**4**	**R 49 231**	0	0	0	1958	1430	58%	0
Potchefstroom	A	2502	1987	3981	50%	R 1.87	6	R 39 995	37	66	36%	1958	1430	58%	37%
	B	2502	2075	4152	50%	R 2.51	12	R 25 356	118	154	43%	1958	1430	58%	39%
	C	2502	2173	4334	50%	R 2.87	14	R 18 610	202	253	44%	1958	1430	58%	26%
Durban	A	1981	2234	3843	42%	R 2.23	8	R 22 384	37	66	36%	1417	1790	44%	37%
	B	1981	2327	4013	42%	R 2.96	15	R 10 368	113	159	42%	1417	1790	44%	39%
	C	1981	2436	4195	42%	R 3.37	18	R 2 858	186	268	41%	1417	1790	44%	26%
Pretoria	A	2506	2016	3985	49%	R 1.89	6	R 36 049	37	66	36%	1933	1460	57%	37%
	B	2506	2105	4156	49%	R 2.53	12	R 24 329	117	155	43%	1933	1460	57%	39%
	C	2506	2206	4338	49%	R 2.90	14	R 17 426	198	256	44%	1933	1460	57%	26%
Cape Town	A	1789	2345	3799	38%	R 2.41	12	R 16 508	36	102	26%	1417	1790	44%	37%
	B	1789	2437	3969	39%	R 3.18	17	R 4 591	115	158	42%	1417	1790	44%	38%
	C	1789	2547	4152	39%	R 3.61	20+	-R 3 008	187	268	41%	1417	1790	44%	25%